INTERFERENCE CANCELLATION FOR COLLOCATED WIRELESS RADIOS

A Thesis
Presented to
The Academic Faculty

by

Anand Raghavan

In Partial Fulfillment
of the Requirements for the Degree
Doctor of Philosophy in the
School of Electrical and Computer Engineering

Georgia Institute of Technology
August 2007

INTERFERENCE CANCELLATION FOR COLLOCATED WIRELESS RADIOS

Approved by:

Dr. Joy Laskar, Advisor
School of Electrical and Computer Engineering
Georgia Institute of Technology

Dr. John D. Cressler
School of Electrical and Computer Engineering
Georgia Institute of Technology

Dr. Kevin Kornegay
School of Electrical and Computer Engineering
Georgia Institute of Technology

Dr. Emmanouil M. Tentzeris
School of Electrical and Computer Engineering
Georgia Institute of Technology

Dr. Chang-Ho Lee
Samsung RFIC Design Center
Atlanta, GA

Date Approved: 20 June 2007

To my parents

ACKNOWLEDGEMENTS

I am grateful to many people for the help I have received in different forms over the last few years, allowing me to reach this point. First, I thank Prof. Joy Laskar who as advisor has been positive and resourceful in his guidance. I would also like to acknowledge Prof. John Cressler for his help and advice during past collaborations. To my dissertation review committee members, Prof. Kevin Kornegay, Prof. Manos Tentzeris and Dr. Chang-Ho Lee, I owe thanks for their time, co-operation and suggestions.

To various former and present members of the Microwave Applications Group, I express my gratitude as their support throughout the course of my research has lightened my task. Of these, the mentorship of Dr. Sudipto Chakraborty in the early years and the direction of Dr. Edward Gebara in the later years are especially significant. I appreciate the advice and contribution of Dr. Chang-Ho Lee, Dr. Kyutae Lim, Dr. Stephane Pinel and Dr. Emery Chen. Thanks are also due to Bevin Perumana and Hyoung-Soo Kim for their assistance during times of need. For the help I have received during my interaction with Dr. Bhaskar Banerjee, Dr. Sunitha Venkataraman, Rahul Bhatia, Umesh Jalan and Dr. Moonkyun Maeng, I am grateful. Most of all, to Dr. Arvind Raghavan who as brother and past member of MAG, has rendered me aid and encouragement in singular fashion, I am indebted.

Through industrial internships I have gained insight into the material impact of my education. For the opportunity to work with them and for their technical suggestions, I thank Dr. Scott Forgues at National Semiconductor and Dr. Bruce Schmukler at Quellan. I also benefited from my discussions with Mike Farrell, Mark Dickman and Dr. Andrew Kim who were colleagues at Quellan. Special thanks are

also due to Patrcik O' Farrell at National Semiconductor for his patience and help on numerous occasions over the years.

The administrative staff at the Georgia Electronic Design Center including Chris Evans, DeeDee Bennett, Korinne Lassiter, and Angelika Braig have been instrumental in creating an atmosphere conducive to the smooth flow of work. I thank the support team for this.

Finally, my deepest gratitude is reserved for my parents who with their love and devotion have made this possible.

TABLE OF CONTENTS

LIST OF TABLES

LIST OF FIGURES

SUMMARY

The area of deterministic noise cancellation in mobile radio communication systems is investigated and analyzed. Several interoperation problems in the mobile wireless radio space are identified and interference concerns for the Bluetooth – WLAN networks are characterized and quantified in the physical layer.

A mathematical framework has been created for describing interference in the 2.4 GHz band. An adaptive noise suppression system has been developed that is able to alleviate the encroachment of the aggressor signal on the victim without sacrificing any of the original signal. This system is demonstrated to improve the victim SNR in a spread spectrum communication scenario.

The research is extended to construct an interference canceller that is easy to assimilate into existing RF front-ends. A low-power small form-factor analog active canceller has been designed in 0.18-μm Si-CMOS IC technology that delivers adequate noise suppression performance while operating in the RF domain. This includes novel implementations of phase rotator circuits based on delay interpolation and an integrated low-current quadrature modulator-based continuously variable analog phase shifter. This canceller is capable of up to 30 dB of in-band cancellation for the Bluetooth – WLAN problem. Other versions of the canceller are configured to protect GPS and DVB-H receivers from unintentional radiators transmitting in the vicinity. These demonstrate noise mitigation of at least 15 dB in their respective bands while generating very low broadband noise at the output. A simple low-power mixed-signal automatic control mechanism is also developed to operate the canceller adaptively.

The work described in this dissertation advances the state-of-the-art in the area of mobile wireless radio coexistence.

CHAPTER I

INTRODUCTION

1.1 The Progress of the Radio: Enabling Information and Mobility

Advancement is a constant of our existence. It is the availability of information that guarantees this. Immanuel Kant had argued that although all our knowledge begins with experience, it does not follow that it all arises out of experience. In a converse analogy, although all our progress does not arise from information, it certainly begins with it! Information is disseminated through an elaborate network that links us to one another. It is thus logical to infer that connectivity is an enabler of progress. The causality of this relationship is uncertain but the association is veritable.

The connectivity we experience today owes itself largely to the steady growth of electronics over the past half of a century. It took root in the development of telegraphy and subsequently telephony during the second half of the 19^{th} century due to the efforts of Samuel Morse and Alexander Bell. Thus began wired connectivity, which relies on a physical medium of linkage. In its present embodiment, a wired link is capable of communicating data with Gb/s throughput over copper wire, or optical fiber after the advent of optical communications in the last few decades. On the other hand, the early mathematical formulations of James Maxwell and the experiments of Heinrich Hertz laid the foundations for electro-magnetism and electro-magnetic (EM) wave propagation. The wireless network ultimately springs from those sources after running a parallel course of development over the 20^{th} century. Key instruments of its growth were Guglielmo Marconi with the first radio and Edwin Armstrong with the concepts that form the backbone of most radios that populate our lives today [1].

The manner of information exchange today is advancing with increasing deference to the convenience of the end-user. Over the years, gains in electronics have enabled data in the form of text, image, audio and video to be communicated at greater speeds between us. Whereas this communication began with the user needing to avail of an existing physical link, it is being accomplished ever more without that constraint. If, a decade ago, a telephone and radio brought us voice and audio, a television or computer supplied video, now, a cell phone alone is beginning to tap into all these media. Wireless connectivity has thus heralded an age of mobility, establishing a paradigm for the march of technology.

Much of the partnership of information and mobility arises from the growth of solid-state electronics, a discipline that sprang from the days of vacuum-tubes with the invention of the transistor by John Bardeen, Walter Brattain and William Shockley in the mid-20^{th} century. This was followed after a gap of about 11 years by the invention of the first integrated circuit (IC) by Jack Kilby in 1958 [2]. The Silicon (Si) bipolar junction transistor (BJT) was followed, among various other semiconductor fabrication technologies, by the Gallium Arsenide (GaAs) and Silicon Germanium (SiGe) heterojunction bipolar transistor (HBT) technologies [3], [4]. Meanwhile, in 1960, the first metal oxide semiconductor field effect transistor (MOSFET) was built, eventually paving the way for current complementary-MOS (CMOS) processes [5], [6]. The impact of these semiconductor technologies and the ability to design solid-state electronic circuitry on them has been multiplied manifold by advancements in other areas of science. Improvements in the processing of materials, optical lithography and the invention of methods such as ultra-high vacuum chemical vapor deposition (UHV/CVD) and molecular beam epitaxy (MBE) have been prime movers. The tremendous complexity involved in translating the precepts of information theory into physical circuitry that may enact the exchange of information, has called for relentless growth in solid-state electronics manufacturing and design. In effect, this

has meant that the circuits that populate an electronic communication device, more so a wireless device, have been subject to the severe and steadily tightening constraints of frugal energy consumption, compaction and economy of manufacture. Rapid scaling of supply voltage and lithographic dimensions in contemporary CMOS technologies [7] among others, has ensured low power dissipation, and high density of componentry, thereby allowing small form factor and low cost devices.

1.2 The Mobile Radio Space and Coexistence

Information is conveyed by a wireless radio through modulation of some characteristic of a radiated EM wave. This began with amplitude modulation (AM) and frequency modulation (FM), and was used to communicated audio. The modulating signal that defines information is superposed by the modulation scheme onto a high-frequency carrier wave. Thus, the communicating device is said to operate at radio frequency (RF). A mobile phone, which is the most common embodiment of such a device, often offers voice communication, short message service (SMS) for text and email, and multimedia messaging service (MMS) for communication of images and video. The mobile phone itself connects wirelessly to a base station that ultimately links to a public switched telephone network (PSTN). The first generation cellular systems used frequency division multiple access (FDMA) and were based on analog FM. In 1979, the first such system - the Nippon Telephone and Telegraph (NTT) was established. This was followed by other mobile telephone systems around the world, such as the Advance Mobile Phone Service (AMPS). In the last two decades of the 20^{th} century, the cellular subscriber numbers had been growing 20% to 50% per year. In 1992, 50% of the total telephone traffic was expected to be cellular by the year 2000 [8].

The second generation (2G) of cellular systems used digital techniques. The advantages of a digital cellular system over the earlier analog systems include but

are not limited to – lower RF transmit power, encryption to provide security of transfer, mobile assisted handoffs, and data services in addition to voice [9]. Most of these employ time division multiple-access (TDMA) or code-division multiple-access (CDMA) methods. However, all wireless communication devices rely on a finite amount of the available electromagnetic spectrum. In the USA, for instance, the Federal Communications Commission (FCC) governs the usage of the spectrum by imposing band regulations. A constant challenge has thus been to achieve data exchange at high speeds over a limited frequency band while maintaining a lower bound on signal quality. This calls for constantly increasing spectral efficiency in the wireless communication method. A variety of wireless air interface standards have consequently been developed to accomplish mobile communication and they use different digital modulation schemes. As mentioned earlier, the multiple-access technique that allows a large number of mobile units to link to a base station also vary. CDMA, for example, uses a spectrum spreading method where the bandwidth that is used to transmit the signal is far greater than the required message bandwidth. It is thus less spectrally efficient than some other methods but provides other benefits in a densely populated cellular environment.

Examples of second generation cellular systems are the Group Special Mobile (GSM) and Digital Cellular System 1800 (DCS1800) first established in Europe, and the IS-54 and IS-95 established in North America. GSM uses TDMA with a Gaussian minimum shift keying (GMSK) modulation technique and operates in the 900 MHz band. DCS1800 operates in the 1710-1785 MHz and 1805-1880 MHz bands. IS-54 uses a TDMA access method and IS-95 employs a direct sequence CDMA (DS/CDMA) technique.

The adoption of mobile wireless devices such as cell phones by the market has been phenomenal and is rapidly increasing. Mobile phones are already the leading communication device in many nations and have started replacing land telephone lines

extensively. In fact, 85% of all telephone subscribers in Africa are presently mobile phone subscribes alone [10]. Figure 1 illustrates the growth of cellular subscribers in the US and worldwide, both by total number and by the fraction per thousand people, based on estimates and forecasts.

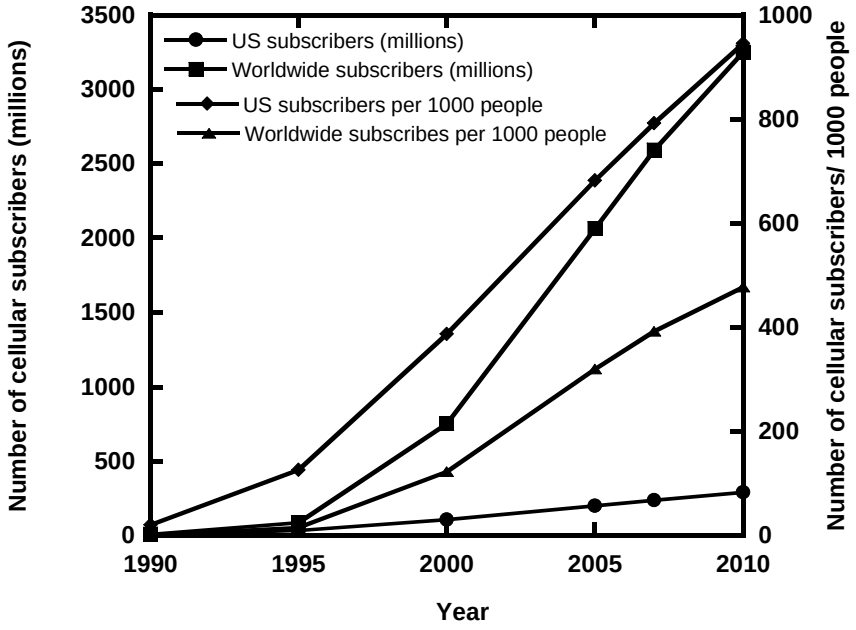

Figure 1: Trend of the number of cellular subscribers in the USA and worldwide.

A change in the course of cellular wireless communication is currently in progress with the replacement of many 2G networks with the third generation (3G) of cellular systems. Many countries have already deployed 3G networks and the next few years are likely to see the complete transformation of mobile phones to the third generation. This is significant because a 3G network is fundamentally different from legacy networks in that it offers competently performing services other than voice communication. Apart from supporting a greater number of voice customers, it also caters to broadband data transfer, typically at 384 kb/s for mobile devices, which is further expandable to 2 Mb/s. This allows functions such as music downloading and video

telephony. Universal Mobile Telecommunications System (UMTS) is a mobile system that has been developed to offer the varied services that a 3G network demands and the transition from 2G to 3G is taking different paths in different regions of the world. In Europe, General Packet Radio Service (GPRS) is being added to the existing GSM network and in North America, Enhanced Data Rates for GSM Evolution (EDGE) forms part of the intermediate generation. A 3G handset operating under the UMTS typically aims to have a music player, camera, video player, web browser and smartcard integrated into it apart from the voice function and most commonly uses a wideband-CDMA (WCDMA) air interface standard.

Advanced smart cellular phones of the present are including non-cellular technologies such as navigation and broadcasting, and are envisioned to co-integrate systems like Digital European Cordless Telephone (DECT), Bluetooth (BT), Zigbee, Remote Keyless Entry (RKE), Global Positioning System (GPS), and RF ID to extend wireless connectivity and service. In fact, the Information Society Technologies (IST) program defined the key steps in the evolution of a 3G network to a future fourth generation (4G) system and noted among other issues [11]:

1. Seamless integration of different wireless systems via network interworking and radio reconfigurable technologies;

2. Guaranteed quality of service levels as required by future applications;

3. Assessment of potential spectrum requirements and coexistence issues.

The expanded flow of media content to the consumer has begun to switch from a one-way donwlink feature to a two-way connection of content and feedback. The accessibility and affordability of broadband services, in conjunction with mobile operator strategies, has penetrated the market in such a way that the user is able to control the timing, format and content of the media itself [12]. Since the advent of digital TV, television broadcast has been making inroads into the mobile market. Numerous

broadcast TV technologies such as Digital Video Broadcasting – Handheld (DVB-H), MediaFLO, Integrated Services Digital Broadcasting – Terrestrial (ISDB-T), and others are being adopted for use with mobile units. Revenues from subscription are expected to reach $13 billion by 2012 with a compound annual growth rate of 83% [13]. Other applications such as mobile gaming are predicted to become more influential in the sales of cellular telephone units. Although not yet pervasive as a means of revenue in cell phone units, mobile gaming consoles have seen their revenues triple from 2004 to 2005. In a parallel development, the pocket personal computer (PC) and personal digital assistant (PDA) have been merging their functions with the cellular phone. In addition to Bluetooth, 2.4 GHz Wireless Local Area Network (WLAN) service is being included for data downstream. Such trends are increasingly enabling applications like video-conferencing and online banking to become available from mobile units, while placing greater demands upon computational power and security measures. Some 3G mobile phones have implemented location service and tracking through GPS beginning in Japan before 2003, and these are expected to become a staple of the cell phone consumer's diet before long.

Speaking from an electronic hardware implementation perspective, by 2003 the total electronic component count in the RF front-end circuitry of a mobile phone had decreased from 500 or 600 units down to 60 and was predicted to reach 40 very soon [14]. Supply voltages for these electronic chips have also been steadily scaling down. The front-end antenna switch is dominated by RF modules, typically including a receive surface acoustic wave (SAW) filter. Further, complete transceivers, filters, power amplifiers, duplexers, and switches are being integrated or are targeted for integration into one single chip-on-board. Where as earlier GSM based radio ICs may have had quad-band functionality, future 3G and higher implementations are likely to provide a more expanded multi-band and multi-mode operation. For example, multi-band operation suggests a radio capable of quad-band 2G cellular, tri-band

3G cellular, and dual-band WLAN in one unit. Multi-mode functionality includes GSM, UMTS, BT, WLAN, GPS, and FM-radio. Such severe requirements are in contemplation only because of the rapid strides the solid-state electronics industry has made towards small form-factor, low-cost and low power semiconductor technology solutions. However, though the confluence of information theory, materials processing and electronic hardware design has enabled an ambitious future plan for wireless communication devices, it is not without its threats.

Signal integrity in radio-frequency (RF) wireless transceivers is a challenging aspect of wireless communications to analyze and design for, as the threats to it are many and varied. In particular, the coexistence of different radio devices in the same region of the frequency spectrum, serving different purposes, compromises signal integrity by mutual interference. The sensitivity requirement of modern radio receivers governs their ability to resolve the desired signal amidst surrounding noise, and is often limited by the state-of-the-art. For efficient and reliable radio operation, containment of noise and a favorable signal to noise ratio (SNR) are essential. Providing users with a wide range of services across different radio technologies and varying bandwidths with near-ubiquitous coverage and mobility through a single terminal is extremely challenging considering the need to maintain the minimum quality of service (QoS). Such a requirement demands interoperable networks. Figure 2 shows an example of an advanced wireless communication system with interoperating wireless networks organized in a layered structure [15].

In this context, various studies in the literature have found mutual interference concerns between the several wireless functions available simultaneously in a crowded environment. Video transmission over WLAN is becoming important for reasons of convenience in the home, mobility in general and corporate information distribution in the enterprise market.This, requiring the transmission and reception of very large amounts of data and being subject to the constraints imposed by time-boundedness,

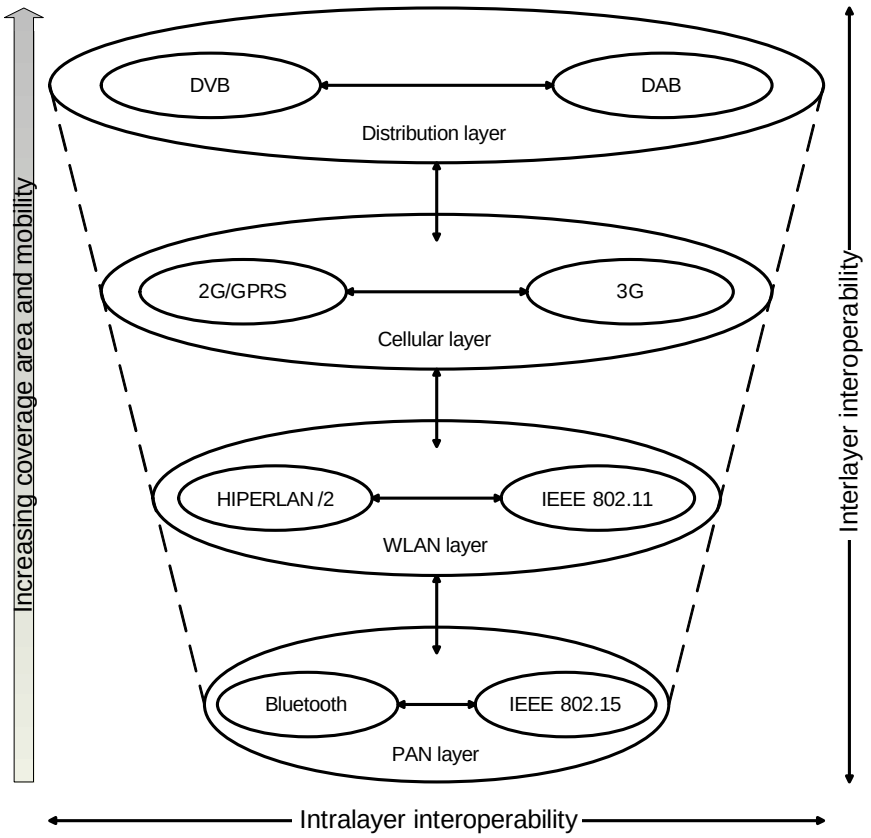

Figure 2: Advanced wireless communication network with a layered structure for interoperation.

is a very challenging application and particularly vulnerable to performance degradation by interference. A series of benchmark tests have revealed that video reception performance over WLAN suffered anywhere between 20% to 64% packet loss when operating in the vicinity of key radio interferers [16]. The interfering devices consisted of another WLAN radio, DECT phone, video camera, and Bluetooth headset among others. Another case of inteference susceptibility is with signals in certain restricted RF bands, such as GPS. The FCC approval for the use of ultra-wide band (UWB) devices in commerical and federal bands has accentuated this concern. UWB signals offer the potential to communicate data at a few hunderd Mb/s rates over short ranges (a few meters) using low radiated power (a few hundred microwatt). One of the unique features of UWB techniques is the ability of a large number of UWB devices

to coexist and operate in a very small area without mutually interfering. However, the impact of a large number of UWB devices operating together in the vicinity of a GPS device has been found to be undesirable. When a software-based GPS receiver was simulated for signal acquisition, it was found to average a 99% success rate in the absence of UWB signals. In the presence of 100 UWB signal sources located about 6 feet from the GPS receiver, transmitting Gaussian monopulse sequences of pulse width 250 ps, the receiver acquistion success rate was found to drop to a worst-case 82% [17].

Recent years have seen concerns raised over two very popular wireless radio technologies – WLAN and wireless personal area network (WPAN), both operating in the unlicensed 2.4 GHz industrial, scientific and medical (ISM) band. From the perspective of interoperation of radios adhering to different wireless standards, mutual interference/ noise needs to be suppressed. This work contributes to the solution of the coexistence problem of interfering radios by developing interference mitigation schemes and implementation procedures, while preserving the desired signal. The sources of interference in multi-radio systems are investigated and noise that may be suppressed is identified and delineated. From the viewpoint of design, though higher layer solutions may be possible such as in the media access control (MAC) layer, this work proposes a unique physical layer (PHY) based method that can be geared towards various radio standards. Among PHY layer schemes, there are some existing methods that function in the baseband frequencies of the radio chain. These are difficult to implement in hardware owing to circuit design complexity and their potential for power-hungry operation, not to mention the excess broadband noise generated and elaborate adaptation mechanisms required. The proposed scheme helps cancel correlated in-band noise originating from an interfering radio and develops the theory of noise cancellation in a radio system with closely spaced interfering devices. The dissertation also encompasses an implementation of the concept in a

contemporary Si-CMOS IC technology featuring novel circuit designs customized for the stated purpose. It is essential in mobile radio applications that the constituent circuits function in a low power mode so as to maximize battery life and mobility, apart from generating as little white noise as possible so that integrity of desired signals is not compromised. Special attention is paid to these two aspects in the circuit designs developed.

A key consideration in the design of such a cancellation scheme is the adaptability of the solution to varying ambient conditions. Therefore, this work also investigates the various issues involved in constructing a control mechanism that governs the adaptation of the interference suppression circuitry. The control loop so developed is of low complexity and can be extended to other applications easily. Although the WLAN – WPAN interference problem is treated as the primary example, implementations are outlined for other coexistence situations also. The generality and versatility of the developed method allow it to be applied to other cases of interoperation in the ISM bands.

1.3 Organization of the Dissertation

The previous sections shed light on the motivation and purpose of the dissertation. The state of the mobile radio application space was briefly discussed and the demands placed upon the constituent electronic ICs were outlined. Attention was drawn to the interoperability criteria of multiple wireless networks with examples cited from the literature. The major coexistence problems dealt with in this work were introduced.

Chapter 2 explores the origin of a problem of interest – coexistence of the WLAN and WPAN networks. A brief description of the IEEE 802.11b/g standard for WLAN devices and the IEEE 802.15 standard for Bluetooth devices is provided with the object of understanding the relevant fundamentals of their operation. The

problem is then mathematically formulated by examining some of the theory surrounding interference in this case. Computational and simulation based evidence is presented for the existence of interference between simultaneously operating WLAN and Bluetooth devices, especially when they are situated in proximity of each other. Such results are also indicated for other interference cases, such as the protection of a GPS device from unwanted radiators. As mentioned before, a wireless radio device may suffer incursions from a variety of sources, such as other high powered transmitting devices in the same room. However, the interference it suffers from a transmitter in its immediate vicinity, for instance one located on the same mobile unit, is of greater interest within the scope of this thesis. With regard to this, the WLAN – BT problem is characterized by a measurement of undesired signal leakage in a representative experimental setup.

Chapter 3 details a method for effecting interference suppression. The theory of adaptive noise cancellation is comprehensively analyzed and a suitable application of the principle to the interference problem is derived. Specific attention is paid to the additive noise generated by the scheme. A modified noise mitigation system is developed for the problem of interest and its ability to effect noise suppression justified while outlining some alternative approaches.

In Chapter 4, a prototype interference cancellation system is described and constructed with off-the-shelf electronic circuit components to portray its operation. This includes a 'core' that generates a cancellation signal and must be controlled externally by an adaptive algorithm. Subsequently, an implementation of the interference canceller in a contemporary 0.18-μm Si-CMOS IC technology is presented. Circuits are developed to perform the requisite functions in the core of the canceller. Several important considerations governing the design of these circuits are analyzed. The designs fabricated primarily address the WLAN – BT problem. A version of these ICs is developed to address GPS protection also and is outlined briefly. In an

alternative approach to one of the central components of the canceller, a third design is proposed and compared with the preceding version. Measured results depicting the performance of the different components of the canceller as well as the whole unit are provided.

Chapter 5 introduces key control mechanisms that may be used to adapt the core of the canceller. The design of an adaptive control unit is very briefly illustrated as the details are largely outside the scope of this dissertation. Aspects of a suitable adaptive algorithm are investigated towards this end and issues pertaining to its operation are outlined.

Chapter 6 enumerates the contributions of this dissertation and speculates about research that may be borne out of this work in the future.

CHAPTER II

ORIGIN AND CHARACTERIZATION OF THE INTERFERENCE PROBLEM

Recent years have seen a steady growth in the assimilation of wireless networking devices into the corporate and personal environment. The increased utilization of the ISM bands is no coincidence since most of these devices rely on the unlicensed portion of the spectrum. While sharing of the spectrum and unlicensed access benefits the end-user, thereby facilitating increased services; it raises questions about network performance in a densely populated frequency space. Lately, these questions have received recognition, and mechanisms that deter interoperability are better understood.

One example of such a concern is in the 2.4 GHz ISM band. The existence of a wide range of commercial products based on WLAN and WPAN calls our attention to their coexistence concerns. Short-range remote signaling devices using the Bluetooth standard [18] and longer range wireless data devices adhering to the IEEE 802.11b/g standard [19] are numerous and present an example of this problem. Their functions are complementary in nature and they both use spread-spectrum communication techniques, yet their deployment in close proximity can and often does result in mutual performance degradation. The study of this problem and its solution forms the core of this work.

2.1 The Bluetooth – WLAN Interference Scenario

Fundamental issues surrounding the interoperability of different networks have been addressed in recent literature. The Bluetooth environment, for instance, is analyzed and simulated with models of the MAC and PHY layer to predict a performance loss

in [20]. The impairment of IEEE 802.11 devices in the presence of Bluetooth interference is partly quantified in [21]. Bluetooth systems conforming to the specifications of IEEE 802.15 and WLAN systems utilizing IEEE 802.11b/g standards, both, operate in the 2.4 GHz ISM band. While the former relies on a frequency-hopping spread-spectrum (FHSS) scheme, the latter may use either an FHSS or a direct-sequence spread-spectrum (DSSS) technique. Often, when operating under closely spaced conditions, the transmitted signals from these devices may collide in both time and frequency causing a reduction in the signal-to-interference ratio (SIR) at the receiver of either system. Early findings [22] indicate that performance degradation of both systems in terms of throughput is severe when the interferers are physically located within 2 m of each other, insignificant beyond 10 m, and moderate for intermediate ranges. Naturally, this is undesirable and methods to understand and mitigate such interference have become necessary.

Various methods have been suggested to combat the coexistence problem in the 2.4 GHz band, as outlined in [23]. Interference is not strictly a physical layer phenomenon; it can impact the performance of MAC and upper layers, much as MAC protocol can affect the interference scenario. The schemes in the literature range from complex TDMA schemes that involve load dependent queuing and scheduling algorithms to other MAC or driver layer solutions. However, most software layer approaches disallow simultaneous operation or otherwise compromise the performance capabilities of one of the transmitting systems. Since interference is a physical phenomenon associated with the wireless RF channel, and is characterized and measured in the PHY layer, a solution constituted in the PHY addresses the problem nearest the source while allowing simultaneous operation. The methods proposed in this work are entirely PHY layer driven and do not impair the inherent abilities of either system.

2.1.1 Operational Specifications

Bluetooth as defined by the IEEE 802.15.1 standard governs the operation of a WPAN device. A WPAN device is intended for very short-range communications – usually up to 10 m and is suited to a battery operated, small, lightweight unit. A Bluetooth network supports both synchronous communication channels for voice and asynchronous communication channels for data. The protocol architecture of Bluetooth is shown in Figure 3.

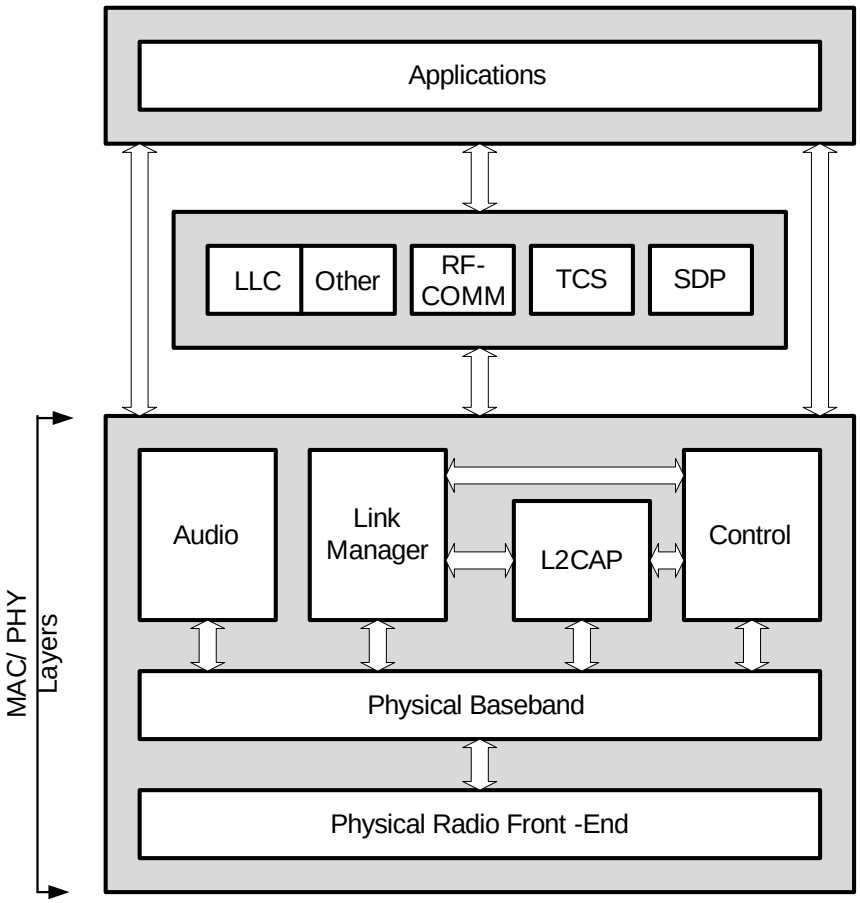

Figure 3: Schematic of the Bluetooth Protocol Architecture

Here, L2CAP refers to logical link control and adaptation protocol, RFCOMM represents a serial port emulator for legacy applications, TCS is telephony control

and signaling, and SDP refers to a service discovery protocol layer that allows inter-device services inquiry. The IEEE 802.15.1 standard only addresses the MAC and PHY layer functions as denoted in the diagram. Further details of the MAC and higher layers are outside the scope of this work.

In the baseband regime of the PHY layer, Bluetooth uses a Gaussian frequency-shift keying (GFSK) continuous phase modulation scheme with a modulation index of 0.3 and a bandwidth bit-period product of 0.5 to transfer information to the carrier signal. This modulation method is preferred owing to relatively low complexity, cost and increased power efficiency as compared to quadrature amplitude modulation (QAM) techniques. A symbol rate of 1 MS/s and channel spacing of 1 MHz over any of 79 RF channels in the 2.4-2.4835 GHz band makes it effectively narrow-band for the purposes of the interference problem. A fast pseudo-random frequency hopping sequence with a maximum rate of 1600 hops/s defines the channel so as to combat co-channel interference and the effects of fading [24]. Consequently, the time-slotted channel that is used has a slot duration of $1/1600 = 625$ μs. The transmitter Gaussian filter spreads each data bit over two symbol durations, causing inter-symbol interference (ISI).

The device function is categorized into three power classes according to the range of transmit powers utilized. This is listed in Table 1. Power control is exercised where required in monotonic steps of output power level between the specified minimum and

Table 1: Power Classes for Bluetooth Devices

Power Class	**Transmit Power Minimum**	**Transmit Power Maximum**	**Power Control**
Class 1	0 dBm	20 dBm	2 dB – 8 dB steps
Class 2	-6 dBm	4 dBm	Optional
Class 3	None	0 dBm	Optional

maximum for that class depending on signal strength feedback from the receiving device.

WLAN devices conforming to the IEEE 802.11 standard are intended for data communications over relatively longer ranges as compared to Bluetooth – up to 100 m, and at higher data rates. Several PHY layer standards have been proposed for use in different frequency bands and to provide a range of data rates. These include 802.11b, 802.11g, and 802.11a among others. A generic protocol configuration of an 802.11 network is shown in Figure 4.

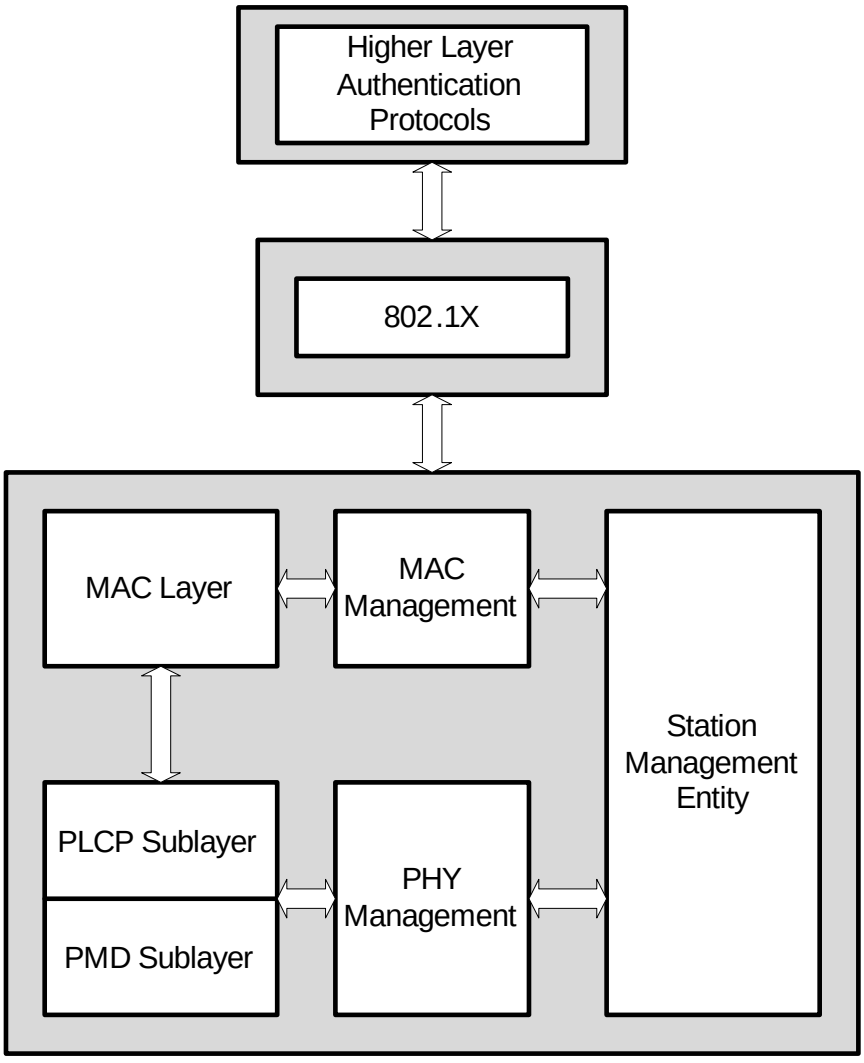

Figure 4: Schematic of the IEEE 802.11 WLAN Protocol Architecture

The data link layer is formed of the IEEE 802.1X and MAC sublayer. PLCP and PMD refer to the physical layer convergence protocol and physical medium-dependent sublayers of the PHY.

The IEEE 802.11 standard specifies several PHY solutions to support different data rates. These employ different modulation schemes and protocol data units. They may use differential binary phase-shift keying (DBPSK), differential quaternary phase-shift keying (DQPSK) or complementary code keying (CCK). In the case of 802.11b, four modulation formats are defined: 1) DBPSK for 1 Mb/s, 2) DQPSK for 2 Mb/s, and 3) CCK for either 5.5 Mb/s or 11 Mb/s transmission [25]. A DSSS method is normally used and the modulated data is spread by an 11-bit Barker sequence entailing a 22 MHz channel bandwidth. The transmission channel may be one of three non-overlapping channels occupying the same 2.4 GHz band as Bluetooth. Whereas 802.11b is a spread spectrum system, the 802.11g standard that was developed later to enable enhanced data rates while transmitting in the same frequency band, is not. A compromise between DSSS and orthogonal frequency division multiplexing (OFDM) is struck and a mandatory PHY employing OFDM is used, with two optional mechanisms. The latter two are DSSS-OFDM and packet binary convolutional coding (PBCC). An extended data rate of up to 54 Mb/s is available under 802.11g.

For the WLAN devices described here, maximum transmit power is specified at 30 dBm in North America and 20 dBm in Europe. Despite a higher ceiling of 30 dBm, many implementations choose to restrict operation to a 20 dBm maximum.

2.1.2 Network Performance Degradation

The theory surrounding the performance criteria of an IEEE 802.11 network in the presence of Bluetooth interferers is vast, and a few key results quantifying this effect are reproduced here. Packet error rate (PER) and number of retransmissions (RT) are taken as performance parameters, and the probability of a collision is denoted

as p(C). A collision is said to occur when an IEEE 802.11b packet is unrecoverable because of a Bluetooth interferer. Whereas WLAN can deter Bluetooth operation by interference, affecting 22 out of the 79 RF channels and decreasing throughput, the reverse interference scenario is found to be more disturbing. In this case, the WLAN device occupies a 22 MHz wide band within the 2.4 GHz ISM band and the Bluetooth device hops over 79 frequencies within the same ISM band. If the Bluetooth device hops on to a frequency in use by the WLAN device, a collision occurs. Thus out of the 79 channels, at any given time 22 are subject to hindrance.

The packet error rate is itself defined as:

$$PER = 1 - (1 - BER)^M \tag{1}$$

where, BER is the bit error rate and M is the number of bits per packet. The WLAN network typically has a variable data rate provision. If the PER is found to be beyond the acceptable threshold, the data rate is lowered. However, lowering the data rate makes the packet longer thereby allowing it to experience interference for a longer period of time. This process, when repeated a number of times leads to instability. If N WLAN packets are transmitted, packet collisions with Bluetooth are independent and identically distributed (i.i.d.), and γ_{PER} represents a PER threshold,

$$p\left(PER \leq \gamma_{PER}\right) = \sum_{n=0}^{k} {}^{N}C_n p\left(C\right)^n \left[1 - p\left(C\right)\right]^{N-n} \tag{2}$$

where, k is one of $[0, 1, ..., N]$, and $p(.)$ denotes probability. Using the standard error function when N is very large, we may approximate the binomial distribution as

$$p\left(PER > \gamma_{PER}\right) = \frac{1}{2}\left\{1 - erf\left[\frac{N\left[\gamma_{PER} - p\left(C\right)\right]}{\sqrt{2\gamma_{PER}Np\left(C\right)\left[1 - p\left(C\right)\right]}}\right]\right\} \tag{3}$$

where, $erf(.)$ is the standard error function. Based on this, graphs of equal probability for $p(PER > \gamma_{PER})$ are shown in Figure 5 [26].

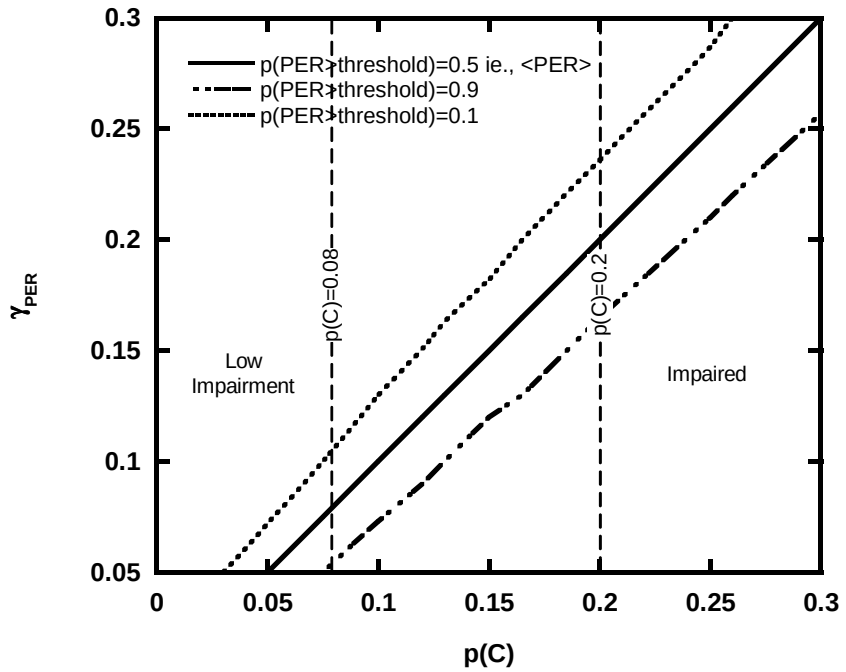

Figure 5: Graph of Equal Packet Error Rate Probability for a WLAN Network

An expected PER or $\langle PER \rangle$ less than 8% is required by IEEE 802.11b. Therefore, the probability that the network is free of impairment may be calculated by setting the PER threshold at 0.08 in (2) or (3) above. The threshold condition for which the WLAN network is said to be significantly impaired is somewhat arbitrary and has been previously assumed to be 0.2 (20% $\langle PER \rangle$).

As noted before, a number of retransmissions may be required to successfully transmit an IEEE 802.11b packet from the access point to the station. Again, if the collisions are assumed i.i.d., and if γ_{RT} is a threshold for RT, the probability that this is not exceeded is calculated as the geometric distribution [27]

$$\begin{aligned} p\left(RT < \gamma_{RT}\right) &= \sum_{n=0}^{\gamma_{RT}} p\left(C\right)^{n} \left[1 - p\left(C\right)\right] \\ &= 1 - p\left(C\right)^{\gamma_{RT}} \end{aligned} \tag{4}$$

The mean $\langle RT \rangle$, and standard deviation σ_{RT} of the number of retransmissions are

easily calculated as

$$\begin{aligned} \langle RT \rangle &= p(C) / [1 - p(C)] \\ \sigma_{RT} &= \sqrt{p(C)} / [1 - p(C)] \end{aligned} \tag{5}$$

The total expected transmission latency of the system can be calculated using the normal transmission latency in the absence of packet collisions, the probability of collision and retransmission, and the latency overhead imposed in case of collision followed by a number of retransmissions.

In evaluating the coexistence scenario, a WLAN station and access point separated by distance d_S are considered with uniformly distributed Bluetooth piconets surrounding the station. The piconet is the basic network unit in a Bluetooth environment. It is a WPAN constituted of one Bluetooth device serving as "master" and a number of other devices serving as "slaves". The slaves may remain either active, or inactive but synchronized with the master. Each piconet has only one master device and all devices in that piconet are aligned with one frequency-hopping channel based on the master's clock. Usually, a practical scenario in WPAN communications will consist of many overlapping piconets forming a scatternet. If γ_{IS} is the interference to signal power ratio threshold beyond which the WLAN signal is jammed, and P_{WL}, P_{BT} are the IEEE 802.11 and Bluetooth transmit powers, then

$$\Gamma = \gamma_{IS} P_{WL} / P_{BT} \tag{6}$$

is the normalized interference to signal threshold. If the aggressor Bluetooth piconets are confined within a radius R of the WLAN station and are uniformly distributed with an areal density of ρ_{BT}, then the expected number of Bluetooth aggressor piconets is

$$N_{BT} = \rho_{BT} A(\Gamma, d_S) \tag{7}$$

where $A(\Gamma, d_S)$ is the effective interference area around the WLAN station within the radius R where the interference signal from the Bluetooth piconets is successfully

encroaching upon the desired WLAN signal. This means that the interference to signal power ratio is greater than the allowed threshold. The interference area is found to depend on the radio propagation characteristics of the physical RF channel.

Further, the area $A(\Gamma, d_S)$ around the station, where interference occurs is determined by methods similar to Jakes multipath fading calculations [28], as follows:

$$A(\gamma_{IS}, d_S) = \int_0^{2\pi} \int_0^R p\left(\frac{P_{BT}[r]}{P_{WL}[d_S]}\right) > \gamma_{IS} r dr d\theta \tag{8}$$

where the expression inside the double-integral represents the probability that the interfering Bluetooth power at radius r exceeds the desired signal power by a factor equal to the interference to signal power ratio threshold. Using log-normal shadowing models, the interference and signal powers can be expressed as

$$\begin{aligned} P_{BT}[r]_{dBm} &= P_{BT,dBm} - \left[P_L(d_0) + 10nlog_{10}\left(\frac{r}{d_0}\right) + X_{BT}\right] \\ P_{WL}[d_S]_{dBm} &= P_{WL,dBm} - \left[P_L(d_0) + 10nlog_{10}\left(\frac{d_S}{d_0}\right) + X_{WL}\right] \end{aligned} \tag{9}$$

where $P_L(d_0)$ is the path loss at an arbitrary distance d_0, n is the path loss exponent, and X_{BT} and X_{WL} are zero-mean log-normally distributed random variables with shadow standard deviations σ_{BT} and σ_{WL}, respectively. If σ_{IS} is the standard deviation of a log-normally distributed random variable representing the interference to signal ratio, some mathematical deliberation is necessary to show that

$$A(\Gamma, d_S) = \pi d_S^2 exp\left\{\frac{2\left[\sigma_{IS}^2 - 10n\Gamma log_{10}(e)\right]}{\left[10nlog_{10}(e)\right]^2}\right\} \tag{10}$$

in the limiting case where R is very large.

Therefore, given typical values of various parameters, interference areas can be found. For instance, P_{BT} = 0 dBm, P_{WL} = 20 dBm, d_S = 20 m, an acceptable interference to signal ratio threshold γ_{IS} = -10 dB [29], office building conditions of $2 < n < 4$, and $5 < \sigma_{IS} < 11$ dB [30] yields $A(\Gamma, d_S) \approx 1m^2$ [26].

Next, the chance of Bluetooth and WLAN packets coinciding in time needs to be evaluated. A simple timing diagram for packet transmission in Bluetooth and WLAN networks is shown in Figure 6. ΔT_{BT} and ΔT_{WL} are the time slot durations of Bluetooth and WLAN ($\Delta T_{BT} = 625\ \mu$s), t_{BT} is the transmission time for Bluetooth, and ΔT_{OFF} is the offset between the two transmissions.

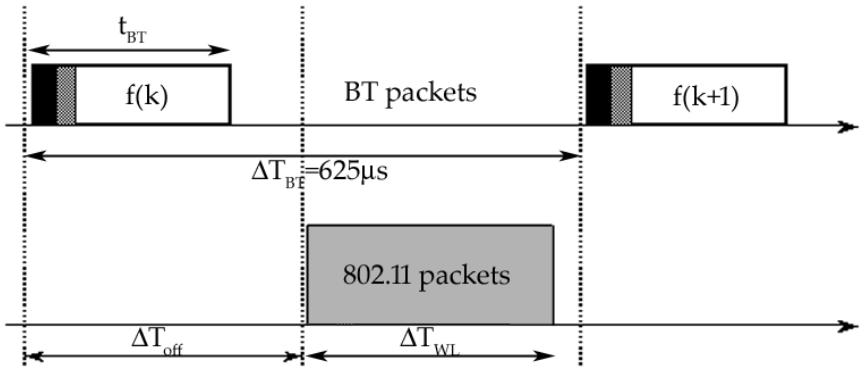

Figure 6: Bluetooth and WLAN Packet Transmission Timing Diagram

If the Bluetooth piconet uses single time slot packets only, the number of Bluetooth packet transmissions overlapping in time with WLAN packets is either n_{ov} or $n_{ov} - 1$, where

$$n_{ov} = \left\lceil \frac{\Delta T_{WL} + t_{BT}}{\Delta T_{BT}} \right\rceil \tag{11}$$

and $\lceil . \rceil$ is the ceiling function. Furthermore, it can be shown that the corresponding probabilities of time-coincidence are

$$\begin{aligned} p(n_{ov} - 1) &= 1 - p(n_{ov}) \\ p(n_{ov}) &= \frac{t_{BT} + \Delta T_{WL} - (n-1)\Delta T_{BT}}{\Delta T_{BT}} \end{aligned} \tag{12}$$

The probability that the signals from the two services are frequency coincident may also be calculated. Using the effects of a continuous-wave (CW) tone on a DSSS signal [31] as a starting point, this probability may be derived. The analysis is complex and not presented here.

Finally, if the probability of activity in a single Bluetooth piconet $p(A)$, is assumed to be i.i.d. for all piconets, and N is the expected number of Bluetooth interferers with an interference level Γ, then the total probability of time-frequency collisions is derived as

$$\begin{aligned} p\left(C\right) &= \sum_{n=0}^{N} {}^{N}C_{n} p\left(A\right)^{n} \left[1 - p\left(A\right)\right]^{N-n} p\left(C_{n}\right) \\ p\left(C_{n}\right) &= \sum_{k=1}^{L} \left\{1 - \left[1 - p\left(C_{1}|\Gamma_{k}\right)\right]^{n}\right\} p\left(\Gamma_{k}\right) \end{aligned} \tag{13}$$

where L is a loading factor for the Bluetooth piconets.

From the foregoing analysis, we may infer that for typical values of parameters noted before, and path loss exponent (n) of 4, the probability of collision is greater than 10% for networks with light Bluetooth traffic and greater than 40% for networks with heavy Bluetooth traffic. Simulations modeling the system under different conditions have revealed significant levels of network performance degradation [32]. For a WLAN data rate of 2 Mb/s, the WLAN system throughput was found to degrade by 25% in a light Bluetooth usage scenario and by 66% in a heavy Bluetooth usage scenario. For a data rate of 11 Mb/s, the corresponding figures were 23% and 66%. In effect, the preceding results indicate that interference is a pressing concern.

The resulting channel overlap is addressed by many methods including MAC layer mechanisms. Some of these are documented in [33]. The schemes are mainly divided into collaborative and noncollaborative mechanisms. In the former method, WLAN and WPAN exchange information over a separate mutual link to minimize conflicts. In the latter method, exchange of information between the two networks is not required. Three collaborative mechanisms are specified here:

1. The two networks have a separate link and their transmissions can be scheduled in non-overlapping time segments.

2. Both networks can decide what type of packet to transmit to minimize interference.

3. The WLAN performs deterministic interference suppression using a programmable notch filter to eliminate the narrowband Bluetooth interferer.

None of these methods allow constraint-free simultaneous operation and in some cases both networks need to act to protect either from unwanted signal. The third method may appear to be free of these requirements, but it should be noted that the WLAN receiver must have an integrated Bluetooth unit in it for this scheme to work. This is necessary so as to provide knowledge of the hopping sequence and timing of the aggressor as the notch filter needs to maintain synchronicity with it. The noncollaborative mechanisms specified are:

1. Adaptive packet scheduling.

2. Packet scheduling on the asynchronous connection-less (ACL) link.

3. Packet selection on the synchronous connection-oriented (SCO) link.

4. Adaptive frequency hopping.

5. Adaptive interference suppression on the WLAN using an adaptive notch filter to eliminate the narrowband Bluetooth interferer.

Again, in the first three methods, compromises are necessary in at least one of the networks to implement scheduling. Some methods will only work on an ACL or only on an SCO. The first scheme usually does not use forward error control (FEC) and thereby decreases protection against noise sources. All of the above, except the last

method require channel estimation or channel classification, which in turn require received signal strength indication (RSSI), BER or PER information. Where channel classification, marking channels as "good" or "bad" according to measured channel conditions is necessary, some bad channels may have to be placed on the hopping sequence if enough good channels are not available.

The last scheme enumerated above uses adaptive interference suppression and is the method of choice for this work. Though notch filters, owing to the extremely wide range of adaptability required, complexity of implementation, and power consumption, have been dispensed with in the remainder of this work, the fundamental premise finds its origin here.

Apart from the interference case treated here, there are other mutual performance degradation scenarios with other radio networks. For instance, in recent times, the GPS network has been recognized as vulnerable. The findings of a US governmental report [34] suggest that systems and procedures to monitor, report, and locate unintentional interference should be implemented or utilized in any application for which loss of GPS is not tolerable. GPS being designed as a low power system in a crowded spectrum, is susceptible to interference – particularly the signal and code structure available to civilian users. GPS radios located in mobile phones have been found to suffer performance degradation due to other higher powered transmitters such as GSM on the same phone, despite operating at different frequency. This occurs mainly due to out-of-band emissions by the aggressor. Such interference is also found to occur when high-speed data communicated through buses inside a mobile unit act as aggressors to the GPS radio by means of sideband spectral content. Corruption may also occur owing to clock related harmonics from microprocessors or charge pump circuits [35]. This is particularly prevalent with GPS as the receiver unit operates at extremely high sensitivity levels of -125 dBm to -155 dBm.

2.2 Coupling Between Collocated Antennas: Characterization

An understanding of the nature of interference in the context of this problem is necessary for achieving any success in suppressing it. We may loosely refer to the undesired energy in the receive antenna of the victim (WLAN) system as noise. Based on this definition, the noise may be separately treated as in-band and out-of-band noise. Since the transmission frequency band of 83.5 MHz width is identical for the two radios, the in-band noise pours energy into frequencies that either transmitter may use. Whereas out-of-band noise also degrades radio performance, it may be rejected by appropriately filtering at the transmit or receive end. This is possible owing to the fact that no desired information is contained in the spectrum outside of the band of interest. However, out-of-band noise is not entirely trivial for two reasons. First, though a transmit channel is precisely defined, it is physically impossible to limit radiation without spreading noise into sidebands depending on the transmit spectral mask. Sideband signals thus produced are a potential source of interference. Second, out-of-band noise at the boundary of a band is as important as noise in-band because of the non-rectangular nature of filters.

Since the goal of this work is separate from the derivation of closed form analytical solutions to the interference problem, a practical case needs be examined. Situations where multiple radio transceivers are located on the same platform in communication products are increasingly prevalent. In the special case that both radios are collocated and are required to operate simultaneously from the same device, the Bluetooth transmitters are well within the interference area of the WLAN receiver as described in the previous analytical treatment of the problem.

To demonstrate this, various paired patch antenna structures were fabricated on flame-resistant 4 (FR-4) material. These were characterized for operation in the 2.4 GHz band and able to transmit IEEE 802.11b/g and Bluetooth data [36]. The

antennae were separated on the board by distances ranging from $\lambda/2$ to $\lambda/10$, where λ is the wavelength of the carrier radiation. These correspond to distances less than 0.1 m at 2.4 GHz, implying that the likelihood of interference is very high and the severity enough to compromise the successful recovery of desired data. The characteristics of the electromagnetic radiation between the antennae were measured and the s-parameters are plotted in Figure 7.

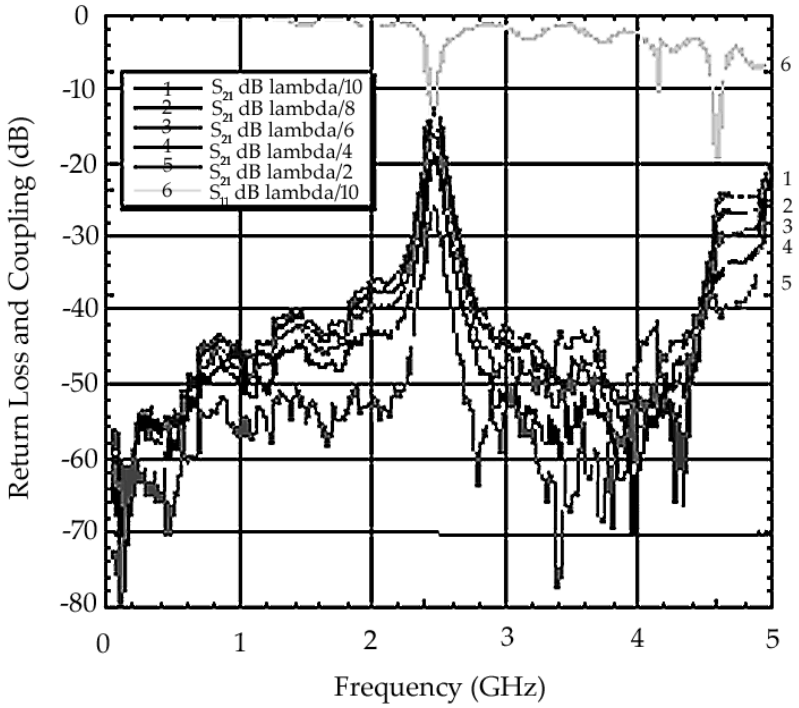

Figure 7: Coupling and Return Loss Characteristics Between Closely Spaced Antennas

The plot shows both the input reflection coefficient for one patch antenna and the coupling between the two antennae for different spacing conditions. As evidenced by the graph, the coupling (or relative interference level) varies from 13 dB to 27 dB. Maximum coupling occurs at the $\lambda/10$ spacing as expected. Such interference levels are formidable and reduce the signal to interference ratio (SIR) at the target receiver. A WLAN receiver has a recommended sensitivity of 75 dBm, and numbers between

85 and 95 dBm are typical. Considering that the transmit level from a Bluetooth radio can be as high as 0 dBm or even 20 dBm (with power control), signal levels at the receiver may be drowned in a sea of noise under these conditions. For receive systems with extreme sensitivity requirements such as GPS, a lower power radiator in its vicinity may act as an aggressor if transmitting in the same frequency band, or even by spectral fallout.

CHAPTER III

THE ADAPTIVE INTERFERENCE CANCELLER

3.1 System Description

The previous chapter outlined mechanisms for enabling coexistence of mutually interfering networks in general terms and indicated an existing method that is closest to the one developed here. The fundamentals of this mechanism are studied in the following sections. A qualitative description of the nature of interference encountered in the present problem, which is also sometimes referred to as noise, is necessary to understand the reason it may be suppressed. A mathematical treatment of the theory of adaptive noise cancellation lends structure to the solution as the two are closely related.

Out-of-band noise, being a minor cause for concern and peripheral to the current treatment of the interference problem, will be ignored. Also, this component of noise may be eliminated by the use of EM filters, although with limitations at the band-edge due to the differences between ideal and practical filters. The nature of a PHY layer solution, therefore, depends squarely on the behavior of in-band noise. Successful negotiation of in-band noise requires further categorization of noise as broadband (white) and band-limited (colored). Broadband noise in the time domain is a random process of statistically uncorrelated impulse energies. This implies non-deterministic behavior and no coordination with any identifiable source. Band-limited noise on the other hand, is deterministic in nature. It is statistically correlated in time to a particular source. Since the aggressor transmitter is the source, and the coupling channel is the means of time-correlation, this deterministic noise is clearly the offshoot of an intentional signal radiation. Also, the noise in-band may be modeled as the

superposition of a broadband and a band-limited component.

Traditionally, most high frequency radio systems are plagued only by broadband noise. As such, their circuit implementations are designed to alleviate white noise only. To minimize confusion, the band-limited component of in-band noise will henceforth be referred to as the interferer. The interference cancellation scheme suggested in this work allows us to suppress the above-mentioned interferer while maintaining adequate broadband noise performance.

The method employed relies on subtracting an internally generated interferer from the signal received at the victim antenna. When the subtraction and intermediate filtration is done adaptively, superior signal-to-noise ratio (SNR) may be obtained compared to direct filtration of the received signal. As such, it is a dual-input, closed-loop adaptive noise suppression scheme.

3.2 The Theory of Adaptive Noise Suppression

3.2.1 Generalized Adaptive Noise Cancellation System

Noise corrupting a desired signal, be it stochastic broadband noise or deterministic in-band noise, may be removed by passing it through a filter. The characteristics of the filter may be fixed if *a priori* knowledge of the signal and noise exists, or adaptable if no *a priori* information is known. This is accomplished using the theory of optimal filtering [37], [38]. The general method of adaptive noise suppression (ANS) makes use of an auxiliary input derived from the field of corrupting noise by means of a sensor. This is then filtered and subtracted from the primary input containing both the desired signal and noise. An adaptable filter is required for this system to work. If performed improperly, the primary signal may suffer an increase in noise. Therefore, adaptation of the filter is critical to its success.

As a starting point to the analysis of a generalized ANS system, the single-input, single-output Wiener filter is considered as depicted in Figure 8. The input signal

is x_j, output signal is y_j, and the desired response is d_j. All signals considered are in discrete-time and statistically stationary. The filter is itself linear, discrete and optimal according to the minimum mean-square error (MMSE) algorithm.

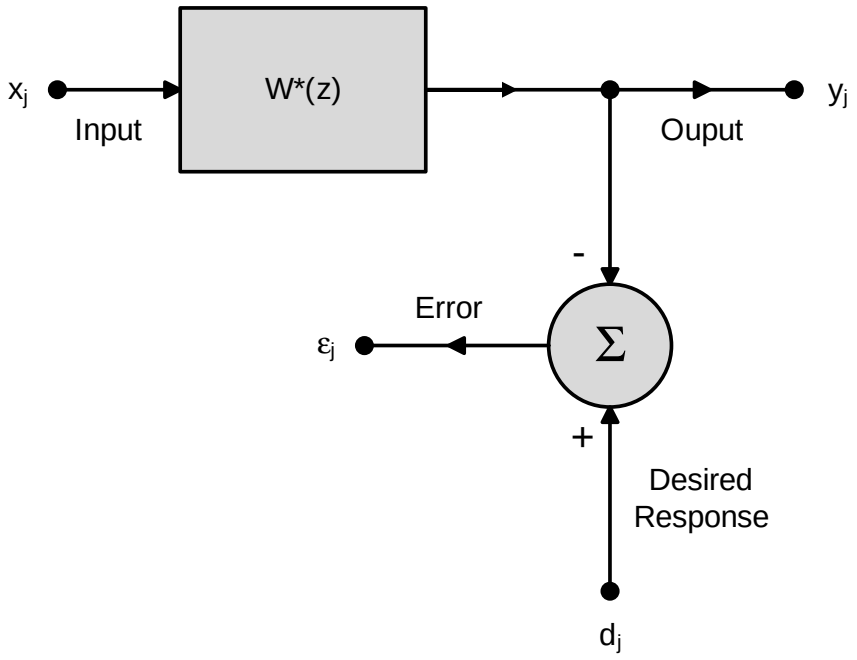

Figure 8: Single Input, Single Output Wiener Filter

The error signal is $\epsilon_j = d_j - y_j$. The autocorrelation function of the input signal x_j, and the cross-correlation function between x_j and d_j are

$$\begin{aligned} \phi_{xx}(k) &= \langle x_j x_{j+k} \rangle \\ \phi_{xd}(k) &= \langle x_j d_{j+k} \rangle \end{aligned} \tag{14}$$

A discrete form of the Wiener-Hopf equation may be used to find the optimal impulse response $w^*(k)$:

$$\sum_{l=-\infty}^{\infty} w^*(l)\, \phi_{xx}(k-l) = \phi_{xd}(k) \tag{15}$$

which is nothing but the convolution

$$w^*(k) * \phi_{xx}(k) = \phi_{xd}(k) \tag{16}$$

Here, the impulse response $w^*(k)$ has been determined for the most general case and can even noncausal and of infinite extent. The power spectral density of the input signal is the z-transform of its autocorrelation function and thus,

$$S_{xx}(z) = \sum_{k=-\infty}^{\infty} \phi_{xx}(k) z^{-k} \tag{17}$$

Similarly, the cross power spectrum between the input signal and the desired response is

$$S_{xd}(z) = \sum_{k=-\infty}^{\infty} \phi_{xd}(k) z^{-k} \tag{18}$$

Now, the transfer function of the Wiener filter is

$$W^*(z) = \sum w^*(k) z^{-k} \tag{19}$$

Therefore, from the preceding equations, the Wiener transfer function is computed as

$$W^*(z) = \frac{S_{xd}(z)}{S_{xx}(z)} \tag{20}$$

A generalized single channel ANS system is shown in Figure 9 [39].The primary input is comprised of signal s_j, stochastic noise m_{0j} that is uncorrelated to any other term in this description, and deterministic noise n_j. The auxiliary input is comprised of another uncorrelated noise term m_{1j} and the noise term $n_j * h_j$, where h_j is the impulse response of the channel with transfer function $H(z)$. The deterministic noise terms n_j and $n_j * h_j$ are uncorrelated to the primary signal s_j. All propagation paths are assumed to be linear time-invariant (LTI). The portion enclosed within the box in Figure 9 is the adaptive filter whose auxiliary input is $x_j = m_{1j} + n_j * h_j$. When the filter converges to the solution by an MMSE-method, the adaptive filter is equivalent to the Wiener filter, and the correspondence is indicated by appropriate nomenclature in the diagram. Using similar notation as before for power spectral

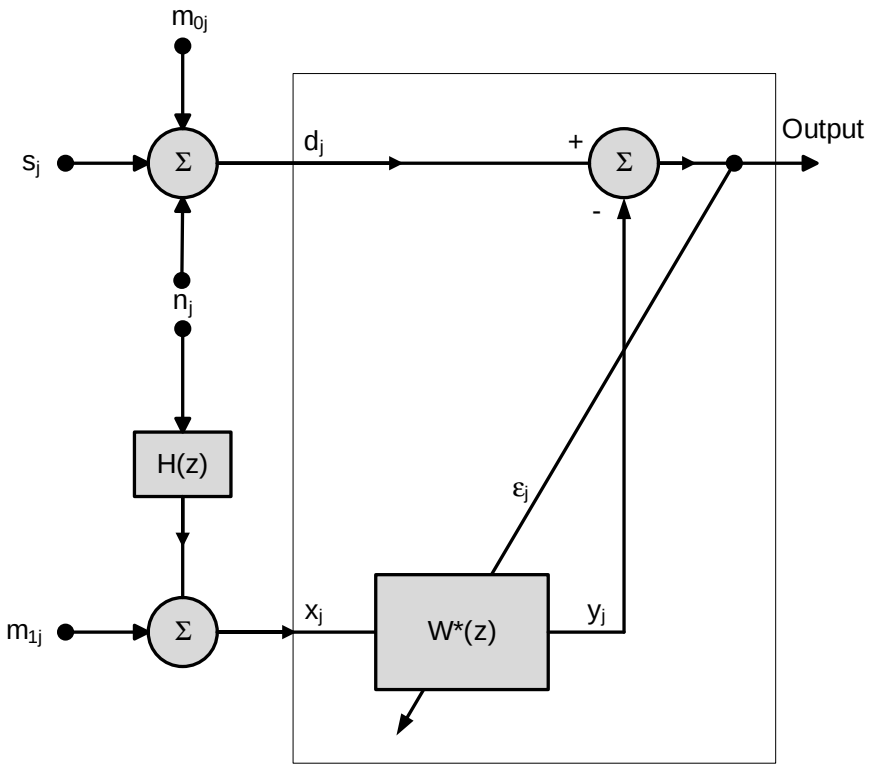

Figure 9: Generalized single channel ANS system

density and recalling that m_{0j} and m_{1j} have zero cross-correlation with all other terms, we have:

$$\begin{aligned} S_{xx}(z) &= S_{m_1 m_1}(z) + S_{nn}(z)\left|H(z)\right|^2 \\ S_{xd}(z) &= S_{nn}(z)\, H\left(z^{-1}\right) \end{aligned} \tag{21}$$

Therefore, from (20), the Wiener transfer function for the generalized ANS system is:

$$W^*(z) = \frac{S_{nn}(z)\, H(z^{-1})}{S_{m_1 m_1}(z) + S_{nn}(z)\left|H(z)\right|^2} \tag{22}$$

It is important to note that the solution for the adaptive filter is independent of the desired signal spectrum $S_{xx}(z)$ or the uncorrelated broadband noise in the primary signal $S_{m_0 m_0}(z)$. Besides, in the special case where there is no uncorrelated broadband noise (m_1) in the auxiliary input, the solution for the adaptive filter converges at exactly the inverse of $H(z)$, thereby cancelling the correlated deterministic n_j completely. In practice this is a trivial case as white noise is always to be expected

in all propagation paths. Also, it is worth noting that the uncorrelated broadband noise m_{0j} in the primary signal path cannot be mitigated by this procedure.

A convenient measure of the performance of the ANS system is obtained by calculating the SNR at the output of the system and its primary input. Here, SNR is used to refer to the ratio of signal and noise power spectral densities and is thus a function of frequency. The input noise power spectrum is found to be:

$$S_{in_{noise}}(z) = S_{nn}(z) + S_{m_0m_0}(z) \tag{23}$$

The output power spectrum consists of many terms. The uncorrelated noise from the primary input is passed through without change while the uncorrelated noise from the auxiliary input is transformed by the adaptive filter. Besides, the correlated noise in the primary path is diminished by the action of the adaptive canceller. Therefore,

$$S_{out_{noise}}(z) = S_{m_0m_0}(z) + S_{m_1m_1}(z)\left|W^*(z)\right|^2 + S_{nn}(z)\left|\left[1 - H(z)W^*(z)\right]\right|^2 \tag{24}$$

The following terms are defined for convenience:

$$\begin{aligned} A(z) &= \frac{S_{m_0m_0}(z)}{S_{nn}(z)} \\ B(z) &= \frac{S_{m_1m_1}(z)}{S_{nn}(z)\left|H(z)\right|^2} \end{aligned} \tag{25}$$

From (22) above,

$$\begin{aligned} W^*(z) &= \frac{\dfrac{H(z^{-1})}{\left|H(z)\right|^2}}{1 + \dfrac{S_{m_1m_1}(z)}{S_{nn}(z)\left|H(z)\right|^2}} \\ &= \frac{\dfrac{1}{H(z)}}{1 + \dfrac{S_{m_1m_1}(z)}{S_{nn}(z)\left|H(z)\right|^2}} \\ &= \frac{1}{H(z)\left[1 + B(z)\right]} \end{aligned} \tag{26}$$

Further,

$$S_{in_{noise}}(z) = S_{nn}(z)\left[1 + A(z)\right] \tag{27}$$

and,

$$\begin{aligned} S_{out_{noise}}(z) &= S_{m_0m_0}(z) + \frac{S_{m_1m_1}(z)}{|H(z)|^2 |1+B(z)|^2} + S_{nn}(z) \left|1 - \frac{1}{1+B(z)}\right|^2 \\ &= S_{m_0m_0}(z) + \frac{1}{|1+B(z)|^2} \left[\frac{S_{m_1m_1}(z)}{|H(z)|^2} + S_{nn}(z) |B(z)|^2\right] \\ &= S_{nn}(z) A(z) + \frac{S_{nn}(z)}{|1+B(z)|^2} \left[B(z) + |B(z)|^2\right] \\ &= S_{nn}(z) \left[A(z) + \frac{B(z)}{1+B(z)}\right] \end{aligned} \tag{28}$$

The ratio of the SNR's at the output and input of the ANS system is thus:

$$\begin{aligned} \frac{SNR_{out}(z)}{SNR_{in}(z)} &= \frac{S_{ss}(z)/S_{out_{noise}}(z)}{S_{ss}(z)/S_{in_{noise}}(z)} \\ &= \frac{S_{nn}(z)[1+A(z)]}{S_{nn}(z)\left[A(z) + \frac{B(z)}{1+B(z)}\right]} \\ &= \frac{[1+A(z)][1+B(z)]}{A(z)+B(z)+A(z)B(z)} \end{aligned} \tag{29}$$

The foregoing analysis describes the dependence of the improvement in SNR from the input of the ANS system to the output as a function of A and B. Upon closer examination, A and B are observed to be ratio of uncorrelated to correlated noise power spectral density in the primary and auxiliary channels, respectively. Therefore, the performance of the ANS system depends strongly on these ratios. If there is no uncorrelated noise in either channel (an unlikely scenario), the performance of the ideal ANS system is perfect with infinite improvement in SNR from input to output. In general, the lower the values of A and B, the better the suppression performance of the ANS system.

Many factors limit the performance of a practical ANS system as compared to the ideal. One of these, which is critical to the current problem and affects how a solution is implemented, is the presence of the primary signal in the auxiliary input. It is intuitive that if a component of the desired signal is added to the auxiliary path, non-zero cancellation of the primary signal will occur at the output of the ANS

system. This effect may also be categorized as signal distortion, which is completely absent in an ANS system provided there is no correlation between the auxiliary signal and the primary desired signal. To understand and quantify this phenomenon, consider the following variation of the ANS system. It is the same as before, except that uncorrelated broadband noise is ignored in both paths and the primary signal is coupled to the auxiliary path after transformation by the filter/ channel $J(z)$. Uncorrelated noise has been omitted for simplicity as it does not affect the key parameters of this manifestation. This scenario is depicted in Figure 10.

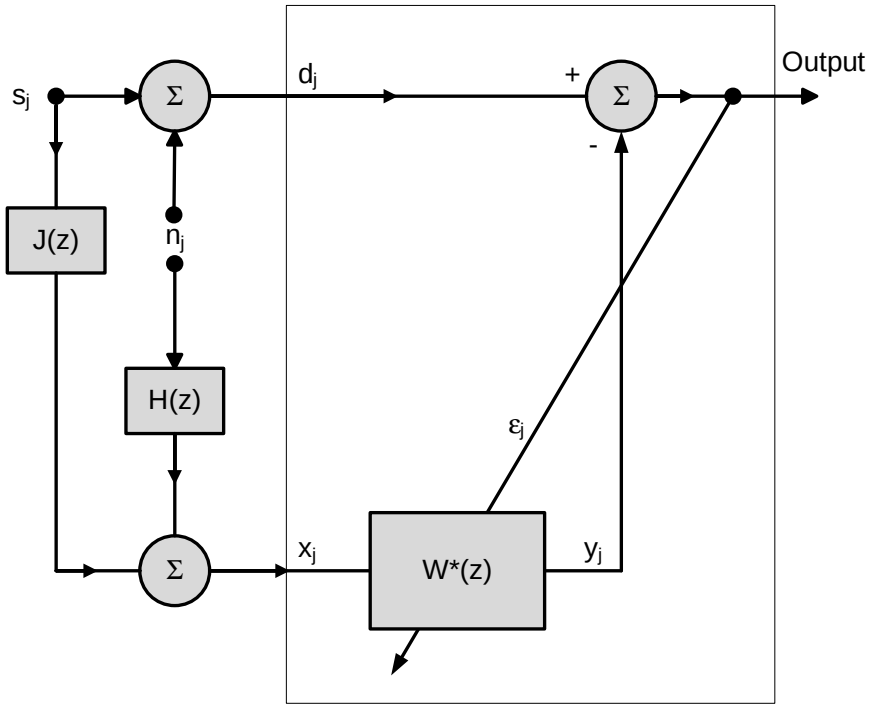

Figure 10: Single Channel ANS System with Component of Desired Signal in Auxiliary Input

Following previous notation, $S_{ss}(z)$ is the power spectral density of the primary desired signal. The spectrum of the auxiliary input x_j is

$$S_{xx}(z) = S_{ss}(z)\left|J(z)\right|^2 + S_{nn}(z)\left|H(z)\right|^2 \tag{30}$$

The cross spectrum between the auxiliary input and the desired response (primary

input), which now contains portion of the primary signal itself, is

$$S_{xd}(z) = S_{ss}(z) J\left(z^{-1}\right) + S_{nn}(z) H\left(z^{-1}\right) \tag{31}$$

From (20) above, the Wiener transfer function after convergence of the adaptive process is:

$$W^*(z) = \frac{S_{ss}(z) J(z^{-1}) + S_{nn}(z) H(z^{-1})}{S_{ss}(z) |J(z)|^2 + S_{nn}(z) |H(z)|^2} \tag{32}$$

Now, the SNR's at the auxiliary input and output may be computed.

$$SNR_{in_{aux}}(z) = \frac{S_{ss}(z) |J(z)|^2}{S_{nn}(z) |H(z)|^2} \tag{33}$$

As the signal gets transformed by $1 - J(z) W^*(z)$ and the noise by $1 - H(z) W^*(z)$ in propagation from input to output, using (32),

$$\begin{aligned} SNR_{out}(z) &= \frac{S_{ss}(z) |1 - J(z) W^*(z)|^2}{S_{nn}(z) |1 - H(z) W^*(z)|^2} \\ &= \frac{S_{ss}(z) \left| \frac{[H(z) - J(z)] S_{nn}(z) H(z^{-1})}{S_{ss}(z) |J(z)|^2 + S_{nn}(z) |H(z)|^2} \right|^2}{S_{nn}(z) \left| \frac{[J(z) - H(z)] S_{ss}(z) J(z^{-1})}{S_{ss}(z) |J(z)|^2 + S_{nn}(z) |H(z)|^2} \right|^2} \\ &= \frac{S_{nn}(z) |H(z)|^2}{S_{ss}(z) |J(z)|^2} \end{aligned} \tag{34}$$

Comparing (34) with (33), the following relation is apparent:

$$SNR_{out}(z) = \frac{1}{SNR_{in_{aux}}(z)} \tag{35}$$

This result implies that the SNR at the output of the ANS system with signal component in the auxiliary input is inversely proportional to the SNR of the auxiliary itself. If a large portion of the primary signal is coupled to the auxiliary input, cancellation is worse at the output.

It is not immediately obvious that the preceding relation is the result of not only worse noise cancellation but distortion of the primary signal also. The following

equations clarify this. Since distortion occurs due to the propagation of the primary signal to the output through the adaptive filter, it is defined as the ratio of the power spectra of the primary signal component at the output arising out of the auxiliary path, and the primary signal at the primary input. Therefore, distortion is

$$\begin{aligned} D(z) &= \frac{S_{ss}(z)\left|J(z)W^*(z)\right|^2}{S_{ss}(z)} \\ &= \left|J(z)W^*(z)\right|^2 \end{aligned} \tag{36}$$

In the subsequent analysis, only the case where the coupled signal component is relatively small is considered, ie., $|J(z)|$ is small. This is desirable in any ANS system. In this case, from the expression for $W^*(z)$ derived in (32) above,

$$D(z) \approx \left|\frac{J(z)}{H(z)}\right|^2 \tag{37}$$

It is noted here that $D(z)$ has no connection to nonlinear harmonic distortion. Using (34), this may be recast as:

$$D(z) \approx \frac{SNR_{in_{aux}}}{SNR_{in}} \tag{38}$$

The obvious inference from this result is that, for a given primary input SNR, the signal distortion at the output is minimized when the SNR at the auxiliary input is minimized. In most situations in communications systems, it is desirable to increase SNR, and the above deduction is not to be confused with this concept. Here, the signal at the auxiliary input is the coupled portion of the desired primary signal present in the auxiliary path, and is unwanted, thus calling for a decrease in SNR.

Finally, the output noise power spectral density in the ANS case with corrupted auxiliary input is derived from (32) using the condition $|J(z)|$ is small, as:

$$\begin{aligned} S_{out_{noise}} &= S_{nn}(z)\left|1 - H(z)W^*(z)\right|^2 \\ &= S_{nn}(z)\left|\frac{S_{ss}(z)\,J(z^{-1})}{S_{nn}(z)\,J(z^{-1})}\right|^2 \\ &= S_{nn}(z)\left|SNR_{in_{aux}}\right|\left|SNR_{in}\right| \end{aligned} \tag{39}$$

Hence, the output noise power spectral density is the input noise power spectral density transformed by the SNR of the auxiliary input and the SNR of the primary input. The $SNR_{in_{aux}}$ factor arises because a lower primary signal component in the auxiliary input causes more perfect noise cancellation at the output. The presence of the SNR_{in} factor indicates that a lower primary signal level relative to noise in the primary input causes the ANS system to be trained better to cancel noise rather than signal.

Other factors that influence the performance of the ANS system and encourage its departure from ideal operation include imperfect adaptation or noise in the adaptive process itself, and impossibility of implementing an adaptive filter of infinite length (or with infinite number of weights). These issues are covered briefly in Chapter 5.

3.2.2 ANS System for Sinusoidal Interference

The generalized scheme presented in the previous section applies to broadband interferences. In the case of a narrow-band aggressor such as a single tone sinusoid, a slightly alternative approach to the analysis of the ANS system is required. The present problem, and indeed most applications in the mobile radio regime, deal with sinusoidal signals as interferers. The undesirable Bluetooth signal for example, is a modulated sinusoid. When dealing with a single sinusoid, a fixed notch filter with the reference frequency implemented in the victim signal path will accomplish the task. However, in spread spectrum systems and owing to drift, in most practical cases, the notch filter needs to be adaptable and may not have knowledge of the reference frequency. A tunable notch filter is in general able to deal with this situation and also when the interferer is a sum of sinusoids. It forms a dynamic solution in which the weights of the adaptive filter are time-varying.

The adaptive filter used in this case is a transversal filter. Consistent with

previous notation, the filter input $x(t)$ is sampled at a rate $1/T$ to form the discrete-time auxiliary/ reference input x_k. This is applied to an N-stage tapped-delay line (TDL). The signals at the N-taps form the N-dimensional reference vector x_k. The filter output is thus $y_k = w_k^T x_k$. A description of adaptation algorithms is provided in Chapter 5. However, it is necessary to summarize the least mean-squares (LMS) algorithm to understand the operation of the ANS system for sinusoidal interference. The following equations govern this adaptation:

$$\begin{aligned} y_k &= w_k^T x_k \\ \epsilon_k &= d_k - y_k \\ w_{k+1} &= w_k + \alpha \epsilon_k x_k \end{aligned} \tag{40}$$

Modification of the above is required to suit the sinusoidal case [40]. The system is recast to define ϵ_k and y_k as the input and output of an LTI-filter with transfer function $G(z)$ as shown in Figure 11.

In order to compute the z-transform of the output $Y(z)$, the i^{th} element of an arbitrary input x-vector is considered. Suppose it has the phase angle θ_i. Then,

$$\begin{aligned} x_{ik} &= C cos\left(\omega_r kT + \theta_i\right) \\ &= \frac{C}{2}\left[e^{j\omega_r kT} e^{\theta_i} + e^{-j\omega_r kT} e^{-\theta_i}\right] \end{aligned} \tag{41}$$

Following the LMS algorithm,

$$\begin{aligned} Z\left\{\epsilon_k x_{ik}\right\} &= \frac{C}{2}\left[e^{j\theta_i} Z\left\{\epsilon_k e^{j\omega_r kT}\right\} + e^{-j\theta_i} Z\left\{\epsilon_k e^{-j\omega_r kT}\right\}\right] \\ &= \frac{C}{2}\left[e^{j\theta_i} E\left(z e^{-j\omega_r T}\right) + e^{-j\theta_i} E\left(z e^{j\omega_r T}\right)\right] \end{aligned} \tag{42}$$

From (40) for the updating of weights, the i^{th} weight becomes

$$W_i(z) = \frac{\alpha C}{2} U(z)\left[e^{j\theta_i} E\left(z e^{-j\omega_r T}\right) + e^{-j\theta_i} E\left(z e^{j\omega_r T}\right)\right] \tag{43}$$

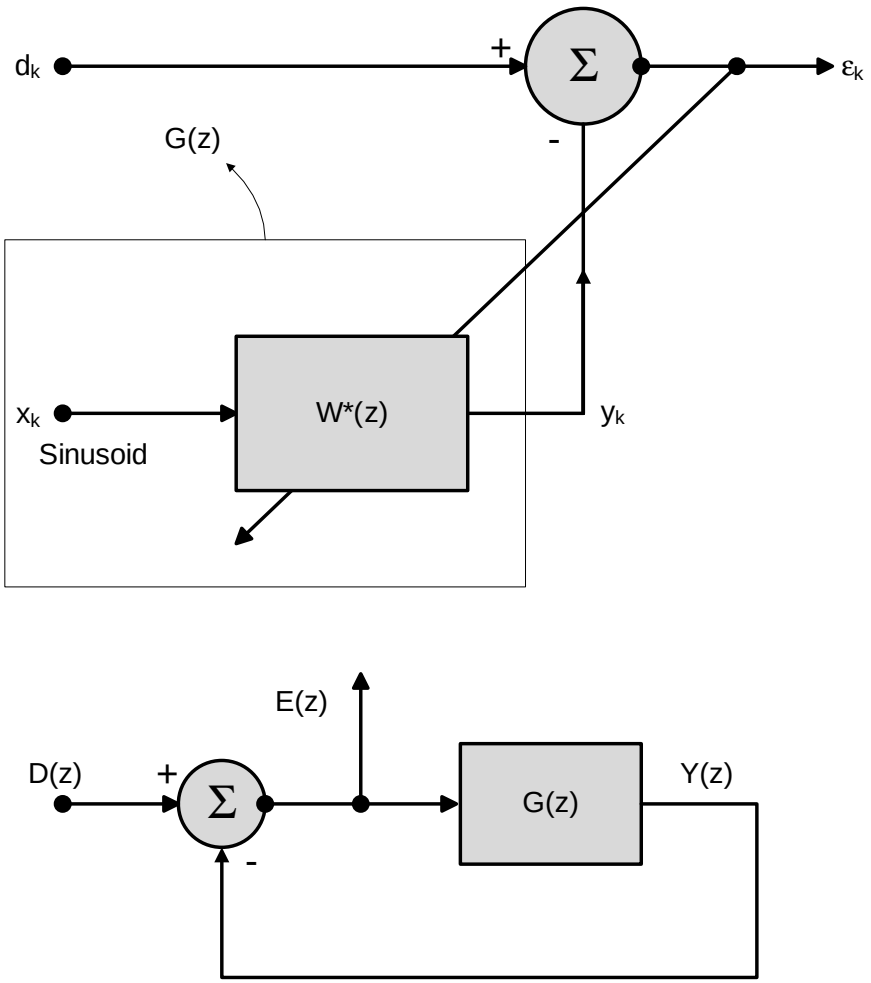

Figure 11: Revised Model for ANS System with Sinusoidal Interferers

where $U(z) = 1/(z-1)$. The i^{th} term in the output is then,

$$\begin{aligned} Y_i(z) &= Z\{w_{ik}x_{ik}\} \\ &= \frac{C}{2}\left[W_i\left(ze^{-j\omega_r T}\right)e^{j\theta_i} + W_i\left(ze^{j\omega_r T}\right)e^{-j\theta_i}\right] \end{aligned} \tag{44}$$

Substituting for W_i from (43) and summing over all terms, it can be shown that:

$$\begin{aligned} Y(z) &= \sum_{i=1}^{N} Y_i(z) \\ &= \frac{N\alpha C^2}{4}E(z)\left[U\left(ze^{-j\omega_r T}\right) + U\left(ze^{j\omega_r T}\right)\right] + \text{time-varying terms} \end{aligned} \tag{45}$$

where the time-varying terms give rise to frequency-shifted components of $E(z)$ in the output. If the proper choice of parameters such as sampling rate is made, it is

possible to neglect these terms so that the transfer function between $E(z)$ and $Y(z)$ is approximated by an LTI-filter. Hence, taking only the first term from (45) and using the definition of $U(z)$,

$$\begin{aligned} G(z) &= \frac{Y(z)}{E(z)} \\ &= \frac{N\alpha C^2}{4}\left[U\left(ze^{-j\omega_r T}\right) + U\left(ze^{j\omega_r T}\right)\right] \\ &= \frac{N\alpha C^2}{2}\frac{zcos\omega_r T - 1}{z^2 - 2zcos\omega_r T + 1} \end{aligned} \tag{46}$$

It is apparent from (46) that $G(z)$ has a complex pole-pair on the unit-circle and a zero. Now, referring to the feedback network in Figure 11 defining $G(z)$, the transfer function from d_k to y_k is found to be

$$\begin{aligned} H(z) &= \frac{1}{1+G(z)} \\ &= \frac{z^2 - 2zcos\omega_r T + 1}{z^2 - 2\left(1 - \frac{N\alpha C^2}{4}\right)zcos\omega_r T + \left(1 - \frac{N\alpha C^2}{2}\right)} \end{aligned} \tag{47}$$

This is the transfer function of a 2^{nd}-order digital notch filter at frequency ω_r, with zeros being located at the poles of $G(z)$. Thus, the construction of an adaptive filter suited to the ANS application with a sinusoidal interferer is described. The following important features of such a filter are noted here.

1. As the null of the notch filter needs to match the reference frequency, it is tunable.

2. The notch can be made arbitrarily sharp at the exact reference single-tone frequency.

3. The converged solution cannot have constant weights. In that case, the reference frequency would be directly passed to the output, without causing any cancellation at nearby frequencies.

3.3 Front-End Noise Cancelling System

The foundations of the various ANS systems suitable to the radio interference problem have been laid in the previous sections. A modified form of these is employed in this work. The canceller is transposed to the RF front-end and moves away from adaptive TDL's or digital notch filters. Some of the key reasons for this choice are related to IC implementation of the system and are outlined in Chapter 4.

A schematic representative of the cancellation process in the front-end is shown in Figure 12.

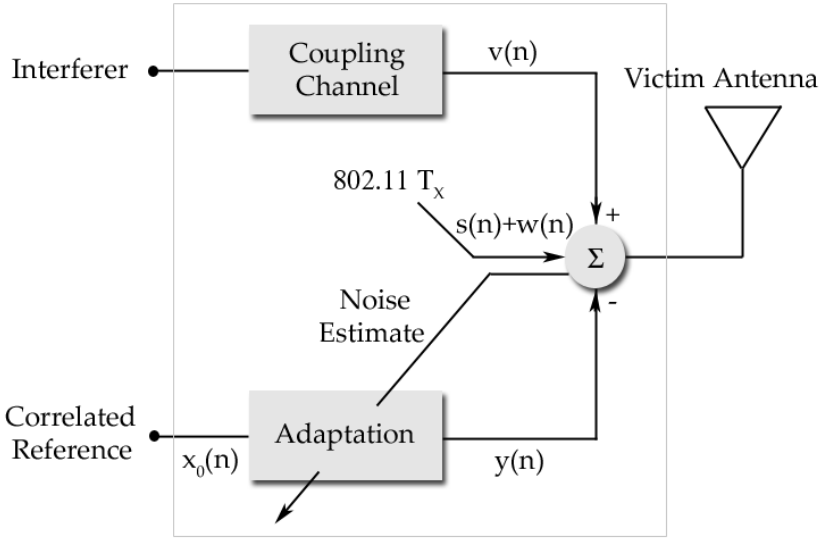

Figure 12: Modified Adaptive Noise Mitigation Scheme for the BT–WLAN Problem

Referring to the diagram, the victim antenna receives a signal

$$x\left(n\right) = s\left(n\right) + v\left(n\right) + w\left(n\right) \tag{48}$$

where $s(n)$ is the information-bearing signal of interest, $v(n)$ is a narrow-band interferer and $w(n)$ is broadband noise. The two noise terms are not correlated to the signal or to each other. Specifically, the expectation

$$\left\langle s\left(n\right) v\left(n-k\right)\right\rangle = 0 \tag{49}$$

for all k.

The cancellation unit receives the reference input $x_0(n)$ that is given by

$$x_0(n) = v_0(n) + w_0(n) \tag{50}$$

where $v_0(n)$ and $w_0(n)$ are narrow-band and broadband noise terms respectively. Whereas, the two broadband noise terms are uncorrelated to any source by definition, and $v_0(n)$ is uncorrelated to the signal $s(n)$, the two narrow-band noise terms are correlated to each other. All signals under consideration are wide-sense stationary. In general, the cross-correlation between the two narrow-band noise terms is unknown and given by

$$\rho(k) = \langle s(n) v_0(n-k) \rangle \tag{51}$$

for a lag k. Traditionally, $x_0(n)$ is processed by an adaptive filter as mentioned before, to produce an output signal

$$y(n) = \sum_{k=0}^{L} g_k(n) x_0(n-k) \tag{52}$$

where $g_k(n)$ are the adaptable weights of the filter and L is its length. The output of the cancellation unit is thus the error signal

$$\begin{aligned} \epsilon(n) &= x(n) - y(n) \\ &= s(n) + v(n) + w_t(n) - y_0(n) \end{aligned} \tag{53}$$

where $y_0(n)$ is the narrow-band correlated noise contribution of $x_0(n)$ to the output, and $w_t(n)$ is the total broadband noise at the victim antenna. If the control mechanism is able to dynamically converge and achieve cancellation, the condition

$$y_0(n) > w_t(n) - w(n) \tag{54}$$

will ensure success.

The implementation described in this work differs from the above general case in that the cross-correlation of (51) is not completely unknown. Since the aggressor antenna, which is the source of correlated noise, is assumed to be located in the

immediate proximity of the victim, the cancellation unit has access to a scaled and delayed version of $v(n)$. Though this approach may slightly affect the aggressor, it obviates the need for large and complex tapped-delay finite impulse response (FIR) filters. However, it must be noted that $v(n)$ is defined not only by the source antenna, but also by the wireless coupling channel. This channel is not expressible analytically in a closed form and thereby still needs to be emulated in order to process $x_0(n)$. Under the operating conditions considered above, measurements show that the coupling channel is largely stationary in its characteristics for a given configuration of the interferers, forming the basis for the design of a simple emulation filter. The filter is endowed with limited tunability to combat dynamic environments.

In either case discussed above, the only correlation among the inputs to the canceller being between $v(n)$ and $v_0(n)$, we may write the mean power of the output as

$$\left\langle \epsilon^2 \right\rangle = \left\langle s^2 \right\rangle + \left\langle (v - x_0)^2 \right\rangle \tag{55}$$

Maximizing the output SNR and performance of the canceller, therefore, requires minimizing the left hand side of (55). This may be accomplished in adaptive filtering schemes by the use of various control algorithms.

Examining the above correlation chain in continuous time, and preserving the same notations as in (48) – (55) we may write

$$y_0(t) = \int_{-\infty}^{\infty} G(f)\, V_0(f)\, e^{j2\pi ft} df \tag{56}$$

where $G(f)$ is the Fourier transform of the filter, and $V_0(f)$ that of the narrow-band noise input to the cancellation unit. This is possible only when the filter is linear and the coupling channel emulated by the filter is assumed linear time invariant. When the filter output is sampled at time $t = T$, this yields

$$|y_0(T)|^2 = \left| \int_{-\infty}^{\infty} G(f)\, V_0(f)\, e^{j2\pi ft} df \right|^2 \tag{57}$$

as the output power due to the interferer. Also, the average power of the total broadband noise at the victim antenna is given by

$$\left\langle w_t^2(t)\right\rangle = \frac{N_0}{2}\left[1 + \int_{-\infty}^{\infty} |G(f)|^2\, df\right] \tag{58}$$

where $N_0/2$ is the power spectral density of $w(t)$. Therefore the SNR before and after cancellation may be expressed as

$$\begin{aligned} SNR_{before} &= \frac{|s(T)|^2}{|v(T)|^2 + \langle w^2(t)\rangle} \\ SNR_{after} &= \frac{|s(T)|^2}{|v(T) - y_0(T)|^2 + \langle w_t^2(t)\rangle} \end{aligned} \tag{59}$$

Here, the powers are measured at a time T, the numerators are constant, and the frequency domain representation of $y_0(T)$ is obtained from (57).

The cancellation technique employed is schematically represented in Figure 13. Shown here, are sources of deterministic noise acting by various physical mechanisms.

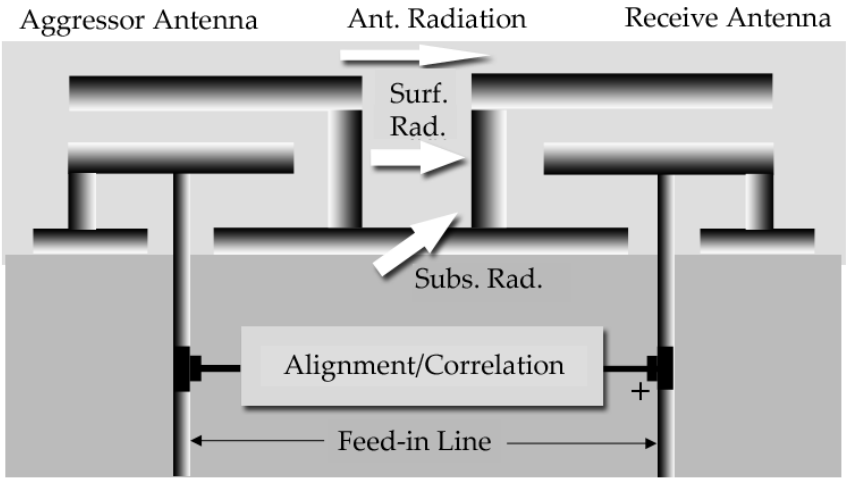

Figure 13: Physical Sources of Correlated Noise in the Radio System and their Suppression

A downscaled replica of the signal at the aggressor antenna is tapped-off by the cancellation unit and used as the input $v_0(t)$ as in (50). This is always accompanied by the white noise $w_0(t)$ present in the aggressor and elsewhere. As long as $|v_0(t)|$ is very small compared to the transmit level in the aggressor, any effect on the Bluetooth transmission is insignificant. Coupling levels to the victim antenna being less than 13 dB, the voltage level of the tapped-off signal needs to be less than 2.5% of the Bluetooth transmit level to accomplish cancellation with a system of unity maximum gain.

A cancellation signal is generated by the unit, which is governed by external controls. Combining this signal with the received signal at the victim (WLAN) antenna at a 180^0 phase differential, effects the suggested interference suppression. Loop cancellation methods that are different from this method have been used before [41] to generate narrow-band nulls at specific frequencies to achieve isolation in full-duplex radios. Correlation and the generation of a cancellation signal within the unit are performed by gain and phase alignment of the input $v_0(t)$, and filtration through $G(f)$ defined in (52) and (56). An issue of significance requiring remark here is that the proposed method creates a cancellation notch in-band that is wider compared to the above-mentioned narrow-band nulls. This is important because very narrow-band nulls are impractical in spread-spectrum communication systems owing to their hopping nature. Also, band limiting through the emulation filter helps prevent the coupled noise from decorrelating for a larger time interval allowing easier cancellation, as suggested in [42]. Besides, as noted in [43], some applications may necessitate the use of non-causal filters in the adaptation path. Deriving the correlated input directly from the aggressor however, negates this requirement since the interferer does not reach the victim before it does the cancellation unit. The importance of this stems from the fact that delays cannot be placed in the primary interference mechanism (air) between the Bluetooth and WLAN radios, thus making it difficult to

violate causality. Also, an advanced implementation of this principle may sense the interferer through the air channel without electrically contacting it. This would not require proximity to the aggressor or access to it, and would rely on magnetic means to couple the reference signal. It is possible to make use of a directional antenna to sample the EM radiation from the aggressor and provide auxiliary input to the canceller. However, it is impossible to guarantee that such a sensing mechanism does not sample the primary desired signal too, thereby factoring in severe performance losses in the canceller due to signal distortion as indicated in the previous section. This, in conjunction with the fact that the carrier frequencies are much higher than the data rates in the present application, implies that interference suppression may be adequately accomplished by means of gain and phase adjustments, and filtration alone.

CHAPTER IV

ACTIVE INTERFERENCE CANCELLERS IN CMOS IC TECHNOLOGY

The previous chapters systematically examined and developed an approach to mitigation of deterministic noise in the mobile radio environment. In this chapter, the preceding theory is translated to design. The construction of the canceller is described at the hardware level and its critical components are introduced. The physical design of these circuits is discussed with reference to their topology and performance parameters. A canceller that is designed to operate at 2.4 GHz for the BT–WLAN problem is presented, along with a version of this design modified for 1.575 GHz operation. The latter is usable as a GPS protection device. Further, a variation on the above design theme offering some performance advantages is developed. All these designs are fabricated in a 0.18-μm Si-CMOS IC technology and measured to demonstrate their effectiveness.

4.1 Canceller Prototype

A prototype of the canceller was constructed on FR-4 material in keeping with the principles discussed earlier [44], [45]. A schematic is shown in Figure 14.

The paired patch antennae of our earlier measurements act as transmitter and receiver in the problem. Inputs to and outputs from the canceller unit are processed by power splitting and combining elements. The board shown is constituted of discrete components available off the shelf. The emulation filter has a band-pass characteristic and is implemented as an LC-section. A varactor diode in shunt with a high-Q discrete inductor provides narrow-band behavior throughout the 83.5 MHz band and

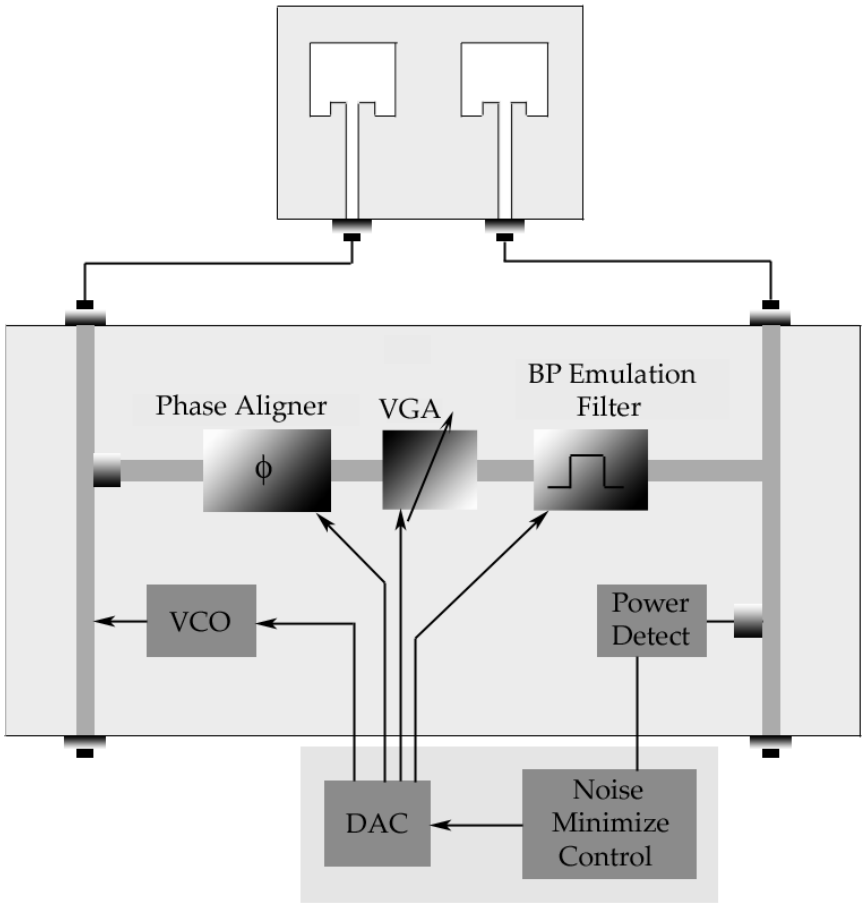

Figure 14: Simplified Schematic of the Interference Cancellation Prototype.

is tunable to compensate for slight channel mismatches.

Gain control is through a variable gain amplifier (VGA) able to provide voltage gain from 0 to 1 or greater. A 360^0 continuously variable phase shifter is used to align the phase of the correlated sample signal with the interferer.

External control involves minimizing the error signal, which is equivalent to finding a minimum for the mean output signal energy as shown in (55) in the previous chapter. As the function of the prototype is merely to demonstrate cancellation ability, it is sufficient to control it manually without the need for an adaptation algorithm. However, a mechanism that makes control easier is also implemented. This involves a simple procedure using pilot signals for reference. Known pilot signals are injected into the canceller unit along with the reference interferer. These pilots

occupy extremely narrow bandwidths and are situated outside the edges of the 2.4 GHz band. Not being in-band, they do not affect canceller performance in the region of interest. It is surmised that the spectrum of the coupled signal after cancellation being smooth, a lowering of energy in-band will correspond with energy reduction at the band edge also. Hence, monitoring and minimizing the energy in a pilot signal at the output of the canceller is equivalent to minimizing coupling within the band.

This however, does not mean the cancellation notch is wide enough to cover the whole 2.4 GHz band. Generating a wide enough notch requires simultaneously minimizing the energy of both pilots. Precise knowledge of the pilot signals and their higher power levels compared to the in-band signals makes this scheme more robust and easier to implement. The result using such a feedback method was measured and an example of the cancellation data within the 2.4 GHz band is shown in Figure 15.

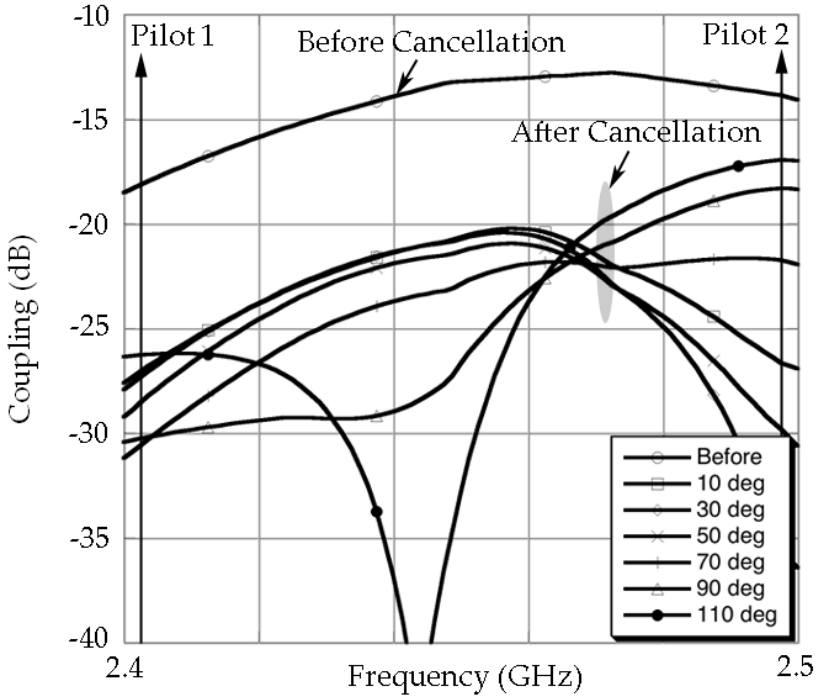

Figure 15: Out-of-band Pilot Tones used for Cancellation In-band by Varying Phase Adjustment.

Various curves in the graph represent different states of control. This result, though preliminary, demonstrates that a wide-band noise suppression of 10–13 dB is easily achievable. It should be noted that such a cancellation notch covers the whole 2.4 GHz ISM band and is not affected by the spread spectrum nature of the communication system. As shown mathematically in the previous chapter, this system generates a noise suppressing signal at frequencies near the reference frequency as well, thereby indicating its adaptive nature.

4.2 Analog Canceller Core: IC Design

Si-CMOS IC technology is a strong contender for RF and high-speed circuit design, including the design of radio front-ends. Most RF applications in the ISM bands between 800 MHz and 6 GHz utilize CMOS ICs to provide front-end functionality. The canceller solution to the interference problem in the 2.4 GHz ISM band proposed in the earlier sections of this document employed discrete components on an FR-4 material to establish validity of the method and outline a feasible solution. The mutually interfering radio devices are often located in close proximity and share the same substrate or circuit board. In order that an interference suppressor be viable as a solution, it is therefore necessary that it operates in the same environment and be easily integrated with existing circuitry.

Designing CMOS ICs to replicate the functionality of the canceller is consequently the most desirable approach. Further, employing a commercial 0.18-μm CMOS technology with a short circuit unity current gain cutoff frequency (f_T) of 30 GHz or greater will allow low power consumption, which is crucial to the feasibility of the method [46]. The remainder of this chapter presents the design of the 'core' of the canceller and delves into the details of the circuits so fabricated. The core comprises the main time-frequency correlation chain of the canceller as described in the previous section. It may be divided into its primary functional components –

a VGA, a phase rotator, and a band-pass filter. Their design, including interfacing with external nodes and performance results are discussed below.

4.2.1 Analog Active CMOS VGA

As described earlier, the high frequency carrier tone of the reference signal needs to be aligned temporally with the interferer. Since the modulated data is of a much larger wavelength than the carrier, on the small spatial scales in consideration, it does not require alignment. This means both the amplitude and phase of the reference input to the canceller must be matched to the undesired interferer separately to enable complete subtraction. Since the interference level is typically less than 15 dB, an alignment system with a maximum gain of unity may be used to achieve suppression while requiring a small input signal strength. Amplitude alignment is therefore implemented by designing a variable gain amplifier (VGA) with an approximate maximum gain of unity or more, and a voltage gain range of 0 to 1. A high attenuation ability is necessary as the interfering signal amplitude may experience large variations.

An amplifier whose gain can be continuously varied from a negative to a positive value is suitable for this purpose. Consider two differential pairs that amplify the input by opposite gains, by varying their tail currents in opposite directions [47]. If the output voltages are summed, as illustrated in Figure 16, the total output voltage of the combination is

$$\begin{aligned} V_{out} &= V_{out1} + V_{out2} \\ &= A_1 V_{in} + A_2 V_{in} \end{aligned} \tag{60}$$

where A_1 and A_2 are controlled by V_{cont1} and V_{cont2}, respectively.

In actual implementation, the summation can be performed in the current domain using differential pair transconductors. V_{cont1} and V_{cont2} must vary the currents through the differential pairs in opposite directions while maintaining a constant total current so that the gain of the amplifier varies monotonically. This may be simply

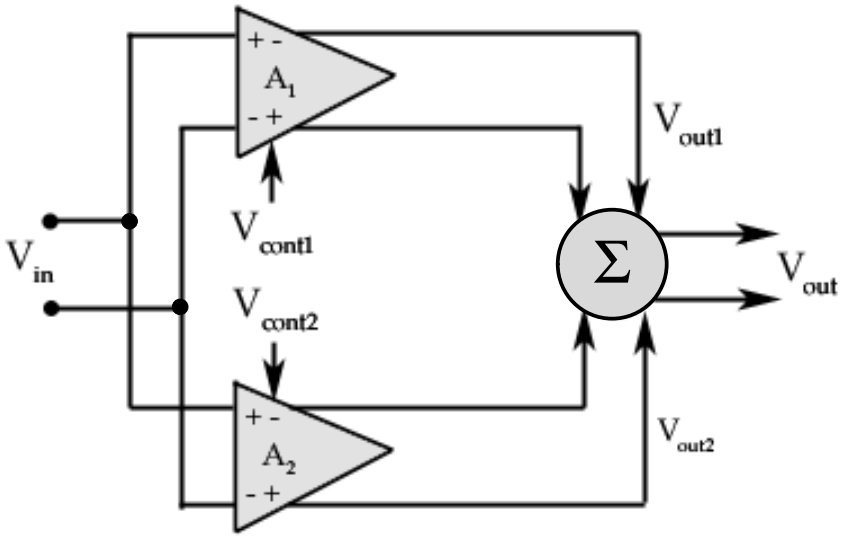

Figure 16: Voltage Domain Summation of Amplifiers.

accomplished by a Gilbert cell [48].

A simplified schematic of the VGA circuit is shown in Figure 17.

The circuit is designed to operate from a 1.8 V power supply. Figure 17(a) shows the RF-signal path of the current steering transconductor. As with a cascode structure, the Gilbert cell consumes greater voltage headroom than a simple differential pair does. Hence, it is also necessary to utilize low headroom circuit topologies in conjunction with the Gilbert cell. The total current in the Gilbert cell, which is constant at all times, is obtained by a folded cascode differential biasing circuit that maintains at least as much output voltage swing, as shown in Figure 17(b). Here, in a PMOS cascode amplifier, the input device is replaced by the opposite type while still converting input voltage to current [49], [50]. It is supplied by a PMOS current source. The currents in the signal path differential pairs are made to vary by changing the control voltage V_{CTRL}. Rather than operate the control differentially, one end has been fixed at the midpoint of the bias control voltage range at the value V_{DC}, which is approximately 0.7 V, while the other is varied around it from 0 to 1.4 V.

In contrast to typical mixed signal broadband designs, the input and output

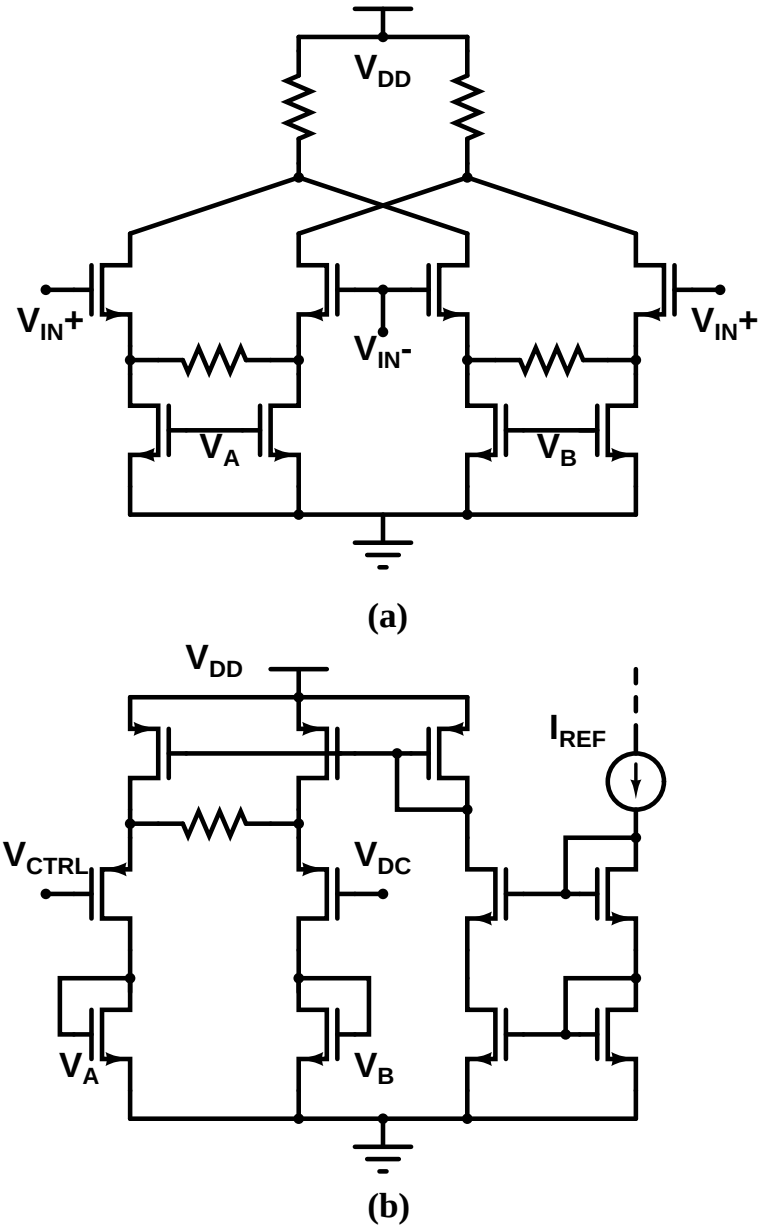

Figure 17: (a) Circuit Schematic of the Gilbert Cell VGA. (b) Schematic of Folded Cascode Current Steering Bias Circuit Operating the VGA

voltage waveforms are not rail-rail swinging square pulses, but rather modulated sinusoids. Therefore, non-linearity in the operating bias range of the Gilbert cell needs to be minimized. Resistive degeneration is used to this end. The current steering cell is resistively degenerated with a 1.5 KΩ poly-poly resistor so as to extend the portion of the control range over which gain magnitude varies linearly with control voltage.

Maximizing this linearity relaxes the control loop design requirements. Since the VGA itself only needs to provide up to unity gain, the size of the signal path devices is optimized to add low noise to the output.

The total delay through the VGA was approximately 40 ps at 2.4 GHz, and phase variation with control voltage was minimal. The s-parameters of the VGA were measured using a 4-port network analyzer. A driver circuit consisting of a two-stage differential amplifier was used to buffer the VGA from the 50 Ω input of the instrument. Time domain measurements were also performed. Shown in Figure 18 is the gain magnitude response of the VGA against frequency for several values of control voltage.

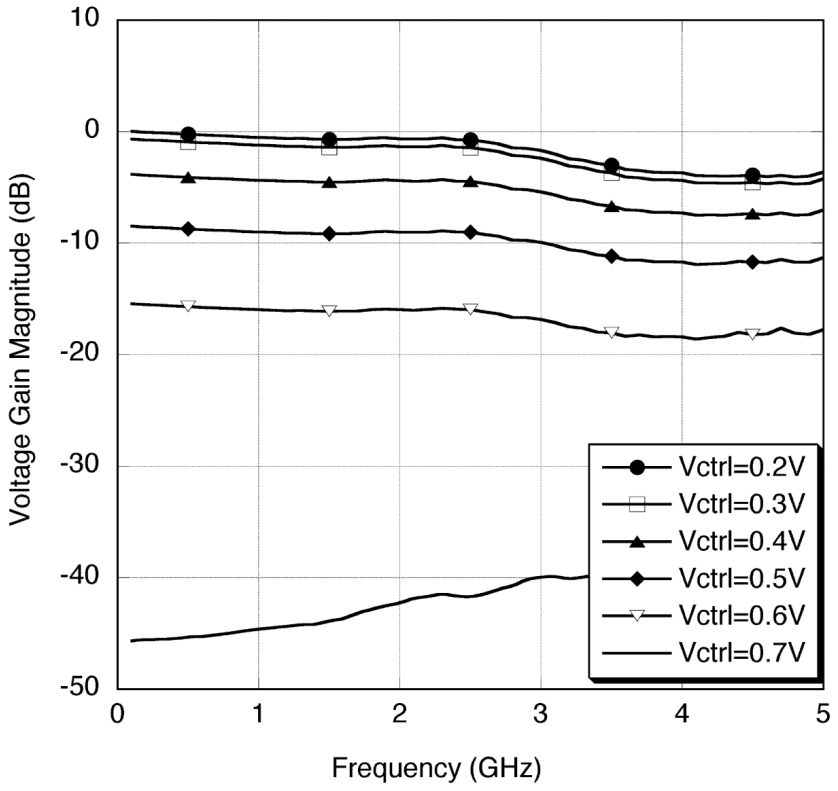

Figure 18: Variation of VGA Gain Magnitude with Frequency.

From the diagram, it is clear that the VGA gain spectrum is quite broadband and has a 6-dB corner well in excess of 5 GHz, while being optimized for operation at 2.4

GHz. Figure 19 shows the phase spectrum of the VGA for different control voltages.

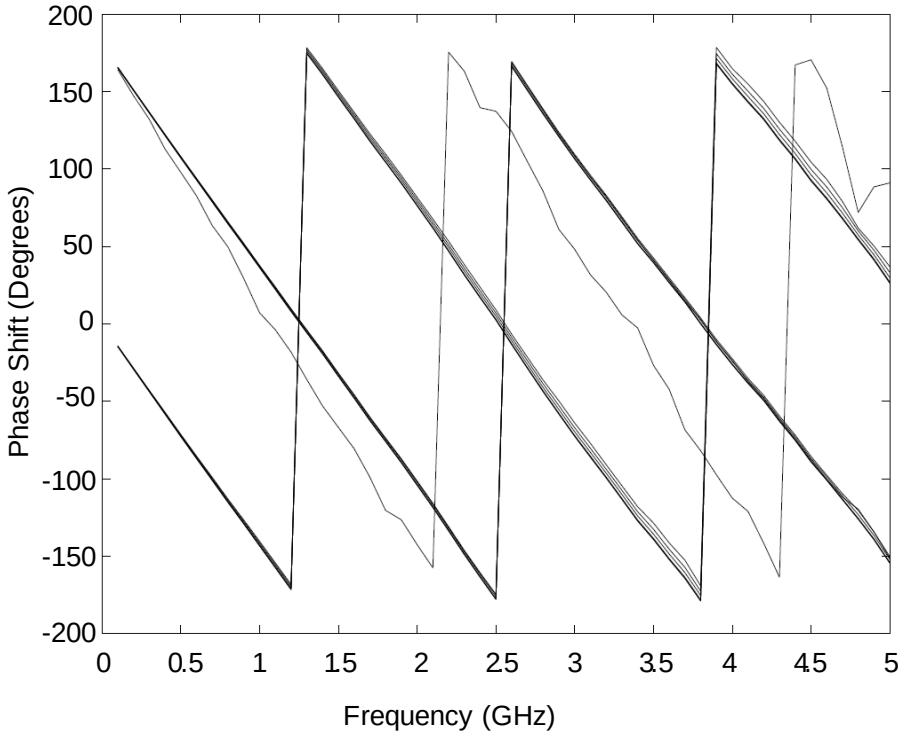

Figure 19: Variation of VGA Phase-Shift with Frequency.

The phase shift is wrapped around every 360^0 for easy interpretation. The parallel sections of the graph show that the slope of the phase-frequency curve is constant over the frequency of interest. In other words, the circuit maintains constant group-delay. There is very little variation of phase with the amplitude control voltage, except at one point – a desirable characteristic. When the amplitude control crosses 0.7 V, which is the midpoint of the control range, the phase-shift across the VGA jumps by 180^0. This mirrors the fact that the VGA gain varies from -1 to +1 – an aspect that is not visible on the gain magnitude spectrum. As a measure of the controllability of the VGA, its gain magnitude and phase shift are plotted against control voltage at 2.4 GHz in Figure 20.

As observed from the plot, the signal amplitude has a controllable range of about 42 dB, although non-linearly, while the phase shift is constant throughout the control

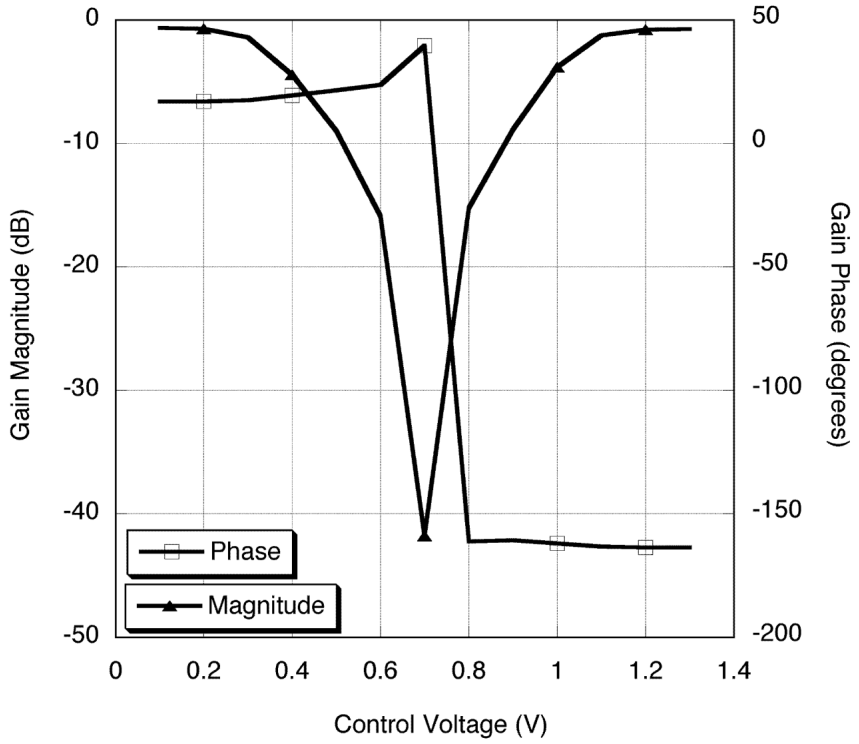

Figure 20: Variation of VGA Gain Magnitude and Phase with Control Voltage at 2.4 GHz.

range except for a 180^0 flip at the center.

4.2.2 Analog Active CMOS Phase Rotator

Temporal alignment of the reference signal for cancellation requires matching of phase in addition to amplitude. Here, the term phase alignment is so generalized as to refer to both delay alignment and true phase shift at the given frequency. Since the interference suppression method proposed uses a channel emulation filter to generate a cancellation notch that is wide band rather than limited to a single tone, the frequency of concern is selected to be the center frequency of the pass band (2.4 - 2.4835 GHz). If the delay through the coupled path is short compared to the wavelength of the carrier modulations, the delay can be modeled as a phase shift thereby eliminating the need for separate delay adjustment. For instance, if the difference in the path delay for the coupled signal and the reference signal is much larger than a single

period, then the remainder of the extra delay beyond one cycle may be equalized by a fixed passive delay element on the circuit board and the rest treated as a phase shift.

This necessitates that the phase rotator designed be a continuously variable shifter with 360^0 of phase range, so as to provide alignment capability for any interference condition. Also, since the VGA described in the previous section is to be designed with unity gain in both the positive and negative directions, it serves additionally as a fixed 0^0 or 180^0 switchable phase shifter. Consequently, a range of only 180^0 is required out of the phase shifter IC. Further, the identical relationship between delay and true phase shift over one carrier cycle allows the design of a circuit that relies on delay manipulation to obtain the necessary phase shift. The equivalent delay range at 2.4 GHz is 208.33 ps.

The phase aligner designed utilizes a delay interpolation technique [51]. The principle of this circuit is that it employs a line of delay cells with voltage-controlled interpolation between multiple taps on the delay line. Various embodiments of this scheme are possible. One method applies NMOS inverter delay cells in the delay line and achieves interpolation by using MOSFETs as voltage controlled resistors [52]. An example of this is shown schematically in Figure 21.

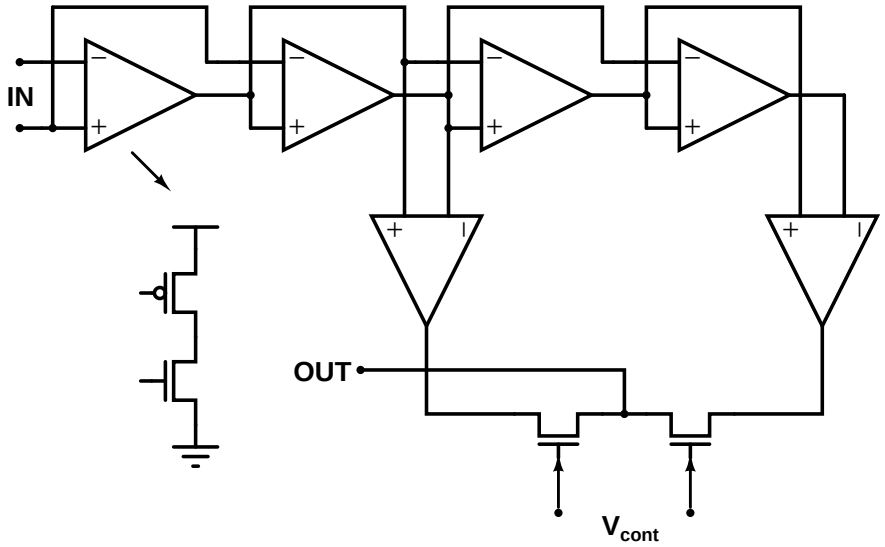

Figure 21: Schematic of a Delay Interpolation Circuit.

Another embodiment of the delay interpolation scheme uses differential amplifier cells in two parallel delay paths, a fast path and a slow path. The outputs of the two paths are summed and their gains are adjusted in opposite directions by a control voltage. In this case, the summing circuit also performs the gain adjustment. The total delay range available is equal to the difference in the delays of the two paths. A schematic representing this method is shown in Figure 22.

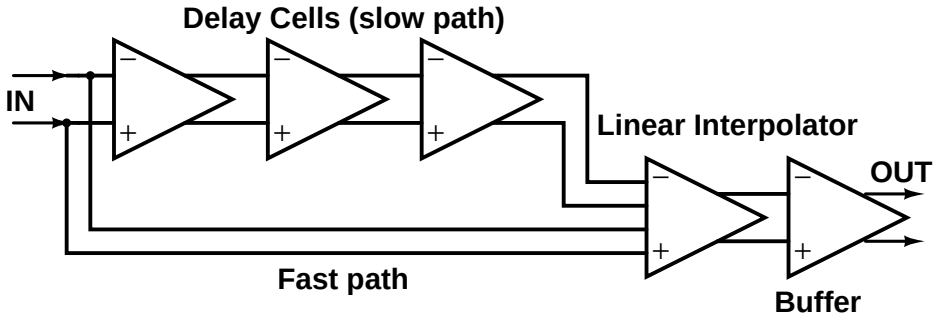

Figure 22: Scheme Used for Delay Interpolation in the Phase Aligner.

This method derives the required path delay using differential amplifier cells. A low impedance driver may be used at the output port to prevent loading of the delay shifter if interfacing with a low-impedance line. A block diagram depicting the operating principle of the phase aligner in terms of its circuit components is shown in Figure 23, and analyzed subsequently.

The portion of the circuit between B and C as shown in the diagram forms the core of the phase aligner. The modified Gilbert cell $G2$ is configured such that each differential amplifier constituting the cell accepts a different set of inputs. Whereas one set of inputs arrives directly from B, the other is delayed by the two cascaded differential amplifiers ($D2$, $D3$) between B and C. The cell $G2$ further sums the currents through each of its halves at the output node so that effectively it interpolates between the delays of its inputs.

The exact delay desired is obtained by adjusting the currents through the two

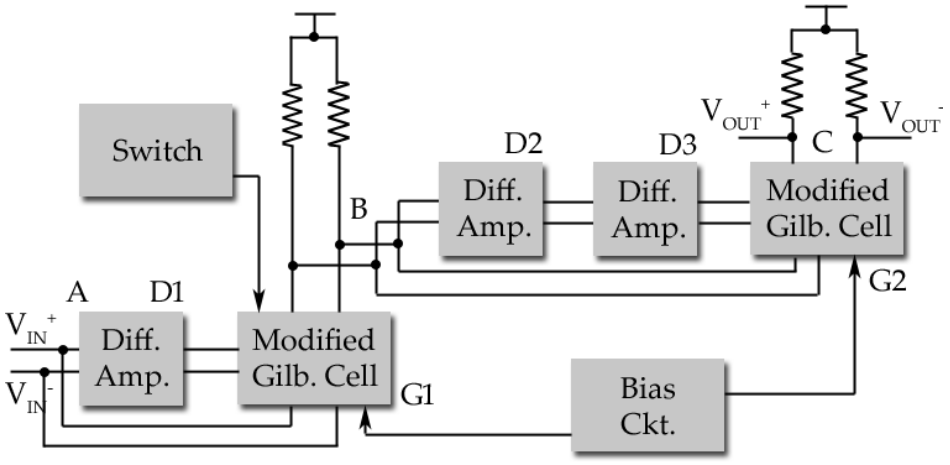

Figure 23: Simplified Block Diagram Showing Phase Shifter Operation and Circuit Components.

halves of $G2$. This is done by means of a control voltage at the folded cascode current biasing circuit of G2 in a manner similar to the VGA.

With reference to Figure 23, τ_{BC} is the delay a signal experiences while propagating between B and C. This delay is variable and controlled by the current steering circuit that biases the modified Gilbert cell $G2$. It varies between $\tau_{BC,min}$ and $\tau_{BC,max}$ at the two extremes of the control range. Therefore, the total controllable delay range is:

$$\Delta\tau_{BC} = \tau_{BC,max} - \tau_{BC,min} \tag{61}$$

Now, the differential amplifier delay cells $D2$ and $D3$ in the schematic have fixed delays τ_{D2} and τ_{D3}. The cell $G2$ interpolates between the two paths from B to C so that at one extreme of the control range, the output signal at C is entirely due to the fast path and at the other, it is entirely due to the slow path through $D2$ and $D3$. Hence, the controllable delay range in (61) above is:

$$\Delta\tau_{BC} = \tau_{D2} + \tau_{D3} \tag{62}$$

The total gain of $D2$ and $D3$ must be unity so that the inputs to $G2$ differ only in phase and not in amplitude. However, despite ensuring the unity gain criterion,

the nature of the interpolator prevents constant gain across the control range. One method of surmounting this is to use dynamic current biasing through the current source. If the tail current through $G2$ is increased non-linearly through the middle of the bias range, a constant effective transconductance may be obtained. Non-linear dynamic biasing through MOSFET devices being difficult to achieve, this method is abandoned in favor of a simpler solution. Increasing the gain range of the VGA enough to ascertain that the total gain of the system is unity at the middle of the phase control range is sufficient.

The total delay range available from the above section of the circuit was around 150 ps, which corresponds to a phase range of 130^0 at 2.4 GHz. The section of the phase rotator circuit from A to B contributes the remainder of the phase control range.

Again, this portion of the circuit consists of a modified Gilbert cell $G1$ that receives inputs directly from A and through the differential amplifier delay cell $D1$. $G1$ is different from $G2$ in that each of its differential amplifier halves is constant current biased. It does not operate by a current steering mechanism. The outputs are summed across the pair of matched load resistors at B. $D1$ is a unity gain stage providing more than 59 ps of delay. This is a fixed delay that can be turned on or off by a switching control circuit that biases the two halves of $G1$. Therefore, if τ_{AC0} and τ_{AC1} represent the delay between A and C when $D1$ is switched off or on,

$$\begin{aligned} \tau_{AC0} &= \tau_{G1} + \tau_{BC} \\ \tau_{AC1} &= \tau_{D1} + \tau_{G1} + \tau_{BC} \end{aligned} \tag{63}$$

But the controllable delay range in each case is equal to $\Delta\tau_{BC}$. The total delay range available over the two modes, which is also the total possible delay range of the

entire circuit is given by

$$\begin{aligned} \Delta\tau_{AC} &= \tau_{AC,max} - \tau_{AC,min} \\ &= \tau_{D1} + \Delta\tau_{BC} \end{aligned} \tag{64}$$

which is more than the required 208.33 ps.

A schematic of the IC implementation of the modified Gilbert cell structure is illustrated in Figure 24. It should be noted that this cell is driven by a folded cascode current steering circuit as with the VGA, to reduce voltage headroom requirement. The control voltage operating the phase aligner is single-ended and varies from 0 to 1.3 V. This acts in conjunction with the switching voltage, to provide another range of phase-shifts also controlled by the same 1.3 V range. The above two ranges have a substantial amount of overlap in terms of the output phase.

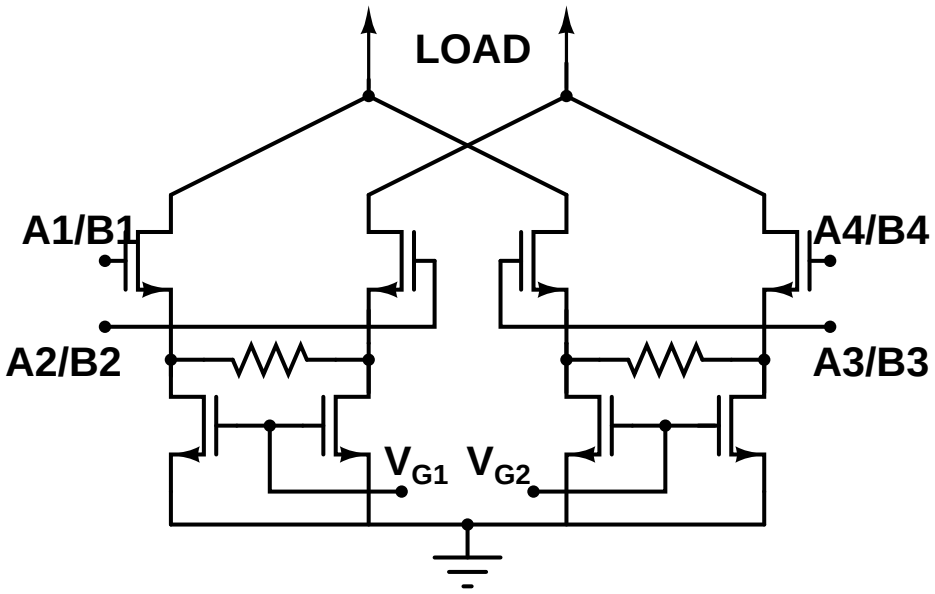

Figure 24: Circuit Schematic of the Modified Gilbert Cell ($G1$, $G2$).

This cell uses source degeneration resistors of 160 Ω in a local series feedback configuration to control gain and linearity. It also transfers current into resistive loads. The unity gain delay line ($D2$, $D3$) consists of three differential amplifier delay

cells. Active cells are used to provide delay rather than passive elements in order to minimize chip area. These delay cells also employ degeneration to limit the gain to unity while providing the required total delay. As this sub-circuit is a significant source of broadband noise in the output by means of MOSFET channel drain noise current, its design needs to balance various factors to achieve optimum performance. The bias current through the differential amplifiers is maintained at low values to contain the total power dissipation and output noise; however, the device sizes are maintained at relatively large values in order to generate the requisite time delay. This threatens to send the devices into sub-threshold operation. Therefore, an increase in MOSFET channel length and a concomitant degradation in noise performance is necessary. All other transistors in the signal path are of minimum channel length.

The switching control used to access the extra phase range of the circuit is illustrated in Figure 25. It relies on an external digital voltage V_{SW} that takes on the values 0 and 1.8 V.

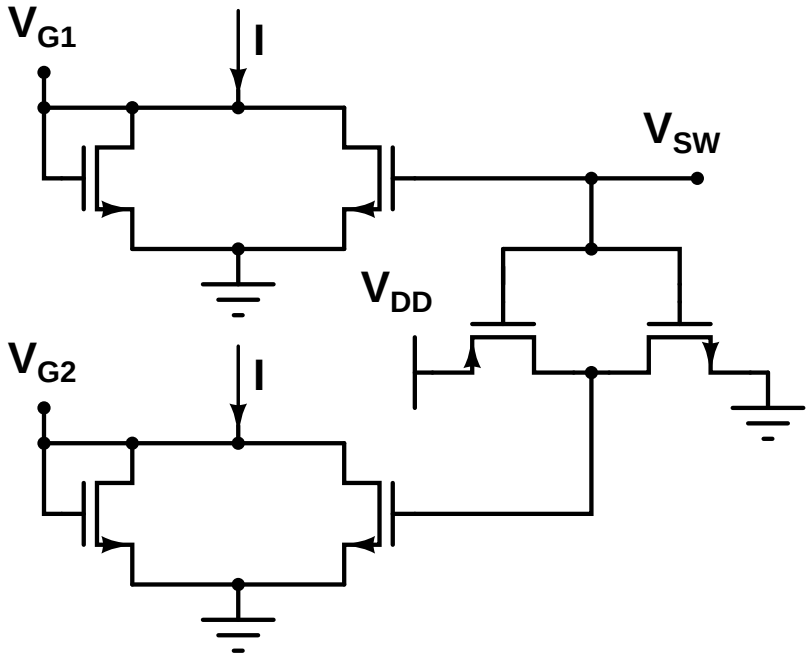

Figure 25: Schematic of Switching Mechanism Used to Control $G1$ and Toggle Extra Delay $D1$.

The interpolating circuit combines the input signals linearly thereby accomplishing delay shift by means of a successive piecewise linear approximation. This is the reason the whole delay range cannot be realized with a single continuous interpolation stage. If it were possible to accomplish a continuous phase range of 180^0 with a single interpolator, at one extreme of the range, the output would correspond to one of the two inputs to the interpolator, and the other extreme, it would be equal to the other input. As the interpolation is linear, at some intermediate point of the control range, the outputs due to the two inputs would be equal and opposite resulting in a trivial zero amplitude signal. Hence the need for segmentation into a fixed and a variable delay range.

To illustrate this, consider the input to the interpolator through the fast path to be $x(t)$. The linearly interpolated output signal may be represented as

$$y\left(t\right) = \alpha x\left(t\right) + \left(1-\alpha\right) x\left(t-\tau\right) \tag{65}$$

where τ is the delay through the slow path, and $\alpha < 1$ is a scalar whose value is controlled by bias current through the top differential pair in the modified Gilbert cell. Consequently, α is governed by the phase control voltage. It is apparent from (65) that when $\alpha = 1/2$, $y(t) = 0$.

Obtaining an effective phase range of 180^0 from the delay shifter requires the inclusion of at least two delay stages in the slow path. Since these architectures involve the design of delay cells to provide a few hundred picoseconds of delay, it is beneficial to partition the total delay into several stages of smaller delay each. This allows more bandwidth efficient circuits. Variations on this theme are possible that decrease current consumption and ease the design of large-delay circuitry required for applications at lower frequencies. One such modification to the above configuration is shown in Figure 26.

Here, a generalized tap-off procedure [53], [54] similar to that used in digital finite impulse response (FIR) filters is represented showing signals tapped-off after

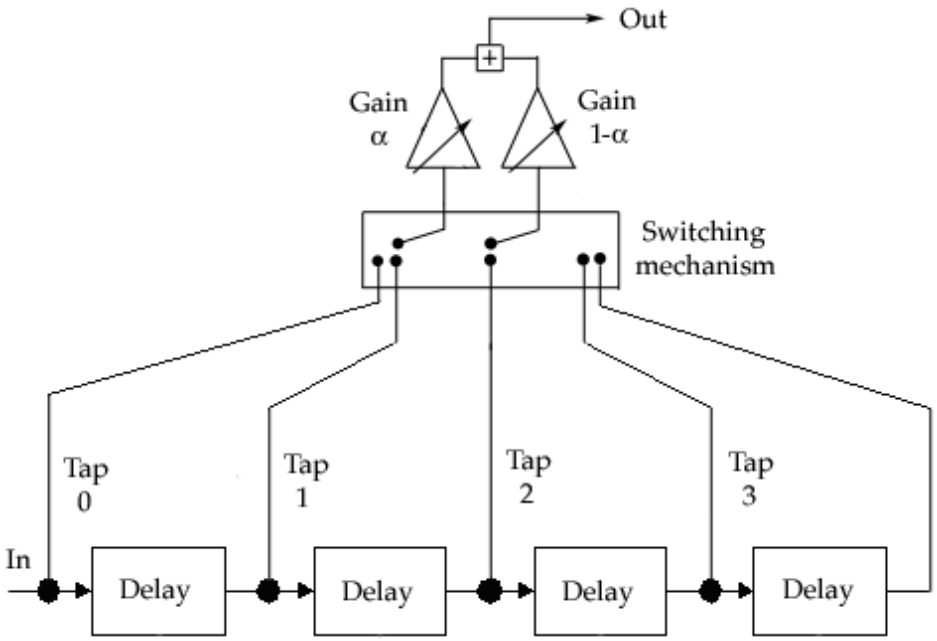

Figure 26: TDL Based Interpolating Shifter.

each delay stage. The interpolator may then mix any pair of them, which can be controlled by a switching mechanism. The continuously variable delay range offered in this case is reduced and equal to the path difference between the two signals used. However, for each choice of tap-offs there is a fixed delay affecting both signal paths that precedes the interpolator-delay cell system. Thereby, the total delay range is partitioned into smaller variable delay ranges each of which is offset from the other by a fixed delay. For instance, a variable 180^0 range is obtained as a variable 60^0 range employed at $0^0 - 60^0$, $60^0 - 120^0$ or $120^0 - 180^0$ by the application of a fixed 0^0, 60^0 or 120^0 offset respectively. A symbolic representation of this method is reproduced in Figure 27 using previously defined mathematical notation.

Referring to the diagram, $r = |y(t)|$ and $\theta = \phi[y(t)]$. The number of delay stages used in the shifter is n and they are identical. Also, the output of each stage is tapped-off and available to the interpolator as an input signal. The continuously adjustable phase range in any mode of operation is π/n radian and the fixed phase offsets used are $k\pi$ where k is an integer between 0 and $n - 1$.

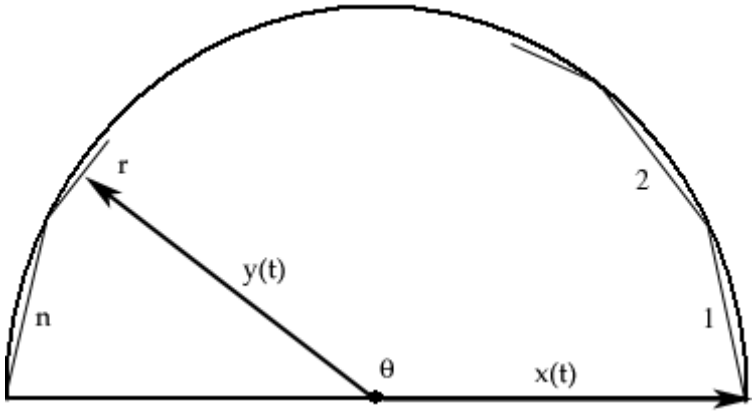

Figure 27: Mathematical Equivalent of Interpolation Scheme with n Tap-Off Delay Stages.

As inferred from the diagram, the phase variation through the shifter is accompanied by gain variation. Similarly, all linear interpolation based phase shifts are not constant magnitude transformations and the concomitant gain dependency on phase shift introduces potential difficulties in the construction of a control loop. The phase rotator circuit for 2.4 GHz operation was however designed with this limitation. In another version of the rotator designed to function at 1.575 GHz in a GPS protection scenario, a variable source degeneration element was used in the modified Gilbert cell to provide non-constant attenuation across the phase control range [55]. This was implemented by means of a MOS resistor that was controlled by the phase adjustment voltage so as to provide roughly uniform amplitude throughout the phase range.

Analog FIR filters may be designed to act as interpolators, however it is difficult to obtain sufficient bandwidth for high frequency applications from these filters. Usually, they also suffer from the need for a large number of passive elements thereby raising chip area [56]. A digital FIR filter may directly be used for the same purpose, where the input signals are sampled and digitized, and a delay line is constructed using a shift register [57] or memory [58]. However, such a design is limited by the extremely high power consumption and circuit complexity required for a digital FIR filter implementation [59].

S-parameter and time domain measurements were performed on the phase rotator fabricated. The measured phase variation at different control voltages as a function of frequency is shown in Figure 28.

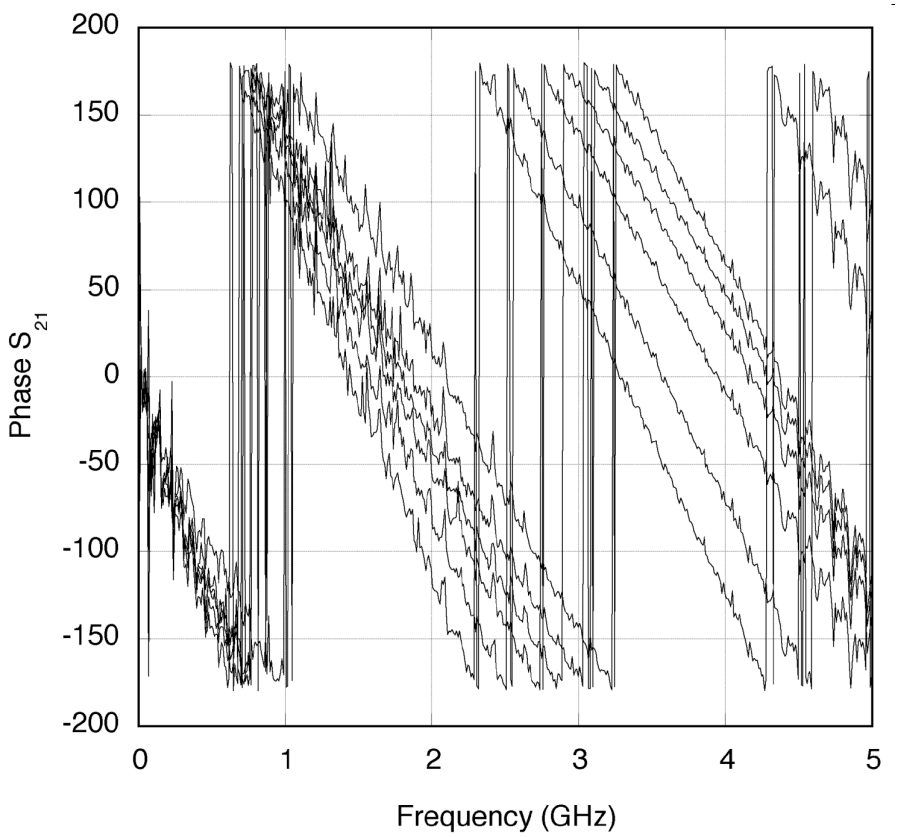

Figure 28: Variation of the Transmission Phase with Frequency for the Phase Aligner at Different Control Voltages.

Generally speaking, for a modulated sinusoid being transmitted through a system with a band-pass characteristic, the carrier is delayed by the phase delay and the modulating data by the group delay. Eliminating phase dispersion, therefore, usually translates to a constant group delay or linear phase response requirement. This is reduced to a triviality in the context of the present problem because the bandwidth of interest (83.5 MHz) is very small compared to the center frequency (2.4 GHz). Phase variation with control in-band illustrating the total phase range and unwanted gain variation are shown if Figure 29.

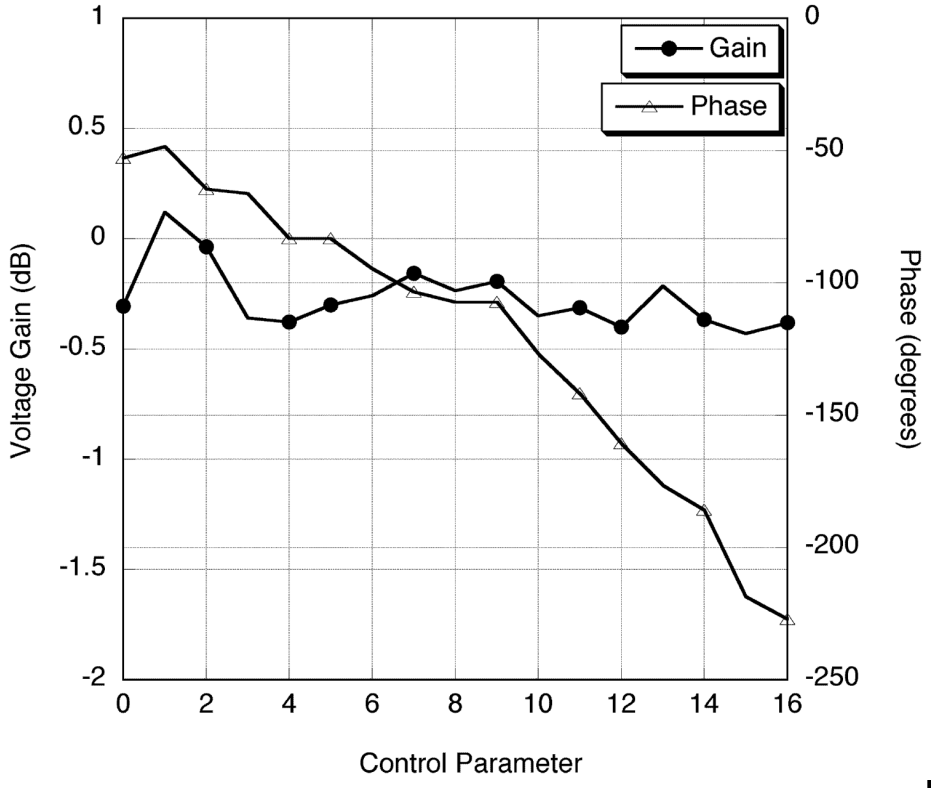

Figure 29: In-band (2.4 GHz) Variation of Gain Magnitude and Phase with a Control Parameter for the Phase Shifter.

Finally, a circuit that is widely used in RF front-end design for quadrature generation [60] may be extended to function as an adjustable phase shifter. This involves two independently controllable VGAs V_a and V_b with voltage gain ranges from -1 to +1, and a quadrature generation circuit. Assuming a sinusoidal input (ignoring modulation), if a and b are the gains of the two VGAs, and f the frequency of the input tone, the output is given by

$$y(t) = asin(2\pi ft) + bcos(2\pi ft) \tag{66}$$

A schematic of this principle is shown in Figure 30.

The output signal can be adjusted to have any amplitude from 0 to $\sqrt{2}$, and any phase shift from 0 to 360^0 with respect to the input, by appropriately varying a and b. The difficulty in this approach stems from the complexity involved in designing a precise high frequency quadrature generator that functions across a frequency band.

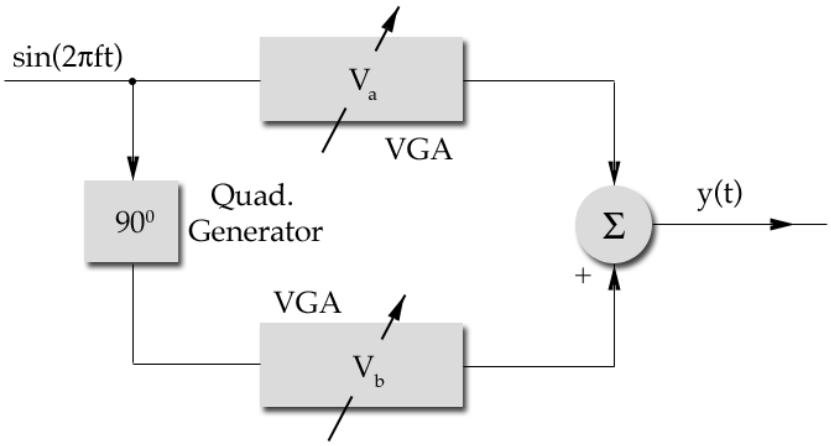

Figure 30: Quadrature Modulator Based Scheme for Design of Phase Aligner.

This circuit may be easily realized as a delay-based shifter or as a true phase shifter depending on the choice of the quadrature generation method. A passive quadrature generator allows true phase shift, but is difficult to implement over a wide bandwidth and at a low cost in area and circuit parasitics.

A number of circuit techniques have been reported in the literature for quadrature signal generation. These may be incorporated in the scheme of Figure 30 different ways. The quadrature element is replaced by an RC-sequence asymmetric polyphase filter in [61]. Digital quadrature modulators with current mode logic (CML) phase shifters are suggested in [62]. Various quadrature voltage controlled oscillators (VCO) have been developed. These range from ring oscillators with frequency doublers generating quadrature outputs [63] to cross-coupled direct quadrature VCOs [64], injection locking and level-locked loop methods [65], [66], and current-controlled quadrature oscillators [67]. Some of these, such as injection-locking, are suitable for high-precision quadrature generation, while others optimize different parameters.

In this work, a variation on the quadrature modulator theme is used to fit the configuration of Figure 30. Here, the orthogonal phase splitting, the VGA, and summing functions are combined into a single, low-power circuit. The concept, as

proposed in [68], is depicted in Figure 31 with minor modification.

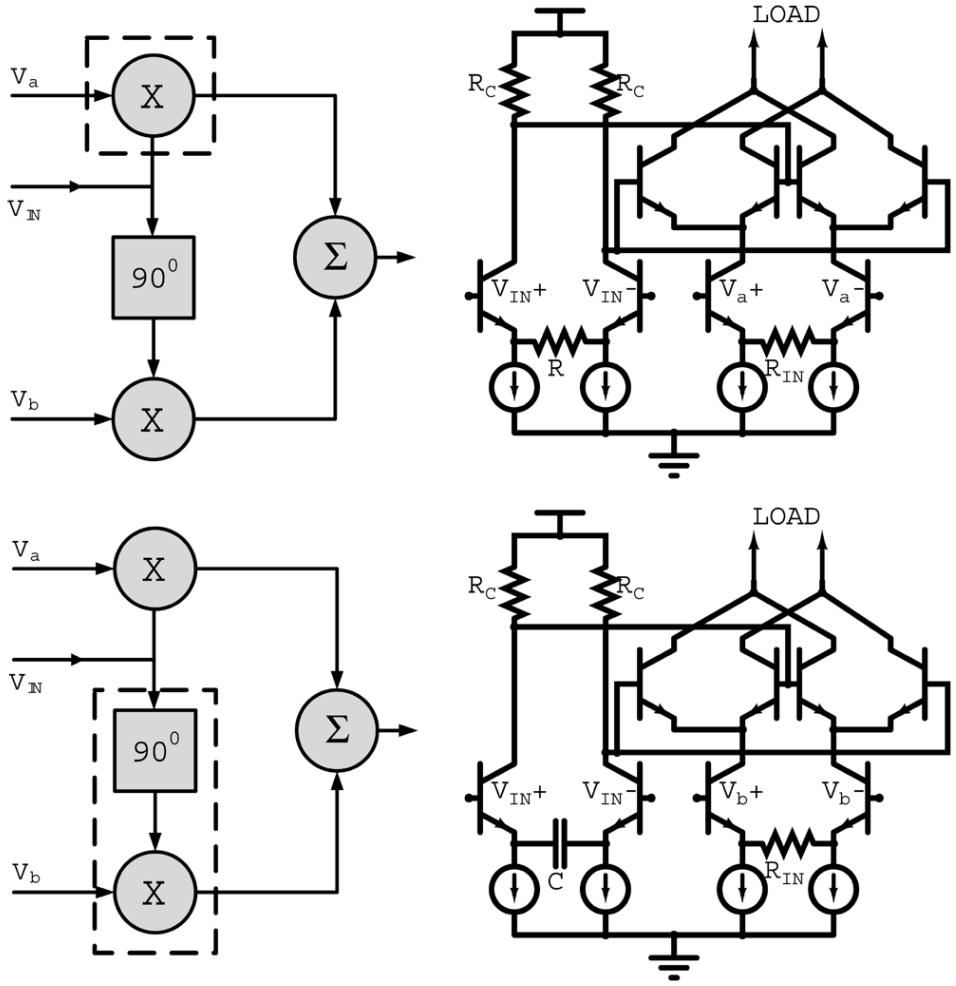

Figure 31: Schematic Illustrating Quadrature Modulator Operation.

Traditionally, in a vector modulator, the carrier tone and its quadrature are multiplied by the in-phase (I) and quadrature (Q) components of the incoming signal. However, in this case, the signal tone and the generated quadrature are multiplied by two DC control voltages (scalars). A brief analysis of its functioning mechanism for a bipolar implementation follows, but is easily extensible to MOSFETs.

The region within the dotted boxes on the left are shown in detail on the right side of the diagram. To first order, the differential signal current in the differential pair which accepts the input V_{IN}, is due to the action of the degeneration resistor, and is given by $\Delta I = \Delta V_{IN}/R$. In the bottom circuit, this current is generated

by the action of the degeneration capacitor, and is given by $\Delta I = \Delta V_{IN}.sC$. This differentiator action provides the 90^0 phase shift before the two signals are multiplied by the scalar control voltages and summed.

To expand upon this, in the top circuit (with R-degeneration), the DC-gain is given by:

$$A_R = \frac{-g_m r_\pi R_C}{R_S + r_b + r_\pi + \frac{R}{2}(1 + g_m r_\pi)} \tag{67}$$

where R_S is the source resistance of the input signal source, r_b is the transistor base resistance, and r_π and g_m are transistor small signal parameters. A frequency response analysis shows a number of poles and zeros generated. The following three poles and a zero can be related to C_{cs}, C_π, C_μ, and C_μ, respectively:

$$p_1 = \frac{R_C + r_0}{2\pi R_C r_0 C_{cs}} \tag{68}$$

$$p_2 = \frac{R_S + r_b + r_\pi + \frac{R}{2}(1+\beta)}{2\pi r_\pi C_\pi \left(R_S + r_b + \frac{R}{2}\right)} \tag{69}$$

$$p_3 = \frac{1}{2\pi (R_S + r_b)\left(1 + \frac{R_C}{R_S + r_b} - A_R\right) C_\mu} \tag{70}$$

$$z_1 = \frac{g_m}{2\pi C_\mu} \tag{71}$$

where β is the current gain.

Similarly, for the bottom circuit (with C-degeneration), the DC-gain is given by:

$$A_C = \frac{-4\pi f g_m C r_\pi R_C}{1 + \beta} \tag{72}$$

Clearly, unlike the R-degenerated circuit, this does not have constant DC-gain. Further, the two poles and two zeros of its transfer function, related to C_{cs}, C_μ, C_μ, and

C, respectively are:

$$p_1 = \frac{R_C + r_0}{2\pi R_C r_0 C_{cs}} \tag{73}$$

$$p_3 = \frac{1}{2\pi \left(R_S + r_b\right) \left(1 + \frac{R_C}{R_S + r_b} - A_C\right) C_\mu} \tag{74}$$

$$z_1 = \frac{g_m}{2\pi C_\mu} \tag{75}$$

$$z_2 = 0 \tag{76}$$

There is also a complex pole-pair (p_4, p_5) related to C and C_{pi} given by the roots of the equation:

$$2C\left(R_S + r_b\right) C_\pi r_\pi s^2 + \left[2C\left(R_S + r_b + r_\pi\right) + C_\pi r_\pi\right] s + \left(1 + g_m r_\pi\right) = 0 \tag{77}$$

From a comparison of the above equations it is apparent that a number of the poles and zeros of the two transfer functions are identical and hence do not contribute to any phase difference between the two outputs. Thus, this phase difference arises from the action of p_2, p_4, p_5, and z_2, and is given by:

$$\begin{aligned} \phi &= tan^{-1}\left[\frac{2\pi f C_\pi r_\pi \left(R_S + r_b + \frac{R}{2}\right)}{R_S + r_b + r_\pi + \frac{R}{2}\left(1 + \beta\right)}\right] \\ &- tan^{-1}\left[\frac{4\pi f C \left(R_S + r_b + r_\pi + \frac{C_\pi r_\pi}{2C}\right)}{2 + g_m r_\pi - 2C\left(R_S + r_b\right) C_\pi r_\pi \omega_2}\right] - \frac{\pi}{2} \end{aligned} \tag{78}$$

It must be noted that p_2 and p_3 do not match exactly and differ slightly because of the Miller factor, causing $A_C \neq A_R$. However, this effect is small. Also, the first two terms above may be made very close to each other so that they cancel out. This requires:

$$\begin{aligned} R &>> R_S + r_b \\ C &<< \frac{1 + \beta}{C_\pi r_\pi \left(R_S + r_b\right) \omega^2} \end{aligned} \tag{79}$$

Under these conditions, the phase difference in the outputs of the two sub-circuits becomes close to 90^0 with the degenerating R and C being the only elements in the two circuits that are not common to them. However, the $R = 1/2\pi fC$ also needs to be satisfied in order to maintain amplitude balance in the quadrature paths. This is not possible over the entire band of interest and leads to some amplitude variation.

The modified version of the phase aligner thus used a MOSFET equivalent of the above circuit. To conserve power and minimize noise generation, the quadrature generating differential pairs were integrated into the Gilbert cell multipliers that ordinarily follow them. Also, it is worth noting that quadrature generation with a MOSFET circuit would typically require more than one stage of differential pairs with R and C degeneration. But one stage was deemed sufficient in the present application. This is owing to the fact that 90^0 of phase separation is not necessary for the proper operation of the canceller core. Referring back to (66) and Figure 30, it may be observed that even if the two signal paths are not in precise quadrature, the output vector spans the whole 360^0 of phase space, although with varying amplitude. The resulting polar diagram that describes its action would resemble an ellipse instead of a circle. Hence, if the two VGA gains (and in this case the gain through the Gilbert cell) are made large enough, the minimum output amplitude can be made to exceed the requirement. A circuit schematic of this modulator is shown in Figure 32.

Again, the Gilbert cells in this circuit are operated by a similar folded-cascode current steering cell as before. Also, unlike the circuits earlier, they utilize a current-mirror load. The modulator was preceded by a preamplifier to suppress its additive noise contribution. A common-gate interfacing stage was used in the preamplifier to match the input to 50 Ω. All the previously described circuits were supplied by a reference current generated on-chip by means of a supply and temperature independent bandgap reference circuit [69], [70].

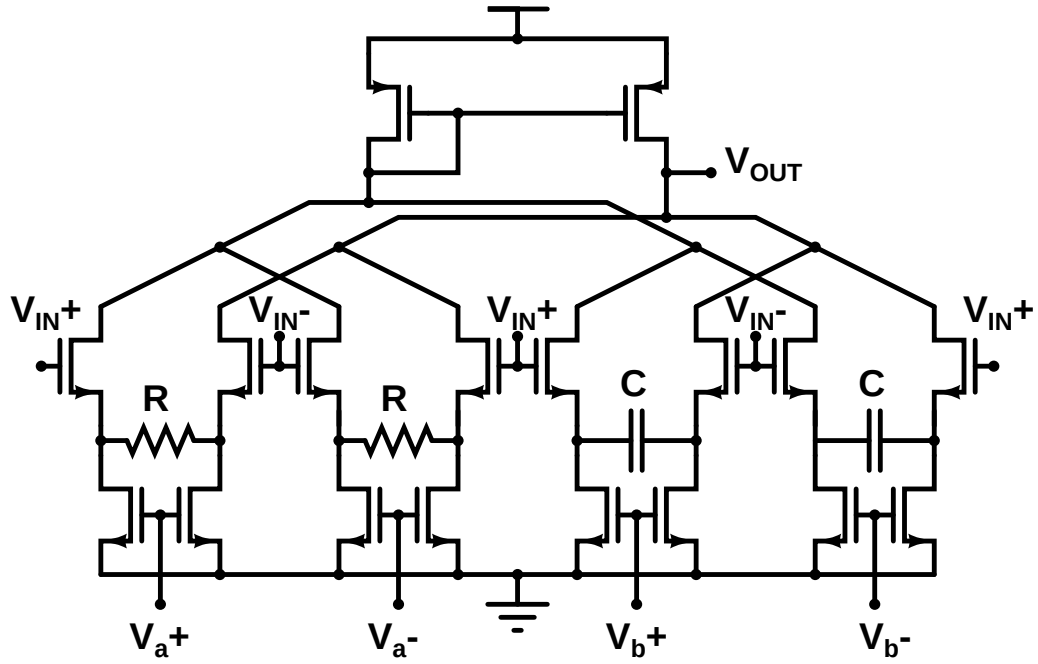

Figure 32: Simplified Circuit Schematic of the Quadrature Modulator Based Phase Aligner.

The band pass emulation filter described earlier in this chapter is adapted to the coupling channel. A schematic of the filter with limited tunability is shown in Figure 33. The varactor diode provides a tuning range of 2.1 to 2.6 pF controllable in steps of 0.1 pF, allowing a wide range of filter Q factors. This inductor was implemented as an external component mounted on-board.

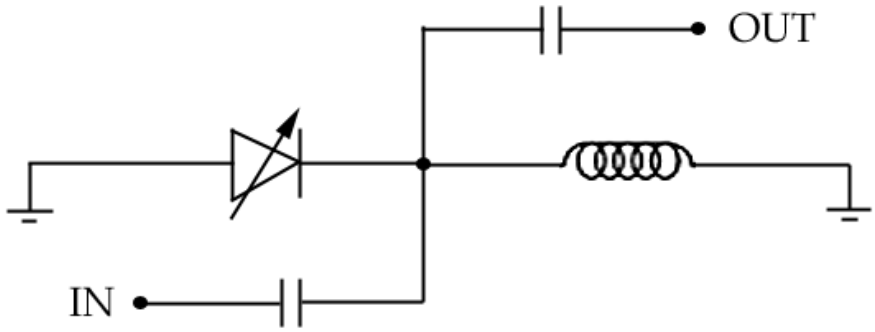

Figure 33: Schematic of On-Board Tunable Band-Pass Emulation Filter.

4.3 Canceller Performance

The IC implementation of the canceller consists of the circuitry described in the previous section as well as some interfacing components. These include input matching circuitry so that the unit may operate from a 50 Ω source, and in the case of the 2.4 GHz solution, a driver to buffer the unit from the load, which is the victim receiver feed-line. The core of the canceller also interfaces with the adaptive control unit that is briefly described in the subsequent chapter.

For the BT–WLAN scenario, the transmission characteristics of the coupling channel, measured before and after cancellation, are shown in Figure 34.

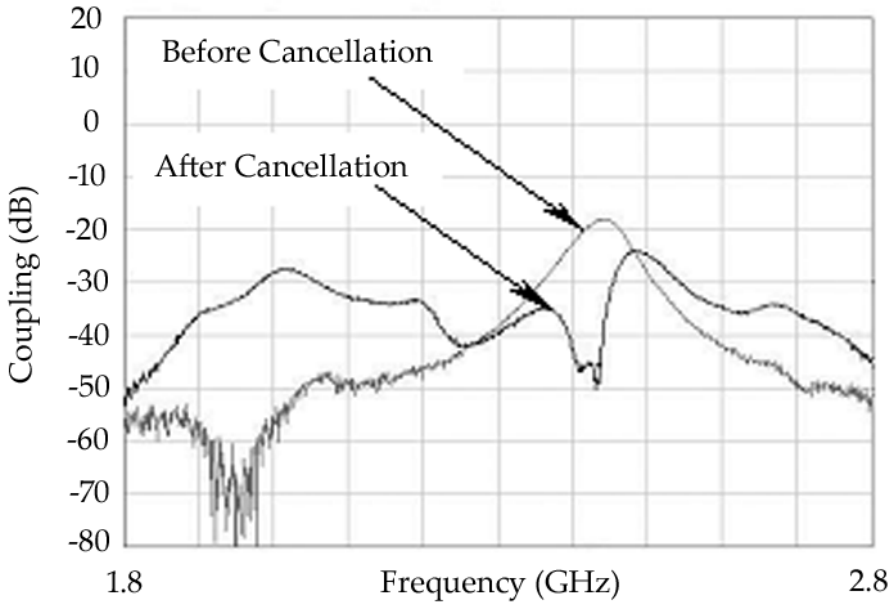

Figure 34: Canceller Performance in the 2.4 GHz Band Showing Magnitude of Coupling Before and After Cancellation for One Physical Configuration of the Aggressor and Victim.

A maximum cancellation of 30 dB is observed in-band, thereby reducing the interference level from 18 dB to 48 dB. When the antennae were arranged at a different distance, the coupling was decreased from 27 dB to 56.6 dB, implying a total cancellation of 29.6 dB. The null created, as noted from the graph, is narrower in bandwidth

than may be desired. Appropriate tuning of the canceller produces a wider band null that provides a lower level of cancellation throughout the band, as noted earlier. These numbers directly translate to an SNR improvement in the victim receiver front-end. The ICs in the canceller core, with the exception of the driver, consume 7.8 mA current. The current consumption in the driver was 16 mA.

An active cancellation result reported in the literature [41] shows improved isolation and reduced transmitter noise leakage into the receive band in a 2 GHz radio duplexer operating in a FDD scheme. A noise cancellation of up to 37 dB has been reported using complex vector attenuators to establish double nulls. However, the narrow band null created and the reference input source are at different frequencies and do not occupy the same band as in the current problem.

The second implementation of the canceller addressed the problem of incursion on a GPS receiver by various possible signal sources in a mobile radio environment. The sources include, for instance, a GSM transmitter and a high-speed bus carrying data between a digital signal processing (DSP) unit and the mobile phone display. Although these sources do not transmit or operate in the same frequency band as the GPS receiver, their sideband spectra contain enough energy to overcome the incoming GPS signal. This is directly due to the fact that the GPS receiver has an extremely high sensitivity requirement. Therefore, a canceller designed to operate in the 1.575 GHz band was also fabricated. This was designed to draw less DC power than the previous implementation and interfaced with the victim receive feed-line by means of a high-impedance node.

The input return loss performance of the 1.575 GHz canceller is shown in Figure 35. It is seen that in the band of interest, the canceller is well matched to the input source with -12.5 dB of S_{11}. An example measurement illustrating the noise suppression performance of this canceller core for one setting of the control mechanism is shown if Figure 36. It is able to suppress noise by about 15 dB.

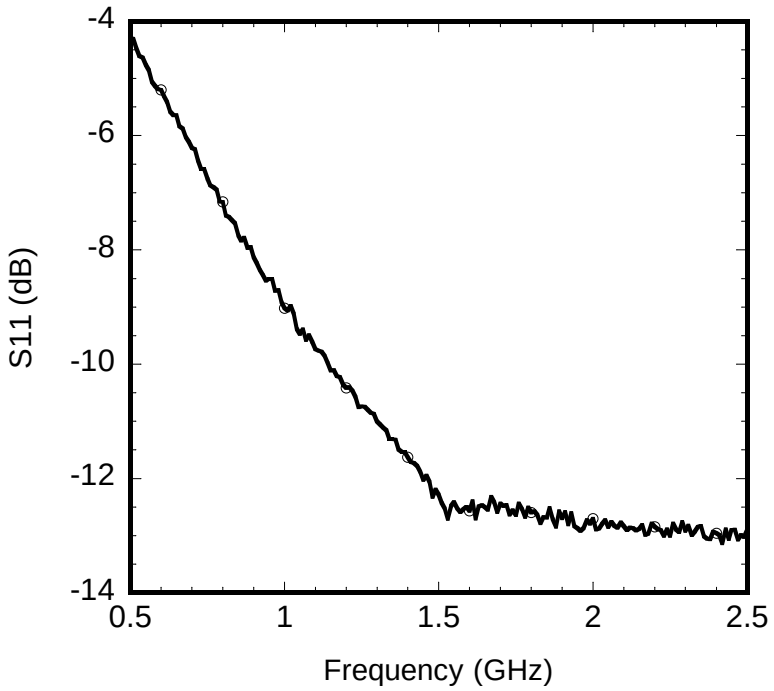

Figure 35: Input Return Loss Characteristic of the Canceller Core for the 1.575 GHz Application.

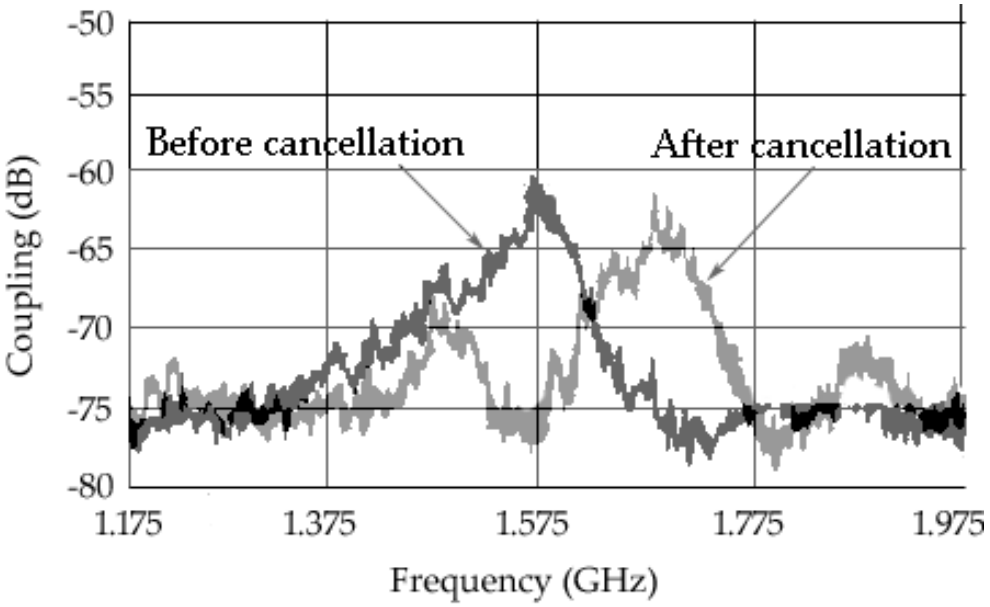

Figure 36: Canceller Performance in the 1.575 GHz Band Showing Magnitude of Coupling Before and After Cancellation for One Physical Configuration of the Aggressor and Victim.

As the expected interfering signal powers are very low, the input power handling range of the cancellers does not need to be very high. This capability is depicted in Figure 37, which is a plot of the gain compression behavior of the 1.575 GHz canceller. It is observed from the graph that the 1-dB gain compression point of the unit is -21.5 dBm (approx.).

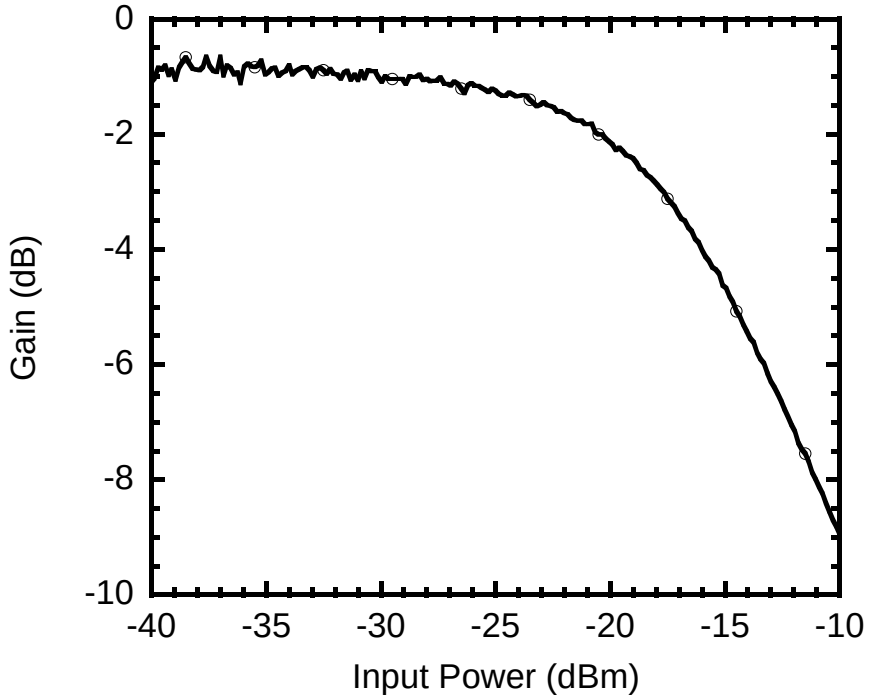

Figure 37: Gain Compression Performance of the 1.575 GHz canceller.

Finally, some results of measurements performed on the quadrature modulator-based canceller are reproduced here. This circuit was designed to operate in the 470 MHz – 750 MHz band. It is intended to protect a digital video broadcast receiver (DVB-H) from unwanted noise leakage. A source of such noise is a nearby GSM radiator operating in the 900 MHz band. As noted before, the two control voltages driving this canceller do not independently control the amplitude and phase of the cancellation signal, but rather form a two-dimensional control space over which this signal can be varied. A graph showing the amplitude control ability and dynamic range achievable from this canceller is plotted in Figure 38.

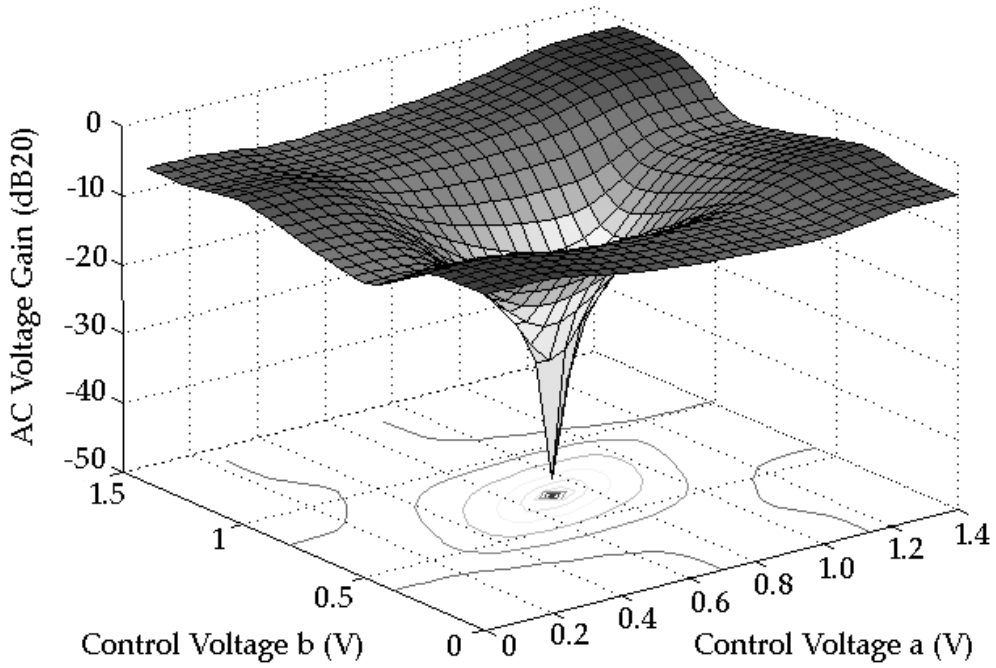

Figure 38: Surface Plot Showing Gain control and Dynamic Range of the Quadrature Modulator-Based Canceller Operating at 750 MHz.

The signal from this canceller is directly coupled to the victim antenna feedline through a capacitor that forms a high-impedance connection. To maintain an insertion loss less than 0.1 dB in the victim feed line, output impedance greater than 2 KΩ is necessary. The canceller unit achieves an output impedance of 6 KΩ or higher throughout the desired band of interest. The noise suppression performance of this version of the canceller is depicted in Figure 39. As seen from the diagram, 40 dB of dynamic range is available for gain control. Noise is mitigated by 16 dB in this case.

Effective interference mitigation at the victim requires that the broadband noise added by the canceller circuitry is minimal and does not degrade the sensitivity of the victim receiver significantly. Since the cancellation signal is added at the victim receive front-end through a voltage summation node, the figure of concern is the noise power spectral density of the canceller rather than its noise figure (NF). Since this version of the canceller incorporates a preamplifier to suppress noise from

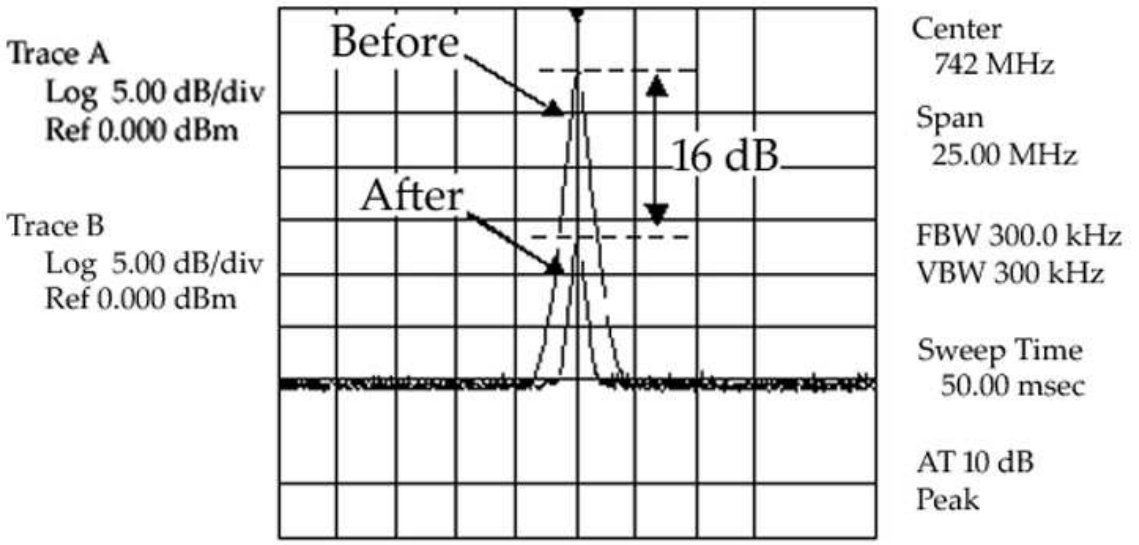

Figure 39: Canceller Performance at 742 MHz Showing Magnitude of Coupling Before and After Cancellation for One Physical Configuration of the Aggressor and Victim.

subsequent stages, it also has a reduced maximum gain requirement. A gain of -10 db is thus sufficient at the higher end of the control range. Concomitantly, the added noise from the canceller core is also diminished. Figure 40(a) shows the noise power spectral density surface of the canceller versus the control variable space and its noise contours. These noise contours are shown in conjunction with the gain contours of the canceller within the same control variable space in Figure 40(b). It is evident from the graph that throughout the useful portion of the attenuation range of the canceller, the output noise power spectral density does not exceed -173 dBm/Hz. Hence, the added broadband noise due to the canceller is well below the noise floor of the victim receive system and does not degrade its noise figure.

Since receiver sensitivity depends directly on the mean noise power spectral density in the receive band, Figure 41 illustrates the effect of cancellation on the sensitivity of the victim.

For high interference levels (> -155 dBm/Hz) sensitivity is improved by up to 15 dB for a given amount of coupled energy. However, a residual effect of the cancellation

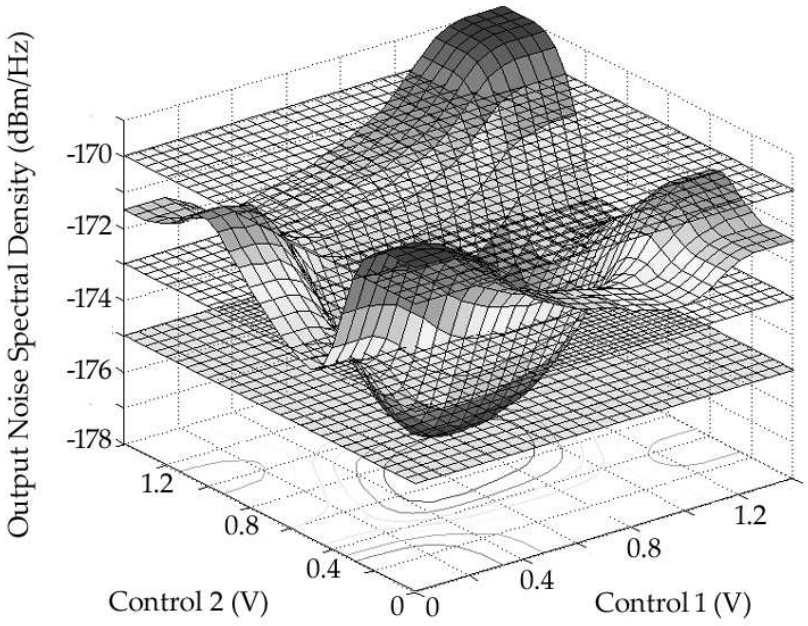

(a)

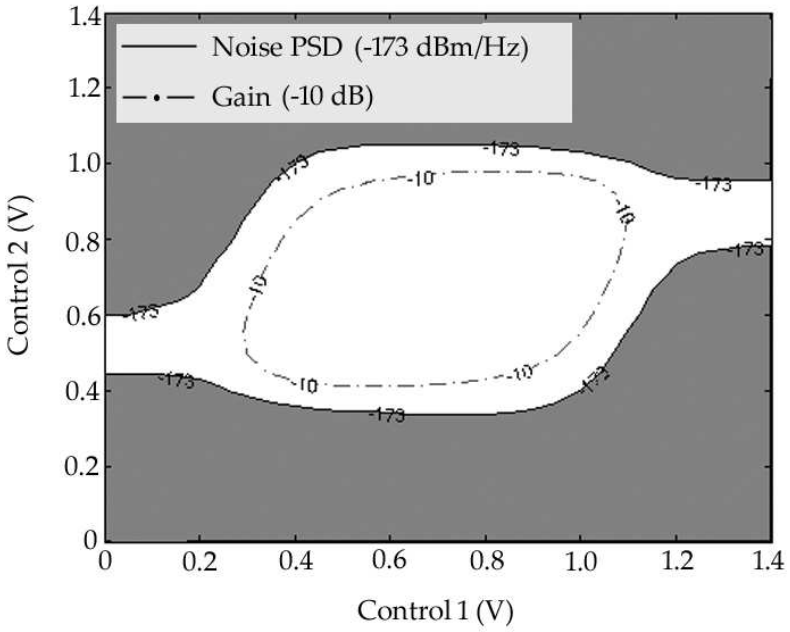

(b)

Figure 40: (a) Noise PSD Surface of the 750 MHz Canceller Core Vs. Control Voltages. (b) Gain and Noise Contours Vs. Control Voltages.

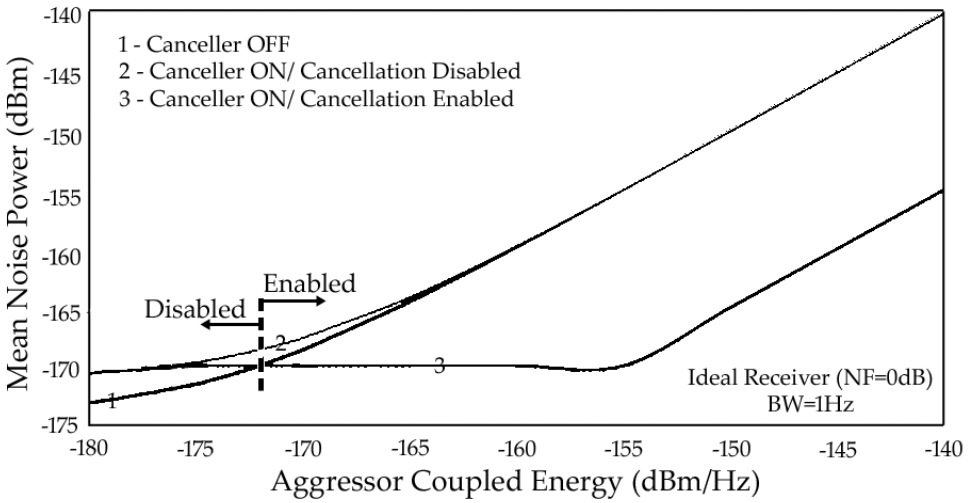

Figure 41: A Measure of Victim Receiver Sensitivity for Various Canceller States.

scheme is that at very low interference levels, victim sensitivity may be degraded by as much as 2.7 dB. This is attributed to the broadband noise added by the canceller circuitry, which is comparable to the victim receiver noise floor.

The performance parameters of the three canceller core ICs is summarized in Table 2.

Table 2: Performance Parameters of the Adaptive Interference Cancellers.

Parameter	2.4 GHz	1.575 GHz	750 MHz
Supply Voltage	1.8 V	1.8 V	1.8V
Power Dissipation	43 mW	21.5 mW	14.5 mW
Amplitude Range	0 to -42 dB	-1 to -33 dB	-2 to -45 dB
Phase Range	$> 360^0$	$> 360^0$	$> 360^0$
Maximum Input Power	-25 dBm	-21.5 dBm	-23 dBm
RF Input Impedance	50 Ω	50 Ω	50 Ω
RF Output Impedance	50 Ω	> 2 KΩ	> 6 KΩ
Available Noise Suppression	> 20 dB	> 15 dB	> 15 dB
Output Noise PSD	$<$ -140 dBm/Hz	$<$ -155 dBm/Hz	$<$ -173 dBm/Hz

CHAPTER V

ADAPTIVE CONTROL UNIT DESIGN

In this chapter, the design of an automatic control unit to adapt the canceller core is examined. The theory of adaptive control and the basis for the algorithms frequently used are introduced with special attention to gradient descent methods. This forms the backbone of the control loop operation mechanism. Schematics describing the controller are presented and circuits central to its design are illustrated. Since the control loop that forms part of the canceller is a mixed-signal design in its final form, it includes a state machine and associated digital circuitry that are in keeping with traditional designs. These borrow from the existing art and are therefore not expanded upon.

5.1 Fundamentals of a Control Mechanism

The dynamically controlled interference canceller can be considered a special case of the generalized adaptive transversal filter. The design of such filters is the domain of optimal filtering, of which noise canceling is a variation. As explained above, a portion of the canceller core may be implemented as a tapped delay FIR filter or otherwise. However, the theory explaining the general case holds. Therefore, suitable methods for adaptive control are briefly analyzed for the general case.

Most feasible adaptation solutions fall into one of two broad categories. Both revolve around measuring the error between the desired output of the filter (canceller) and the actual output at any iteration, and using this in a feedback configuration with the input to change the control variables. The error, which is a function of the inputs and the control variables, describes an n-dimensional surface in the control variable-space. The methods are divided according to the approach used to traverse the error

surface while converging at a solution for the controls.

In the context of the present problem, the dimensionality of the control variable-space is two, and the variables themselves are the gain and phase control voltages. A minor difference exists in the third canceller solution based on the quadrature modulator, where the two control voltages are not separately identifiable as governing the amplitude and phase of the cancellation signal. Instead, the amplitude and phase characteristic are each functions of the two control variables. With reference to the above, the two most practically realizable categories of control algorithms are the gradient descent and random search schemes.

To understand these methods, the following relations bear consideration. First, if the input signal vector at a discrete time instant j is given by

$$X_j = [x_{1j}, x_{2j}, ..., x_{nj}]^T \tag{80}$$

and the control variable vector is given by

$$V^T = [v_1, v_2, ..., v_n] \tag{81}$$

then the j^{th} output signal is

$$y_j = V^T X_j \tag{82}$$

Now, if the desired response is d_j, the error at j^{th} time is

$$\begin{aligned} \epsilon_j &= d_j - y_j \\ &= d_j - X_j^T V \end{aligned} \tag{83}$$

and the mean square error is

$$\begin{aligned} \xi &= \left\langle \epsilon_j^2 \right\rangle \\ &= \left\langle d_j^2 \right\rangle - 2P^T V + V^T R V \end{aligned} \tag{84}$$

where

$$\begin{aligned} P &= \langle d_j X_j \rangle \\ R &= \left\langle X_j X_j^T \right\rangle \end{aligned} \tag{85}$$

By differentiating (84) with respect to the control variable vector we get the gradient vector

$$\nabla = -2P + 2RV \tag{86}$$

which can be set to zero for the exact Wiener-Hopf solution.

All gradient descent methods operate on the basis of the above equations. For the noise cancellation case with two variables, the error surface is a hyperbolic paraboloid that never goes negative. The calculation or estimation of the gradient of (86) may be performed differently in various algorithms. Two algorithms of practical significance are the differential steepest descent (DSD) and least mean squares (LMS) algorithms [71].

The former technique directly measures the derivatives of the mean squared error by perturbing the control variables in both the positive and negative directions by a small percentage and calculating the gradient by a finite difference equation. Though this method is straightforward to implement, it is computation intensive compared to the LMS technique and involves more complex circuitry. The LMS algorithm however, does not directly calculate derivative. It relies on estimating the gradient by squaring the single value of error at any instant of time and differentiating it as if it were the mean square error. Since a new gradient estimate is obtained with each data sample, an adaptive iteration is effected with the arrival of each sample. This reduces the computational requirements on the circuitry and does not perturb the control variables, but is noisier and less accurate. The complete mathematical treatment of this approach is lengthy and provides insights into the stability of control loops based

on such methods. A detailed investigation of this behavior has been performed in the literature [72].

Finally, the random search method abandons the systematic search of the error surface for an optimum point in favor of making random changes to the adaptation variables [73]. The mean square error is measured before and after the change and the measurements compared. If an error reduction is caused by the change, it is accepted. If not, it is rejected and another random change tried. A linear random search algorithm employs a variation on this theme by making the control variable change proportional to the change in error performance, thereby introducing memory into the random search procedure. A simplification of this procedure is possible in the two variable cancellation problem. As each control variable has a known operating range and can be monotonically swept through that range, the adaptation processor can make a random change to it and depending on the error performance either accept the change or reverse its direction. This is pursued iteratively and alternately for each variable, independent of the other. The bidirectional search technique described is uniquely suited to the problem owing to its simplicity of implementation and minimal computational requirement.

5.2 Design of the Control Loop

A brief implementation procedure for the control mechanism on the basis of the DSD variation of gradient descent is as follows. The canceller core and control loop are established as shown in Figure 42. Here, the emulation channel consists of the filtering elements that replicate the effect of the actual interference. This comprises the VGA, primary emulation filter and the phase aligner. The control loop for the gain and phase control voltages themselves may be designed independently and can be identical to each other.

An example of an amplitude control loop that fits into the appropriate box in the

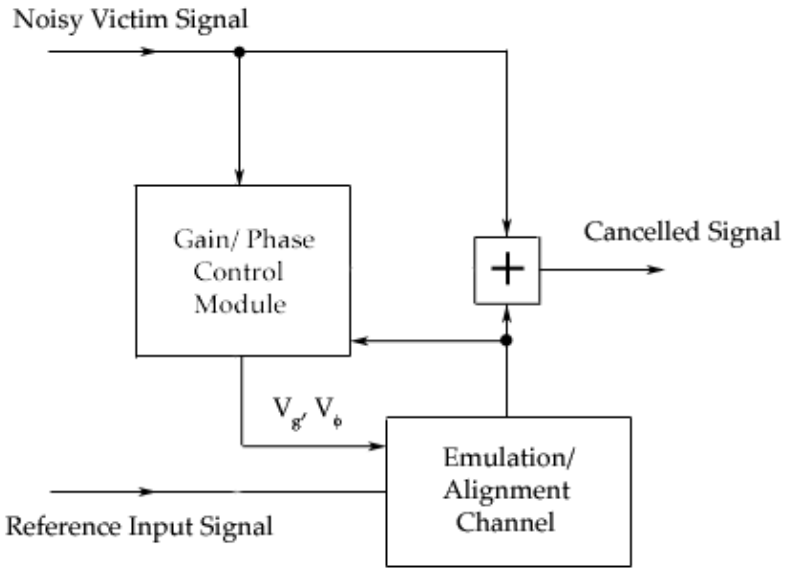

Figure 42: Illustration of Generalized Control Mechanism in the Interference Canceller.

previous diagram is shown in Figure 43. This is a fully analog circuit implementation of the steepest descent concept.

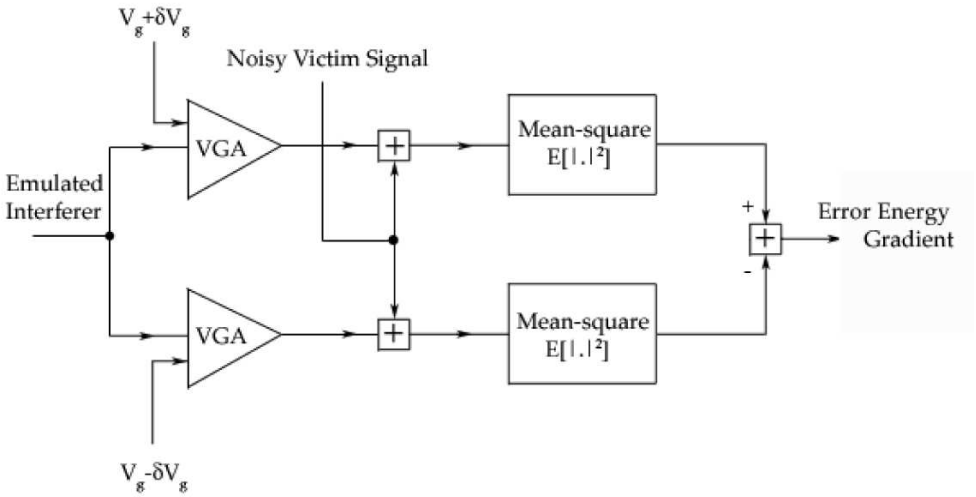

Figure 43: Analog Gain Control Loop Operating by the DSD Principle.

A similar loop may be used for phase control also. Around any given state of the control voltage, small and equal perturbations are applied to it in both directions. The

mean-squared values of the results are determined by squaring and low-pass filtering. They are then mutually subtracted and integrated. The energy in the cancelled signal is the sum of the energies in the victim signal alone and the residual coupled aggressor signal. Consequently, subtraction after the low-pass filters produces the difference in mean energies of the aggressor component alone at the two perturbations. Mathematically, this is the directional derivative of the error energy with respect to the gain control voltage. Reducing this gradient to zero iteratively determines the optimal solution, and the integral of the error energy gradient in the above diagram represents the optimal control voltage.

The above implementation involves the design of analog circuitry alone. An analog control mechanism suffers from convergence difficulties when it encounters discontinuities in the control variable state space. When the control voltages reach the extremities of their range during the adaptation process, a discontinuous jump in the voltage is often required. This affects the stability of the loop and prevents convergence. This prompts the design of a digital controller. A hybrid control loop has been used effectively in the literature for various problems [74]. This allows a coarse solution to be found using a digital state machine and refined by an analog controller.

A simplified random search may alternatively be employed with the aid of a mixed-signal control loop. This was the method of choice for the previously described canceller cores. The phase and gain control voltages are treated independently during alternate cycles of a low frequency digital clock signal (200 kHz). Again, identical treatment of each control voltage is possible thereby minimizing redundancy in the circuitry. The gain (phase) control voltage is incremented during alternate clock cycles, starting from a random value. This incrementation is done by a digital counter circuit/ register circuit. The resulting energy in the cancelled victim signal is estimated using an analog power detector that is designed in keeping with traditional

methods [75], [76]. The power detector produces a small analog voltage that is amplified by an op-amp with an offset cancellation circuit. This sample is held on a sample-and-hold circuit using a capacitor and applied to a comparator. The state of the comparator then determines whether to keep changing the gain (phase) control voltage in the direction that produced the gradient in the power detected, or to reverse it. Eventually, the two control variables descend to their optimum values. At this point, they both begin to oscillate around their final values for the remaining cycles.

The mechanism described here produces a digital code from the state machine. The code is converted to an analog gain (phase) control voltage by means of two digital-to-analog converters (DAC). Each DAC designed has 9-bit resolution and is of a voltage-scaling type [77], [78], [79]. It has a typical R-2R ladder structure and produces a voltage output capable of driving an off-chip 20 pF load. Figure 44 shows a schematic of the DAC.

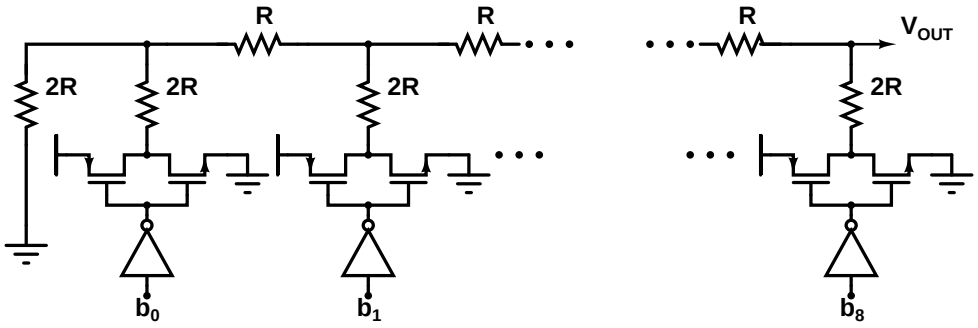

Figure 44: Simplified Schematic of 9-bit R-2R Ladder Voltage-Scaling DAC.

The 5% settling time of the DAC is less than 1 μs. Also, the resolution of the DACs directly governs the controllable resolution of the canceller core and hence the amount of cancellation possible. Open loop tests performed on the control loop demonstrated stable operation. Under closed loop conditions, the adaptation process converged to an optimal solution without encountering local minima in each of the three canceller implementations, thereby achieving substantial noise suppression.

CHAPTER VI

CONCLUSIONS AND FUTURE WORK

6.1 Contributions and Impact of the Dissertation

The contributions of this work can be summarized as follows:

1. It investigates and analyzes the hitherto unexplored area of deterministic noise cancellation in mobile radio communication systems. Several interoperation problems in the mobile wireless radio space are identified and interference concerns in the physical layer of operation are investigated. In particular, the Bluetooth – WLAN coexistence issue is characterized and quantified. This demonstrates the severity of performance degradation in a WLAN network operating in close proximity with a Bluetooth radio, and shows that for mutual separations of the order of a single circuit board, the probability of conflict may be as high as 40%. Requirements for the mitigation of interference in a typical IEEE 802.11b mobile radio receiver from a Bluetooth source are delineated.

2. A mathematical framework has been created for describing interference in the 2.4 GHz band and the deterministic noise mitigation problem has been cast to fit this framework. An adaptive noise suppression system has been developed that is able to alleviate the encroachment of the aggressor signal on the victim without sacrificing any of the original signal or otherwise corrupting it. This system is demonstrated to improve the SNR at the victim receiver. It is also able to handle a spread spectrum communication system as it does not rely on a narrow band cancellation notch.

3. The research is extended to construct an interference canceller that is both viable and easy to assimilate into existing RF front-ends, with emphasis on its universality and application independence. A small form-factor canceller has been designed in 0.18-μm Si-CMOS technology that delivers adequate noise suppression performance while placing the least possible strain on the front-end system. Owing to the large size and poor performance of passive devices on traditional Si-CMOS substrates, and the lengthy modeling cycle associated with them, the solution is active in nature, taking minimal recourse to passives. Robust and versatile circuitry is developed to achieve the amplitude and phase alignment required for correlation of signals. This includes novel implementations of phase rotator circuits based on delay interpolation and an integrated low-current quadrature modulator-based continuously variable analog phase shifter. The canceller so designed is capable of up to 30 dB of cancellation in-band for the Bluetooth – WLAN problem. Other versions of the canceller are configured to protect high-sensitivity GPS receivers from unintentional radiators, and to insulate receivers in the 500 – 750 MHz portion of the spectrum (such as DVB-H) from higher power transmitters in the vicinity. These demonstrate noise mitigation of at least 15 dB at 1.575 GHz and 750 MHz, respectively. The additive broadband noise power spectral density generated in these cancellers reach low values of the order of -170 dBm/Hz, which is unprecedented for such a function. All of the above are achieved with DC power dissipation values as low as 15 mW.

4. Issues relevant to developing automatic control mechanisms to operate the cancellers are examined. As a consequence, a simple low-power mixed-signal control loop is designed to effect the adaptation process required to ensure an optimal cancellation solution regardless of the dynamics of the interference environment. This is based on the principle of bidirectional random search and accomplishes

repeatable convergence in a high-sensitivity two-dimensional control problem.

The key contributions of this work are envisioned to be the development of controllable interference cancellation systems that allow the coexistence and simultaneous operation of multiple collocated high frequency wireless mobile radio devices, and advancement in the understanding of adaptive noise suppression in this context. Filtering methods being severely limited in their application to interference mitigation, this approach provides a unique alternative to combat a difficult coexistence environment, and is expected to have a significant impact on wireless communication front-ends.

6.2 Scope for Future Research

The body of work presented in this dissertation only scratches the surface of the coexistence problem in modern mobile wireless communication systems and multimedia devices. In recent years, solutions to this concern have been suggested at various levels of the communication system hierarchy. The central aspect of non-collaborative methods that allow simultaneous operation is an adaptive filtering scheme with a low-power circuit implementation. The interoperation problem is expected to be aggravated in the near future with the increasing complexity of services and equipment populating the spectrum. This raises the need for better solutions to the potentially debilitating problem.

Whereas a more far reaching answer involves designing a communications structure that directly addresses the sources of interference and outlines a method for operating outside the realm of conflict, this is extremely difficult to achieve for all possible interoperability scenarios. Therefore self-correcting or noise suppressing systems will need to be implemented for the foreseeable future. Two possible alternatives for such an adaptive suppression scheme are those designed to function at the RF front-end

and those targeted to work at the back-end baseband. This work proposes a methodology in keeping with the former, and a system comprising of adaptive tunable notch filters addresses the latter. While the baseband solution has some advantages, it is also more difficult to integrate into existing transceiver chipsets. With this in perspective, a hybrid implementation involving both the RF front-end and the baseband may offer an excellent compromise by exploiting the advantages of both. Future work can involve investigation of a hybrid approach.

To make any answer to the interference problem constituted in the physical layer more powerful and versatile, it needs to be able to combat a variety of aggressor – victim situations. Often, access to the aggressor is not available or is not practical. In other cases, a victim may be subject to corruption by numerous aggressors, some remote. In order to withstand these, the solution proposed in this dissertation should be expanded in its ability and scope. Thus, future research may be envisioned to develop 'receive only' systems, where the aggressor is irrelevant. As a preliminary step towards this, a electromagnetic element may be used to sample the aggressor signal without altering its electrical characteristics. This also eliminates interfacing issues at the input end. However, obtaining a sample of the aggressor signal in this manner in exclusion to the desired victim signal is fraught with difficulties. Any amount of the latter signal coupled into the reference input reduces the effectiveness of the canceller. A possible implementation that obviates the need for access to the aggressor stems from the concept of generating a reference signal *in-situ*, wherein, a more complex adaptation process is required to train the correlator and reference input to the corrupting signal. The investigation of such a system provides much ground for research and is rewarding in terms of the potential performance insights achievable.

APPENDIX A

PUBLICATIONS

1. A. Raghavan, S. Chandramouli, E. Gebara, and J. Laskar, "A low additive noise interference canceller for high sensitivity applications," being submitted to *Radio and Wireless Symposium 2008*.

2. A. Raghavan, E. Gebara, E. M. Tentzeris, and J. Laskar, "Analysis and design of an interference canceller for collocated radios," *IEEE Transactions on Microwave Theory and Techniques*, vol. 53, pp. 3498-3508, Nov. 2005.

3. A. Raghavan, E. Gebara, E. M. Tentzeris, and J. Laskar, "An active interference canceller for multistandard collocated radio," *2005 IEEE International Microwave Symposium Digest*, June 2005.

4. A. Raghavan, U. Jalan, S. Chakraborty, C.-H. Lee, J. Laskar, E. Chen, J. S. Lee, J. D. Cressler, G. Freeman, and A. Joseph, "A millimeter-wave linear low-noise amplifier in SiGe HBT technology with substrate parasitic model," *34th European Microwave Conference*, Oct. 2004, vol. 1, pp. 21-24.

5. S. Venkataraman, B. Banerjee, A. Raghavan, C.-H. Lee, and J. Laskar, "Small signal and RF noise analysis and modeling of 0.12-mm MOSFETs at liquid nitrogen and liquid helium temperatures," being submitted to *IEEE Transactions on Electron Devices*.

6. B. G. Perumana, S. Chakraborty, S. Sarkar, P. Sen, D. A. Yeh, A. Raghavan, D. Dawn, C.-H. Lee, S. Pinel, and J. Laskar, "A SiGe sub-harmonic mixer for millimeter-wave applications," to be presented at the *2007 European Microwave*

Symposium.

7. H. S. Kim, A. Raghavan, E. Gebara, and J. Laskar, "Backplane equalization comparison for 10-Gb/s data communication with 0.25-mm SiGe BiCMOS and 0.18-mm CMOS feed-forward equalizers," *2007 IEEE International Microwave Symposium Digest*, June 2007.

8. J. Laskar, A. Raghavan, C.-H. Lee, E. Gebara, E. M. Tentzeris, and T. Stelliga, "An active integrated circuit wireless interference cancellation solution," *IEEE Radio and Wireless Symposium*, pp. 559-562, Jan. 2006.

9. S. Chakraborty, A. Raghavan, B. G. Perumana, and J. Laskar, "Fundamental design considerations of integrated silicon radio circuits in nanometer geometries," *International Conference on MEMS and Semiconductor and Nanotechnology*, Dec. 2005.

REFERENCES

[1] H. Sobol, and K. Tomiyasu, "Milestones of Microwaves," *IEEE Transactions on Microwave Theory and Techniques*, vol. 32, pp. 1170–1181, Sep. 1984.

[2] "In Memoriam – Jack Kilby (1923-2005) Inventor of the Integrated Circuit," *IEEE Signal Processing Magazine*, vol. 22, pp. 6–7, Sep. 2005.

[3] H. Kroemer, "Quasi-Electric and Quasi-Magnetic Fields in Non-Uniform Semiconductors," RCA Review, vol. 18, pp. 332–342, 1957.

[4] H. Kroemer, "Theory of a Wide-Gap Emitter for Transistors," *Proceedings of the IRE*, vol. 45, pp. 1535–1537, 1957.

[5] D. Kahng, "A Historical Perspective on the Development of MOS Transistors and Related Devices," *IEEE Transactions on Electron Devices*, vol. 23, pp. 655-657, Jul. 1976.

[6] C. -T. Sah, "Evolution of the MOS Transistor – From Conception to VLSI," *Proceedings of the IEEE*, vol. 76, pp. 1280–1326, Oct. 1988.

[7] R. H. Dennard, F. H. Gaensslen, H. -N. Yu, V. L. Rideout, E. Bassous, and A. R. LeBlanc, "Design of Ion-Implanted MOSFETs with Very Small Physical Dimensions," *IEEE Journal of Solid–State Circuits*, vol. 9, pp. 256–268, Oct. 1974.

[8] S. Chia, "The Universal Mobile Telecommunication System," in *IEEE Communications Magazine*, vol. 30, pp. 54–62, Dec. 1992.

[9] G. L. Stuber, *Principles of Mobile Communication*, Norwell, MA: Kluwer Academic Publishers, 1996.

[10] "2007 Global Mobile Communications – Statistics, Trends and Forecasts," Paul Budde Communication Pty. Ltd., Feb. 2007.

[11] M. Di Benedetto, F. Tosco, and F. Vatalaro, "Mobile Radio Advances in Europe: Third Generation and Beyond," *IEEE Communications Magazine*, vol. 38, pp. 125–126, Sep. 2000.

[12] "The Convergence of Telecoms, Media and Technology: How Mobile Services will Accelerate Changing Media Consumption," Frost and Sullivan, March 2007.

[13] "The Mobile Broadcast TV Market: Subscription Revenue Numbers, 2006-2012," Datamonitor, March 2007.

[14] J. Fenk, "RF-Trends in Mobile Communication," *Proceedings of the 29th European Solid-State Circuits Conference*, pp. 21–27, Sep. 2003.

[15] T. Al-Gizawi, K. Peppas, D. I. Axiotis, E. N. Protonotarios, and F. Lazarakis, "Interoperability Criteria, Mechanisms, and Evaluation of System Performance for Transparently Interoperating WLAN and UMTS-HSDPA Networks," *IEEE Network*, vol.19, pp. 66–72, July–Aug. 2005.

[16] "The Effects of Interference on Video over Wi-Fi," Farpoint Group, Jan. 2007.

[17] Y. P. Morton, M. P. French, Q. Zhou, J. B. Y. Tsui, D. M. Lin, M. M. Miller, and D. Janning, "Software Approach to Access UWB Interference on GPS Receivers," *IEEE Aerospace and Electronic Systems Magazine*, vol. 20, pp. 28–33, Jan. 2005.

[18] B. P. Crow, I. Widjaja, L. G. Kim, and P. T. Sakai, "IEEE 802.11 Wireless Local Area Networks," *IEEE Communications Magazine*, vol. 35, pp. 116–126, Sep. 1997.

[19] J. C. Haartsen, "The Bluetooth Radio System," *IEEE Personal Communications*, vol. 7, pp. 28–36, Feb. 2000.

[20] N. Golmie, "Impact of Interference on the Bluetooth Access Control Performance: Preliminary Results," IEEE 802.15/00-322r0, May 2000.

[21] G. Ennis, "Impact of Bluetooth on 802.11 Direct Sequence," IEEE 802.11-98/319, Sep. 1998.

[22] S. Shellhammer, "SCORT – An Alternative to the Bluetooth SCO Link for Operation in an Interference Environment," IEEE 802.15-01/145r0, March 2001.

[23] J. Lansford, A. Stephens, and R. Nevo, "Wi-Fi (802.11b) and Bluetooth: Enabling Coexistence," *IEEE Network*, vol. 15, pp. 20–27, Sep.–Oct. 2001.

[24] IEEE Std. 802.15.1–2005, "IEEE Standard for Information Technology – Telecommunications and Information Exchange Between Systems – Local and Metropolitan Area Networks – Specific Requirements – Part 15.1: Wireless Medium Access Control (MAC) and Physical Layer (PHY) Specifications for Wireless Personal Area Networks (WPANs)."

[25] IEEE 802.11g–2003, "IEEE Standard for Information Technology – Telecommunications and Information Exchange Between Systems – Local and Metropolitan Area Networks – Specific Requirements Part II: Wireless LAN Medium Access Control (MAC) and Physical Layer (PHY) Specifications."

[26] I. Howitt, "WLAN and WPAN Coexistence in UL Band," *IEEE Transactions on Vehicular Technology*, vol. 50, pp. 1114–1124, July 2001.

[27] R. V. Hogg, and E. A. Tanis, *Probability and Statistical Inference*, New York: Macmillan, 1977.

[28] W. C. Jakes, *Microwave Mobile Communications*, New York: Wiley-Interscience, 1974.

[29] J. Zyren, "Extension of Bluetooth and 802.11 Direct Sequence Model," IEEE 802.11-98/378, Nov. 1998.

[30] T. S. Rappaport, *Wireless Communication Principles and Practice*, New York: IEEE Press/Prentice-Hall, 1996.

[31] J. Proakis, *Digital Communications*, New York: McGraw-Hill, 1995.

[32] Jung-Hyuck Jo, N. Jayant, "Performance Evaluation of Multiple IEEE 802.11b WLAN Stations in the Presence of Bluetooth Radio Interference," *IEEE International Conference on Communications 2003*, vol. 2, pp. 1163–1168, May 2003.

[33] C. F. Chiasserini, and R. R. Rao, "Coexistence Mechanisms for Interference Mitigation in the 2.4-GHz ISM Band," *IEEE Transactions on Wireless Communications*, vol. 2, pp. 964-975, Sep. 2003.

[34] "Vulnerability Assessment of the Transportation Infrastructure Relying on the Global Positioning System," http://www.volpe.dot.gov/gps/gpsvuln.html, Aug. 2001.

[35] G. Gerten, "Protecting the Global Positioning System," *IEEE Aerospace and Electronic Systems Magazine*, vol. 20, pp. 3–8, Nov. 2005.

[36] A. Raghavan, E. Gebara, M. M. Tentzeris, and J. Laskar, "An Active Interference Canceller for Multistandard Collocated Radio," *IEEE MTT-S International Microwave Symposium Digest*, June 2005.

[37] N. Wiener, *Extrapolation, Interpolation and Smoothing of Stationary Time Series with Engineering Applications*, New York: Wiley, 1949.

[38] T. Kailath, "A View of Three Decades of Linear Filtering Theory," *IEEE Transactions on Information Theory*, vol. 20, pp. 145–181, Mar. 1974.

[39] B. Widrow, J. R. Glover Jr., J. M. McCool, J. Kaunitz, C. S. Williams, R. H. Hearn, J. R. Zeidler, Eugene Dong Jr., and R. C. Goodlin,"Adaptive Noise Cancelling: Principles and Applications," *Proceedings of the IEEE*, vol. 63, pp. 1692-1716, Dec. 1975.

[40] J. Glover Jr., "Adaptive Noise Canceling Applied to Sinusoidal Interferences," *IEEE Transactions on Acoustics, Speech, and Signal Processing*, vol. 25, pp. 484–491, Dec. 1977.

[41] S. Kannangara, and M. Faulkner, "Adaptive Duplexer for Multiband Transceiver," *Proceedings of the Radio and Wireless Conference*, pp. 381–384, Aug. 2003.

[42] G. Marsh, and T. Sutton, "Analog Active Cancellation of a Wireless Coupled Transmit Signal," U.S. Patent 6 539 204, March 25, 2003.

[43] S. Boll, and D. Pulsipher, "Suppression of Acoustic Noise in Speech Using Two Microphone Adaptive Noise Cancellation," *IEEE Transactions on Acoustics, Speech, and Signal Processing*, vol. 28, pp. 752–753, Dec. 1980.

[44] A. Raghavan, E. Gebara, E. M. Tentzeris, and J. Laskar, "Analysis and Design of an Interference Canceller for Collocated Radios," *IEEE Transactions on Microwave Theory and Techniques*, vol. 53, pp. 3498–3508, Nov. 2005.

[45] J. Laskar, A. Raghavan, C.-H. Lee, E. Gebara, M. Tentzeris, and T. Stelliga, *Ac Active Integrated Circuit Wireless Interference Cancellation Solution*, *IEEE Radio and Wireless Symposium*, pp. 559–562, Jan. 2006.

[46] P. H. Woerlee, M. J. Knitel, R. van Langevelde, D. B. M. Klaassen, L. F. Tiemeijer, A. J. Scholten, and A. T. A. Zegers-van Duijnhoven, "RF-CMOS Performance Trends," *IEEE Transactions on Electron Devices*, vol. 48, pp. 1776–1782, Aug. 2001.

[47] B. Razavi, *Design of Analog CMOS Integrated Circuits*, New York: McGraw Hill, 2000.

[48] B. Gilbert, "A Precise Four-Quadrant Multiplier with Subnanosecond Response," *IEEE Journal of Solid-State Circuits*, vol. SC-3, pp. 365–373, Dec. 1968.

[49] R. J. Baker, H. W. Li, and D. E. Boyce, *CMOS Circuit Design, Layout and Simulation*, New York: Wiley-IEEE Press, 1997.

[50] M. Banu, J. M. Khoury, and Y. Tsividis, Fully Differential Operational Amplifiers with Accurate Output Balancing, *IEEE Journal of Solid-State Circuits*, vol. 23, pp. 1410-1414, Dec. 1988.

[51] B. Lai, and R. C. Walker, A Monolithic 622 Mb/sec Clock Extraction and Data Retiming Circuit, *ISSCC Digest of Technical Papers*, pp. 144–145, Feb. 1991.

[52] S. K. Enam, and A. A. Abidi, NMOS ICs for Clock and Data Regeneration in Gigabit-Per-Second Optical-Fiber Receivers, *IEEE Journal of Solid-State Circuits*, vol. SC-27, pp. 1763-1774, Dec. 1992.

[53] L. R. Rabiner, and B. Gold, *Theory and Application of Digital Signal Processing*, Englewood Cliffs, NJ: Prentice-Hall, 1975.

[54] S. Haykin, *Adaptive Filter Theory*, Englewood Cliffs, NJ: Prentice-Hall, 2001.

[55] S. Otaka, G. Takemura, and H. Tanimoto, "A Low-Power Low-Noise Accurate Linear-in-dB Variable-Gain Amplifier with 500-MHz Bandwidth," *IEEE Journal of Solid-State Circuits*, vol. 35, pp. 1942–1948, Dec. 2000.

[56] Z. Ciota, A. Napieralski, J. L. Noullet, "Analogue Realisation of Integrated FIR Filters," *IEE Proceedings Circuits, Devices and Systems*, vol. 143, pp. 274–281, Oct. 1996.

[57] K. Azadet, and C. Nicole, "Low-Power Equalizer Architectures for High-Speed Modems," *IEEE Communications Magazine*, vol. 36, pp. 118–126, Oct. 1998.

[58] B. C. Rothenberg, J. E. C. Brown, P. J. Hurst, and S. H. Lewis, "A Mixed-Signal RAM Decision-Feedback Equalizer for Disk Drives," *IEEE Journal of Solid-State Circuits*, vol. 32, pp. 713–721, May 1997.

[59] H. Wu, J. A. Tierno, P. Pepeljugoski, J. Schaub, S. Gowda, J. A. Kash, and A. Hajimiri, "Integrated Transversal Equalizers in High-Speed Fiber-Optic Systems," *IEEE Journal of Solid-State Circuits*, vol. 38, pp. 2131–2137, Dec. 2003.

[60] B. Razavi, *RF Microelectronics*, NJ: Prentice-Hall, 1998.

[61] S. H. Galal, H. F. Ragaie, M. S. Tawfik, "RC Sequence Asymmetric Polyphase Networks for RF Integrated Transceivers," *IEEE Transcations on Circuits and Systems II: Analog and Digital Signal Processing*, vol. 47, pp. 18–27, Jan. 2000.

[62] J. Hakkinen, T. Rahkonen, and J. Kostamovaara, "An Integrated 100 MHz to 1 GHz I/Q Modulator with CML Phase Shifter," *IEEE CAS Region 8 Workshop on Analog and Mixed IC Design*, pp. 11–15, Sep. 1996.

[63] A. W. Buchwald, and K. W. Martin, "High-Speed Voltage-Controlled Oscillator with Quadrature Outputs," *Electronics Letters*, vol. 27, pp. 309–310, Feb. 1991.

[64] P. Andreani, "Very Low Phase Noise RF Quadrature Oscillator Architecture," *Electronics Letters*, vol. 37, pp. 902–903, July 2001.

[65] P. Kinget, R. Melville, D. Long, and V. Gopinathan, "An Injection-Locking Scheme for Precise Quadrature Generation," *IEEE Journal of Solid-State Circuits*, vol. 37, pp. 845–851, July 2002.

[66] S. Navid, F. Behbahani, A. Fotowat, A. Hajimiri, R. Gaethke, and M. Delurio, "Level-Locked Loop: A Technique for Broadband Quadrature Signal Generation," *Proceedings of the IEEE Custom Integrated Circuits Conference*, pp. 411–414, May 1997.

[67] A. Leelasantitham, and B. Srisuchinwong,"A High-Frequency Low-Power Sinusoidal Quadrature Oscillator Using Only CMOS Current Mirrors," *Proceedings of the 15th International Conference on Microelectronics*, pp. 404–408, Dec. 2003.

[68] M. Steyaert, and R. Roovers, "A 1-GHz Single-Chip Quadrature Modulator," *IEEE Journal of Solid-State Circuits*, vol. 27, pp. 1194–1197, Aug. 1992.

[69] K. E. Kujik, "A Precision Reference Voltage Source," *IEEE Journal of Solid-State Circuits*, vol. SC-8, pp. 222–226, June 1973.

[70] G. Tzanateas, C. A. T. Salama, and Y. P. Tsividis, "A CMOS Bandgap Voltage Reference," *IEEE Journal of Solid-State Circuits*, vol. SC-14, pp. 655–657, June 1979.

[71] B. Widrow, and J. M. McCool, "A Comparison of Adaptive Algorithms Based on the Methods of Steepest Descent and Random Search," *IEEE Transactions on Antennas and Propagation*, vol. 24, pp. 615–637, Sep. 1976.

[72] B. Widrow, J. M. McCool, M. G. Larimore, and C. R. Johnson Jr., "Stationary and Nonstationary Learning Characteristics of the LMS Adaptive Filter," *Proceedings of the IEEE*, vol. 64, pp. 1151–1162, Aug. 1976.

[73] C. I. Marrison, and R. F. Stengel, "Robust Control System Design Using Random Search and Genetic Algorithms," *IEEE Transactions on Automatic Control*, vol. 42, pp. 835–839, June 1997.

[74] E. Graf, and J. P. Wiedmer, "Parallel Analog and Digital Control Loops for Phase Locking Precision Oscillator to Reference Oscillator," U.S. Patent 4107623, Aug. 1978.

[75] P.-C. Huang, Y.-H. Chen, and C.-K. Wang, "A 2-V 10.7-MHz CMOS Limiting Amplifier/ RSSI," *IEEE Journal of Solid-State Circuits*, vol. 35, pp. 1474–1480, Oct. 2000.

[76] C.-P. Wu, and H.-W. Tsao, "A 110-MHz 84-dB CMOS Programmable Gain Amplifier with Integrated RSSI Function," *IEEE Journal of Solid-State Circuits*, vol. 40, pp. 1249–1258, June 2005.

[77] T. Miki, Y. Nakamura, M. Nakaya, S. Asai, Y. Akasaka, and Y. Horiba, "An 80-MHz 8-bit CMOS D/A Converter," *IEEE Journal of Solid-State Circuits*, vol. 21, pp. 983–988, Dec. 1986.

[78] P. E. Allen, and D. R. Holberg, *CMOS Analog Circuit Design*, Oxford University Press: New York, 1987.

[79] F. Maloberti, R. Rivoir, and G. Torelli, "Power Consumption Optimization of 8 Bit, 2 MHz Voltage Scaling Subranging CMOS 0.5 μm DAC," *Proceedings of the IEEE International Conference on Electronics, Circuits, and Systems*, vol. 2, pp. 1162–1165, Oct. 1996.

VITA

Anand Raghavan received his Bachelor of Technology (B. Tech.) degree in Electrical Engineering from the Indian Institute of Technology Madras in 2001, and the Master of Science (M.S.) degree in Electrical and Computer Engineering from the Georgia Institute of Technology, Atlanta, in 2003. His research interests include analog and RF front-end circuit design, semiconductor device physics, and IC design for high-speed and collaborative signal-processing applications. He has worked as a graduate intern at National Semiconductor Corporation, Tucson, AZ during summer 2002, and at Quellan Inc., Atlanta, GA during the fall of 2005 and spring of 2006.